Report
P-17-16
December 2018

Modelling of resaturation in the Bentonite-Rock Interaction Experiment with conditioning to dismantling data

Task 8F of SKB Task Forces EBS and GWFTS

Steven Baxter
Giovanni Carta
David Holton

SVENSK KÄRNBRÄNSLEHANTERING AB

SWEDISH NUCLEAR FUEL
AND WASTE MANAGEMENT CO

Box 3091, SE-169 03 Solna
Phone +46 8 459 84 00
skb.se

SVENSK KÄRNBRÄNSLEHANTERING

ISSN 1651-4416
SKB P-17-16
ID 1693430
December 2018

Modelling of resaturation in the Bentonite-Rock Interaction Experiment with conditioning to dismantling data

Task 8F of SKB Task Forces EBS and GWFTS

Steven Baxter, Giovanni Carta, David Holton
Amec Foster Wheeler

Abstract

Radioactive Waste Management (RWM) has been established to manage the safe disposal of high level wastes and spent fuel within a Geological Disposal Facility (GDF). The UK does not currently have a final disposal concept for its GDF; instead RWM is considering a number of generic designs which include the possible use of bentonite as a buffer material, forming part of an engineered barrier system (EBS) to surround certain containers being considered for disposal.

The final subtask (i.e. Task 8F) of the Bentonite Rock Interaction Experiment (BRIE) at the Äspö Hard Rock Laboratory (HRL), is the focus of this study. The scope of this task is the simulation of the BRIE experiment, with specific emphasis placed on the investigation of hydraulic interactions at the interface of the fractured bedrock and the emplaced bentonite. To achieve this, models need to be able to capture length scales of the order of a centimetre to accurately capture the wetting behaviour of the bentonite. The main objectives of the analysis are:

- Evaluation and comparison of the predictive modelling completed in the earlier tasks with the new updated model that incorporates the new description of the local 'identified' fractures that intersect the boreholes containing the bentonite,
- Application of an integrated modelling approach (to represent both the geometrical complexity of the fractures in the rock, the rock 'matrix' and the key processes in the bentonite) to improve the ability of the model to represent the range of factors able to influence the wetting process,
- Sensitivity studies so as to gain an insight into the consequences of parametric uncertainty on the modelling results.

The result of the integrated modelling suggests that:

- An accurate representation of the discrete fracture network system intersecting the bentonite is essential to capture the highly heterogeneous wetting of the bentonite,
- Conditioning the parameters of the rock matrix, fractures and bentonite can substantially improve the comparison between model results and the experimental measurement of wetting,
- Conditioning models to a limited set of sensor data has shown the possibility for producing multiple, complementary model parameterisations that predict equally valid resaturation with the sensor measurements (i.e. the calibration process results in a non-unique parameterisation of a model).

Sammanfattning

Organisationen Radioactive Waste Management (RWM) har inrättats för att hantera en säker förvaring av högaktivt avfall och använt bränsle i en geologisk deponeringsanläggning (GDF). Storbritannien har för närvarande inte ett slutförvaringskoncept för sin GDF. I stället överväger RWM ett antal generiska konstruktioner som inkluderar en möjlig användning av bentonit som buffertmaterial, som då skulle utgöra en del av det ingenjörsbarriärsystem (EBS), som ska omge vissa behållare i förvaret.

Den slutliga deluppgiften (det vill säga Task 8F) av projektet Bentonit Rock Interaction Experiment (BRIE) vid Äspö Hard Rock Laboratory (HRL) är i fokus för denna studie. Omfattningen av denna uppgift är simuleringen av BRIE-experimentet, med särskild tonvikt på att undersöka hydrauliska interaktioner vid gränsytan mellan det sprickiga berget och den inplacerade bentoniten. För att uppnå detta måste modellerna kunna hantera längdskalor i storleksordningen av en centimeter för att fånga bentonitens vätningsbeteende tillräckligt bra. De viktigaste målen med analysen är:

- Utvärdering och jämförelse av den prediktiva modellering, som avslutades i de tidigare modelleringsuppgifterna, med den nya uppdaterade modellen som innehåller den nya beskrivningen av de lokala ”identifierade” sprickorna som skär borrhålen innehållande bentonit.
- Applikation av ett integrerat modelleringsförfarande (för att representera både geometrisk komplexitet av sprickorna i berget, bergmatrisen och nyckelprocesserna i bentoniten) för att förbättra modellens förmåga att representera de faktorer som kan påverka vätningsprocessen.
- Känslighetsstudier för att få insikt i konsekvenserna av en parametrisk osäkerhet i modelleringsresultatet.

Resultatet av den integrerade modelleringen indikerar att:

- En korrekt representation av det diskreta spricknätverkssystemet som skär bentoniten är väsentligt för att fånga den starkt heterogena vätningen av bentoniten.
- Konditionering av bergmatrisen, sprickor och bentonitparametrar kan väsentligt förbättra jämförelsen mellan modellresultat och experimentellt uppmätt vätning.
- Konditionering av modeller till en begränsad uppsättning sensordata har påvisat möjligheten att producera multipla komplementära modellparametriseringar som förutspår lika giltig återmättnad med avseende på sensormätningarna (det vill säga kalibreringsprocessen resulterar i en icke-unik parametrisering av en modell).

Executive summary

Radioactive Waste Management is studying and considering the safe disposal of high level wastes and spent fuel within a Geological Disposal Facility (GDF). A range of potential concepts are being considered, and include the use of bentonite as a buffer material as part of an engineered barrier system (EBS) to surround the disposal containers. Required safety functions to be performed by the bentonite buffer include protecting the disposal containers from detrimental thermal, hydraulic, mechanical and chemical processes as well as retarding radionuclides released from any waste container.

Participation in the Äspö EBS Task Force offers RWM the unique opportunity to strengthen and extend the UK's capabilities by assisting the development of modelling tools relevant to bentonite, applicable either to the current generic GDF concepts, or to future site-specific stages of the UK disposal programme. Specifically, the Äspö EBS Task Force provides an opportunity for considering coupled processes of a bentonite buffer material, with two research areas currently active:

- THM: coupled thermal (T), hydraulic (H), and mechanical (M) processes.
- THC: coupled thermal (T), hydraulic (H), and chemical (C) processes.

Within both of these research areas, modelling tasks have been identified to further the understanding of coupled processes. One of these tasks consists of modelling the Bentonite Rock Interaction Experiment (BRIE) at the Äspö Hard Rock Laboratory (HRL), denoted Task 8, and is a collaborative exercise between the Äspö EBS and Äspö Groundwater Flow and Transport of Solutes (GWFT) Task Forces. Task 8 currently consists of five subtasks (8A – 8F) of increasing complexity, from initial scoping analysis up to site-scale models, including predictive modelling of various aspects of the BRIE. The final subtask, Task 8F, is the focus of this report; providing the opportunity to consider hydraulic interactions at the interface of a fractured bedrock and emplaced bentonite on the scale of 30 cm diameter overcored boreholes. By participating in Task 8F, a UK modelling team has been able to develop modelling approaches as part of a collaborative international project, providing RWM with the opportunity to:

- compare and verify techniques and processes developed for modelling the bedrock bentonite interface with other teams participating in the Task Force,
- derive a methodology to integrate the approach taken to both the rock and bentonite,
- develop methodologies for refining models of the fractured rock using additional site measurements as they become available, and
- advance modelling techniques, allowing accurate representation of the interaction between the groundwater flow from the rock, and the resaturation of emplaced bentonite.

Through modelling the BRIE, the feasibility of using a physically realistic approach to simulate the interface between bentonite and fractured host rock has been demonstrated. In the Task 8C study, the saturation rate of bentonite emplaced in overcored boreholes located in a fractured host rock were found to be significantly affected by both the locations and total volume of groundwater ingress. During Task 8D, water producing fractures within these overcored boreholes were specified deterministically and through conditioning the local fracture network, the resaturation rates and profiles of emplaced bentonite were somewhat constrained. In Task 8F, updated descriptions of fractures intersecting the overcored boreholes have been provided. In addition, model conditioning has been performed based on the response of the relative humidity sensors from the experiment. As such, Task 8F provides significant refinement of the numerical models developed for simulating resaturation of the emplaced bentonite.

Key achievements

- The relative humidity, calculated from water content measurements of samples of the bentonite blocks taken post-completion of the BRIE have been compared against the data acquired by the RH sensors for both borehole KO0017G01 and borehole KO0018G01. At all sensor locations, the samples have been shown to be in good agreement, never differing by more than 6.5 %.
- For Task 8F, the description of the deterministic fractures intersecting the overcored boreholes has been updated. With this updated, simulations of 100 realisations of the stochastic background fracture network have been generated to provide an indication of the variability of the rock, with inflows to the boreholes calculated. The realisations which provided the best agreement between measured and modelled inflows have been selected for subsequent calculation of the resaturation of emplaced bentonite, including the evolution of relative humidity at the twelve RH-sensors.
- Measurements from the relative humidity sensors located in the dry section of borehole KO0017G01 have been used to condition model parameters describing the evolution of the pressure front through the bentonite. Subsequent model predictions at the remaining relative humidity sensors are in good agreement with the experimental data.
- Using models conditioned to both fracture observations in the deposition holes, as well as the short-term (less than 2 year) responses measured at the twelve relative humidity sensors, long-term predictions of the resaturation of emplaced bentonite have been performed for 100 years post emplacement (as requested by the Task Force). This timescale was selected to capture the major resaturation processes of bentonite emplaced on the scale of the BRIE.

Key conclusions:

This report demonstrates the feasibility of using a physically realistic approach to simulate the rock bentonite interface through modelling Task 8F and validation with the BRIE data. The approach adopted explicitly represents the heterogeneity of the fractured bedrock necessary to accurately predict resaturation times and profiles of emplaced bentonite. In addition, methodologies have been developed for conditioning models of the bentonite using additional site measurements as they have become available. In summary, the developed approach has identified:

- The saturation of bentonite is highly heterogeneous, especially at early times after emplacement. An accurate representation of the discrete fracture network system intersecting the bentonite is essential to capture the highly heterogeneous wetting of the bentonite. In addition, a detailed representation of the surrounding fractured bedrock is important to constraining the supply of groundwater to the bentonite.
- Conditioning the parameters of the rock matrix, fractures and bentonite can substantially improve the comparison between model results and the experimental measurement of wetting.
- Conditioning models to a limited set of sensor data has shown the possibility for producing multiple, complimentary model parameterisations that predict equally valid resaturation with the sensor measurements (i.e. the parameterisation of the model is not unique calibration process results in a non-unique parameterisation of a model).
- The ability of the software, ConnectFlow, to simulate the heterogeneous hydration of the bentonite.

Finally, although models to date have been developed that are specific to the BRIE at the Äspö HRL, the tools, conditioning techniques and methodologies developed are generic, and are directly applicable to any future work carried out on UK specific issues for the simulation of bentonite hydration in a higher strength rock.

List of acronyms and abbreviations

BRIE	Bentonite Rock Interaction Experiment
CAD	Computer Aided Design
CONNECTFLOW	A software package, developed by Amec Foster Wheeler, for modelling groundwater flow and transport on a variety of scales
CPM	Continuous Porous Medium
DFN	Discrete Fracture Network
EBS	Engineered Barrier System
ECPM	Equivalent Continuous Porous Medium
GDF	Geological Disposal Facility
GWFT	Groundwater Flow and Transport of solutes
HRL	Hard Rock Laboratory
NDA	Nuclear Decommissioning Authority
RH	Relative Humidity
RWMD	Radioactive Waste Management Directorate
SDM	Site Descriptive Modelling
THC	Coupled Thermal (T), Hydraulic (H), and Chemical (C) Processes
THM	Coupled Thermal (T), Hydraulic (H), and Mechanical (C) Processes
TOUGH2	A software package, developed by Lawrence Berkeley National Laboratory, for simulating nonisothermal, multiphase fluid flows in both porous and fractured media

Contents

1 Introduction and objectives

In the UK, the management and delivery of geological disposal for higher-activity radioactive wastes is the responsibility of Radioactive Waste Management Limited (RWM). The safe disposal of these wastes utilises a multiple barrier concept to isolate the wastes from the biosphere. Although the UK does not currently have a defined concept for its Geological Disposal Facility (GDF), for all geological environments but disposal in salt, the generic designs for a UK GDF (NDA RWMD 2010b) may use a bentonite buffer material as part of an engineered barrier system (EBS). This bentonite buffer is used to surround the disposal container. A bentonite buffer material is also proposed in the GDF concepts of a number of other countries, for example in Sweden and Finland is KBS-3 concepts (SKB 2006). The required safety functions to be performed by the bentonite buffer are detailed in NDA RWMD (2010a) and Holton et al. (2011) and include:

- protecting the disposal containers from detrimental processes, including thermal, hydraulic, mechanical and chemical effects,
- retarding the release of radionuclides from any failed waste container.

It is therefore apparent that the understanding of bentonite behaviour in the context of a GDF is relevant to the current generic UK disposal concept; with RWM reviewing UK specific factors influencing the performance of the bentonite barrier (Wilson et al. 2012) as part of their research programme. During 2011, RWM decided to provide support for a UK modelling team to participate in the Äspö EBS Task Force, a collaborative international project. Through participation, RWM intends to strengthen and extend the UK's capabilities by assisting the development of models of processes relevant to bentonite, applicable either to current GDF concepts, or to future site-specific stages of the UK disposal programme.

1.1 Background to the EBS Task Force

The Äspö EBS Task Force programme considers coupled Thermal (T), Hydraulic (H), Mechanical (M) and Chemical (C) processes relevant to bentonite buffer materials. Current research is split into two areas, one considering the coupled modelling of THM processes, and the other considering THC processes. Active projects within the Task Force considering coupled THM processes include:

- the modelling of the Bentonite Rock Interaction Experiment (BRIE), which is an investigation of hydraulic interactions between the bedrock and the bentonite buffer,
- the homogenisation of bentonite as it hydrates,
- a sensitivity and verification analysis, and
- the modelling of the "prototype repository".

Research into THC processes includes the investigation of diffusion of chemical species through bentonite.

The collective modelling task of the BRIE is denoted Task 8 and it is a collaborative research project between the Äspö Task Force on Groundwater Flow and Transport of Solutes (GWFT) and Engineered Barrier Systems (EBS). Task 8 of the EBS Task Force considers the interaction between engineered and natural barriers and provides an assessment of a fractured bedrock description in the wetting processes of bentonite at deposition tunnel scale (Vidstrand et al. 2017). As detailed in the task description (Vidstrand et al. 2017), findings from Task 8 will improve:

- the scientific understanding of the exchange of water between the sparsely fractured rock and the bentonite,
- the predictions of the wetting of the buffer,
- the characterisation methods of container deposition boreholes, and
- the methods used for establishing deposition hole criteria.

In Task 8 the BRIE provides an opportunity to model the resaturation of bentonite. The BRIE is being run concurrently to Task 8 and intends to address Vidstrand et al. (2017):

- selection criteria/suitability for deposition holes,
- the drilling of central boreholes and subsequent characterisation of the site using borehole logging and hydraulic tests, and
- the characterisation of two central boreholes for the installation of a bentonite buffer.

Participation in Task 8, as part of a collaborative, international project, provides the opportunity to:

- compare and verify techniques and processes developed for modelling the bedrock / bentonite interface with other teams participating in the Task Force,
- identify the important data used to parameterise the rock, to provide a basis for resaturation,
- develop methodologies to represent the interaction between the groundwater flow from the rock and the resaturation of the bentonite material,
- build confidence in the ability to model the resaturation processes by comparison with experimental observations,
- investigate processes for refining models of the fractured rock using additional site measurements as they become available, and
- explore important parameter uncertainty and evaluate consequences (e.g. rock matrix permeability).

Task 8 is not intended to be a fully coupled modelling exercise (Vidstrand et al. 2017); i.e. fully incorporating thermal, chemical, or mechanical aspects[1]; instead, it aims to improve the knowledge of the bedrock-bentonite interface with regard to how groundwater flow resaturates the bentonite.

Task 8 is split into a number of subtasks and, specifically, it is the modelling results of Task 8F that are the focus of this study. Task 8F follows on from Task 8C and Task 8D, which have previously been modelled by Amec Foster Wheeler, supported by RWM, and documented in Baxter et al. (2014a, b). Task 8C and Task 8D were concerned with the prediction of resaturation of the central probe boreholes of the BRIE, with limited data available for conditioning models. Task 8F revisits the BRIE, refining resaturation predictions using additional geometric and hydraulic data provided as part of the task description (Wilson et al. 2011).

Whilst the models developed are specific to the BRIE at the Äspö Hard Rock Laboratory (HRL), the tools, techniques and methodologies developed are generic and so are directly applicable to any hard fractured rock environment. In the UK's preparatory phase this work is therefore of relevance to higher strength rocks (HSR) in which a bentonite buffer may provide part of the EBS.

1.2 Scope of Task 8F

Task 8 consists of five subtasks (8A – 8D, 8F) of increasing complexity, from initial scoping analysis to site-scale models, designed to provide predictive modelling of various aspects of the BRIE. Previous analysis of Task 8C (Baxter et al. 2014a) provided predictions of inflow to central boreholes planned for the TASO tunnel (located at a depth ~420 m at the Äspö HRL) of the BRIE experiment based on site-scale statistics. In addition, the resaturation profiles of bentonite emplaced in proposed over-cored boreholes of the BRIE were predicted. Task 8D (Baxter et al. 2014) extended this analysis to provide predictions of inflow and wetting of the bentonite emplaced in two 30 cm diameter overcored boreholes selected for the BRIE experiment using local characterisation of these holes.

[1] It is noteworthy that a number of material properties, especially those associated with the bentonite, are dependent on the swelling pressure sustained by the bentonite during resaturation. This dependency would require coupled hydraulic-mechanical models to be developed and is beyond the scope of this study.

Task 8F involves the use of additional geometric and hydraulic data (not available at the time of Tasks 8C and 8D) evaluated post-completion of the BRIE experiment. The additional data set provided as part of Task 8F includes:

- refinement of the geometrical details of the deterministic fractures observed in the boreholes,
- geometric details for fracture traces in KO0018G01, interpreted from the emplaced bentonite,
- water content data of the bentonite removed from both overcored boreholes KO0017G01 and KO0018G01.

Participation in Task 8F provides RWM with the unique opportunity to develop methodologies to understand the resaturation of the bentonite buffer material. By considering the additional data available during site characterisation and post-completion of the experiment, it is possible to determine the significance of such data for understanding the resaturation profiles of the bentonite, thus informing future investigations.

1.2.1 Objectives

Task 8F provides an opportunity to further develop existing models of the BRIE experiment. Whereas previous subtasks have involved predictive modelling of the bentonite resaturation, within Task 8F, the experimental results post-completion of the BRIE (Fransson et al. 2017) are available to:

- provide detailed evaluation of the resulting wetting of the bentonite installed in two overcored boreholes,
- improve the knowledge of the bedrock-bentonite interface with regard to understanding how groundwater flow resaturates bentonite,
- evaluate the predictive modelling completed in the earlier tasks, enabling comparison with the latest modelling results,
- perform a back-analysis (inverse modelling), to determine how to improve the numerical models.

1.3 Report structure

This report details modelling results and conclusions from Task 8F and is structured as follows:

- Chapter 2 provides an overview of the previous modelling work performed (Task 8D (Baxter et al. 2014b)), detailing the methodologies and data on which Task 8F will be based.
- The tools used for simulating resaturation of the emplaced bentonite are reviewed in Chapter 3. In addition, the numerical model definition including computational domain, boundary conditions and the mesh used are detailed.
- Chapter 4 presents the additional experimental data provided by the Task Force (Fransson et al. 2017) post-completion of the BRIE and available for Task 8F modelling.
- Using the Task 8D description, a basecase model is defined in Chapter 5. This model undergoes a series of conditioning steps as reported in Chapter 6, providing refined simulations of the BRIE experiment.
- Using the conditioned models from Chapter 6, a number of variants of the underlying fracture system are considered in Chapter 7.
- Chapter 8 provides long-term predictions of the resaturation profiles of the emplaced bentonite, extending to 100 years after installation.
- The key conclusions from this study are documented in Chapter 9.

2 A review of modelling in Task 8D

Task 8F modelling of the BRIE involves the use of additional geometric and hydraulic data (not available at the time of Task 8C and 8D) evaluated post-completion of the experiment. Chapter 2 provides a review of the Task 8D data and modelling performed by Amec Foster Wheeler (Baxter et al. 2014b), emphasising the additional information made available for Task 8F. In particular, this chapter details:

- the 3D geometry, material specification, design of the bentonite installation, and fracture statistics,
- the modelling assumptions, such as boundary and initial conditions, and
- the stages of model calibration performed for Task 8D.

Task 8F is a continuation of previous modelling studies (Task 8C (Baxter et al. 2014a) and Task 8D (Baxter et al. 2014b)) of the BRIE experiment designed to refine predictions of the resaturation of bentonite emplaced in overcored boreholes located in a fractured high strength granitic rock. This section provides an overview of the data and modelling assumptions used in this study, comparing the approach with the predictive modelling performed pre-completion of the BRIE (Task 8D). Specifically, additional information available for Task 8F are highlighted. The following aspects of data and modelling are considered:

- geometrical set-up of the BRIE experiment,
- the bentonite installation process,
- the fracture statistics of the bedrock local to the experiment,
- fracture interpretations within the boreholes overcored for emplacement of bentonite,
- modelling assumptions for the boundary and initial conditions,
- the specification of the rock matrix, fractures and bentonite,
- a summary of Task 8D predictive modelling.

2.1 Geometrical data

The BRIE is situated in the TASO tunnel, and the geometrical set-up for Task 8F is identical to the Task 8D specification, and defined in the Swedish RT90 coordinate system. The chosen model domain occupies an approximate cubic volume of $(40)^3$ m^3, and is constrained by the set of coordinates given in Table 2-1 of Baxter et al. (2014b) reproduced from the task description (Vidstrand et al. 2017). The model domain proposed for Task 8F, relative to the Äspö HRL, is shown in Figure 2-1.

Geometrical specification was provided as part of task description (Vidstrand et al. 2017) via a series of CAD files, the key features from which are illustrated in Figure 2-2 and Figure 2-3. The proposed model domain is illustrated in Figure 2-4. Boundary conditions are based on the larger scale Darcy-Tools model (Vidstrand et al. 2017), as provided by the Task Force. Additional details about the model domain can be found in Section 2.1 of Baxter et al. (2014b).

Boreholes KO0014G01 through KO0020G01 have been drilled in the TASO tunnel floor as part of the BRIE, the positions of which are shown in Figure 2-5. During the second stage of the experiment, the central probe boreholes of the TASO tunnel, KO0017G01 and KO0018G01 were overcored to a diameter of 30 cm for the emplacement of the bentonite stacks. Additional details can be found in Section 2.1 of Baxter et al. (2014b).

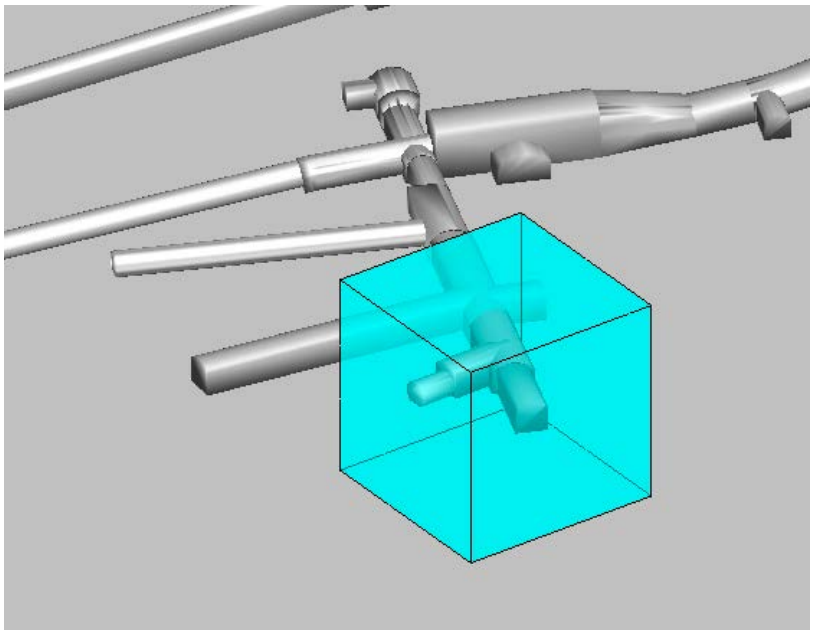

Figure 2-1. *Illustration of the suggested model domain at the Äspö HRL. The model domain includes the TASO tunnel and is approximately (40)^3 m^3. This figure is reproduced from the task description (Vidstrand et al. 2017).*

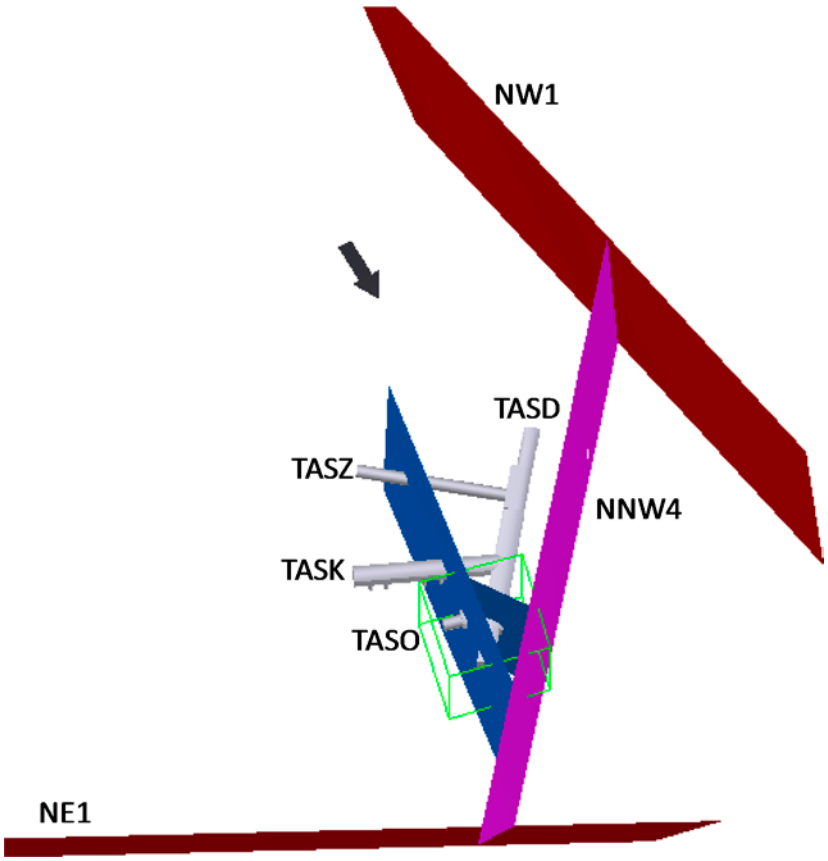

Figure 2-2. *Illustration of the CAD data and the suggested model domain. The large structures are named according to the Äspö HRL structural model. The tunnel names are given to provide a reference orientation. The thick black arrow indicates the principal rock stress orientation. This figure is reproduced from the task description (Vidstrand et al. 2017).*

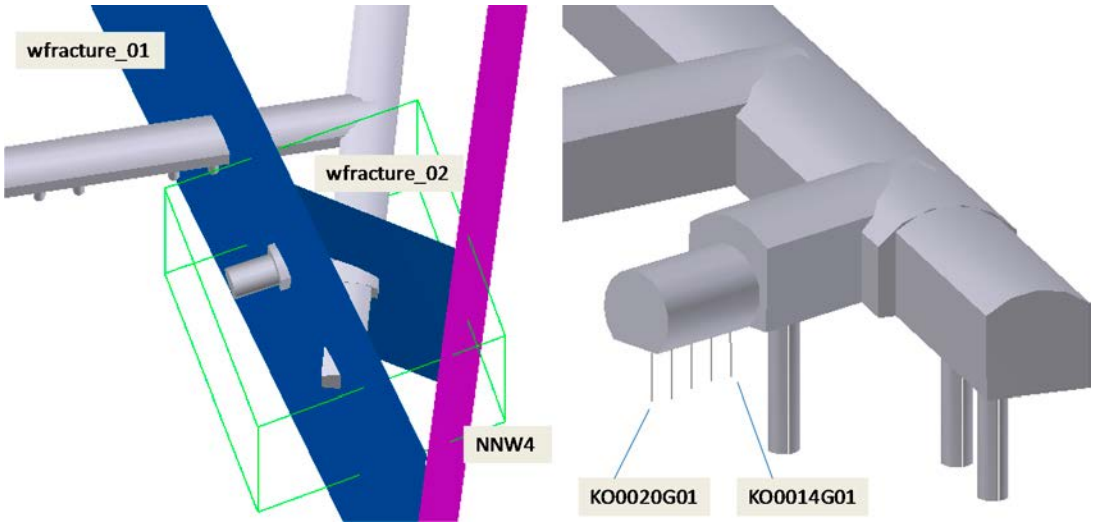

Figure 2-3. *Illustration of CAD data provided local to the TASO tunnel, the three deterministic hydrogeological structures contained in the suggested model domain are named. The figure on the right includes an indication of the location of the five probe boreholes. Figure 2-5 shows the names of the probe boreholes. This figure is reproduced from the task description (Vidstrand et al. 2017).*

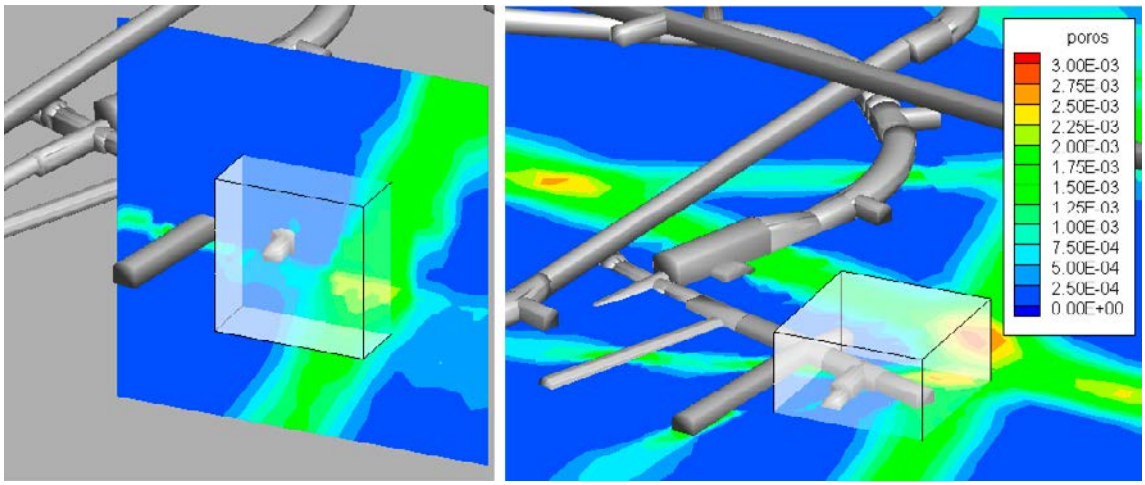

Figure 2-4. *Illustration of the proposed model domain, set within a larger scale DarcyTools model domain. One of the bounding sides broadly corresponds to a large structure, NNW4 as identified in Figure 2-2. This figure is reproduced from the task description (Vidstrand et al. 2017).*

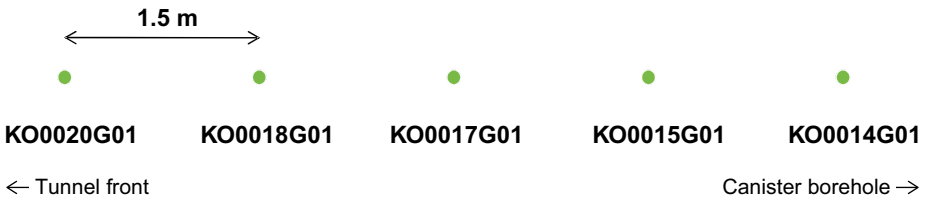

Figure 2-5. *Illustration of probe borehole spacing and naming. This figure is reproduced from the task description (Vidstrand et al. 2017).*

2.2 Design of bentonite installation

This section summarises the bentonite installation process for the 30 cm overcored boreholes KO0017G01 and KO0018G01 of the BRIE experiment. For a detailed description, the reader is referred to Section 2.2 of Baxter et al. (2014b). Cylindrical blocks of compacted bentonite, drilled and machined to obtain well-defined properties and dimensions are threaded onto a central tube. Confining plates, welded to the top and bottom of the central tube hold the bentonite blocks in place. Details are presented in Table 2-2 of Baxter et al. (2014b) and in Figure 2-6.

The cylindrical blocks have a dry density slightly higher than the target dry density, as the blocks will swell to fill the outer slot between the bentonite and the overcored borehole wall.

The bottom of overcored boreholes KO0017G01 and KO0018G01 were both filled with macadam (labelled as "sand" in Figure 2-6) to a depth of 2 – 4 mm.

The bentonite parcels are both instrumented in two sections:

- KO0017G01 at 2.3 m and 2.6 m.
- KO0018G01 at 2.3 m and 2.7 m.

In each of these four sections, two instrumented blocks of bentonite are installed, with the top block containing relative humidity sensors, and the bottom block pressure sensors. A photograph of these instrumented bentonite blocks is shown in Figure 2-7. For each of the four sections, sensors within the bentonite blocks were located identically. On emplacement in the overcored boreholes, sections were oriented in the plane, so that pore pressure sensors were located as close as possible to the fracture of interest in each overcored borehole (see Figure 2-7 and Figure 2-8). For further details of the sensor installation and recorded data the reader is referred to Fransson et al. (2017).

Installations of the bentonite occurred at the following times:

- KO0018G01: 13-09-2012 17:12.
- KO0017G01: 14-09-2012 10:19.

Three photographs from the bentonite installation phase of KO007G01 are shown in Figure 2-9.

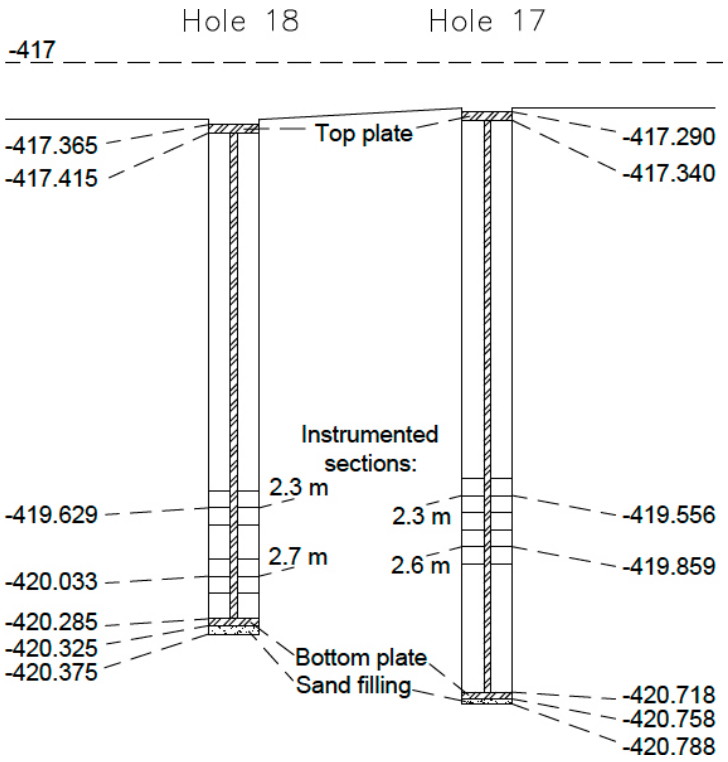

Figure 2-6. *Outline of the of the BRIE bentonite pack installations, reproduced from Vidstrand et al. (2017).*

Figure 2-7. *Instrumentation of blocks; left: block with pressures sensors; right: block with relative humidity sensors. This figure is reproduced from Vidstrand et al. (2017).*

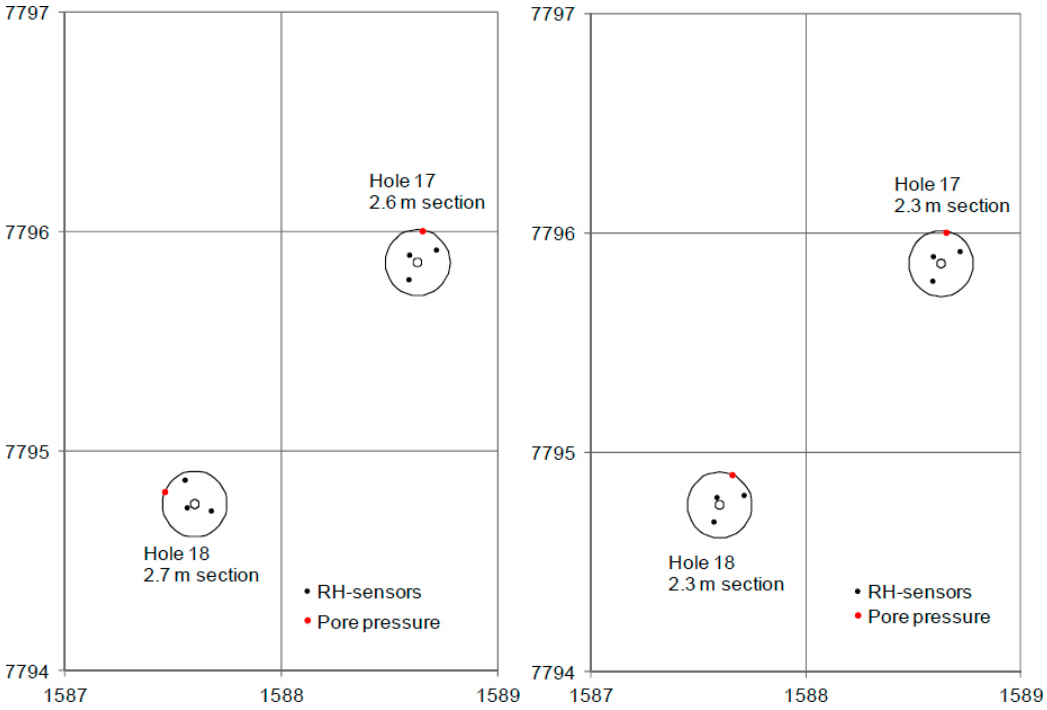

Figure 2-8. *Illustration of sensor positions in overcored boreholes KO0017G01 and K0018G01, and reproduced from Vidstrand et al. (2017).*

Figure 2-9. *Installation of the bentonite blocks in KO0017G01. Photographs are reproduced from Vidstrand et al. (2017).*

2.2.1 Filling the outer slot

The process for filling the outer slot of both overcored boreholes is detailed in Subsection 2.2.1 of (Baxter et al. 2014b). For KO0018G01, 3.1 litres of formation water was poured into the outer slot (between the borehole wall and the top-plate of the bentonite installation); and for KO0017G01, 6.85 litres of formation water was poured through the sand filling[2] and 1.05 litres was poured into the outer slot, the technical details responsible for this difference can be found in Subsection 6.2.5 of Fransson et al. (2017).

2.3 Fracture statistics local to the BRIE

The BRIE at the Äspö Hard Rock Laboratory (HRL) is located in a granitic bedrock, with groundwater flow occurring through a series of interconnected fractures. Site specific fracture statistics for the bedrock local to the BRIE are given as intensity, size and orientation data, forming the basis of the stochastic fracture network. Fracture statistics provided as part of the task description (Vidstrand et al. 2017) for Task 8F are unchanged from those used in the Task 8D (Baxter et al. 2014) and Task 8C (Baxter et al. 2014a) modelling, as summarised in Section 2.3 of Vidstrand et al. (2017).

With fractures dominating groundwater pathways through the bedrock, characterisation of this highly heterogeneous flow system is necessary to describe the spatial variability of the rock. Consequently, it is expected that a Continuous Porous Medium (CPM) modelling approach, using bulk hydraulic properties, will be insufficient to statistically represent accurately the local flow and transport pathways within the fractured bedrock. As a CPM approach is a form of representing the rock by its average properties, this will significantly restrict the extent to which inflows and resaturation profiles can be predicted for the two central probe boreholes of the BRIE. Alternatively, modelling the bedrock as a Discrete Fracture Network (DFN) explicitly represents the flow conducting fractures, providing representation of the flow and transport at a local level. By simulating the groundwater flow through this series of interconnected fractures, predictions for both heterogeneous inflows to probe boreholes, and resaturation profiles of emplaced bentonite, are possible.

Only a handful of large structures local to the Äspö HRL can be specified deterministically; details are presented in Section 2.4 of Baxter et al. (2014b). The remainder of the fracture network is unknown, although statistics for fracture intensity, orientation, size and transmissivity can be inferred from fracture traces on tunnel walls, fracture intersections with boreholes, and hydraulic testing of the boreholes. These statistical distributions can then be used to sample parameters for fractures within a hydrogeological DFN model of the bedrock local to the TASO tunnel and the BRIE. Characterisation of the site local to the BRIE identified three distinct orientations of fractures (fracture sets). Of these sets, one corresponds to sub-horizontal fractures, dipping gently to the south-east, with the other two sets sub-vertical, corresponding to steeply dipping fractures aligned approximately N-S and E-W. For all sets, the orientations of fractures are modelled using a Fisher distribution. Section 2.3 of Baxter et al. (2014b) discusses the development of statistical parameters used to generate the fracture models, as summarised in Table 2-1.

Table 2-1. Fracture statistics to be used for DFN modelling local to the TASO tunnel, supplied as part of the task description (Vidstrand et al. 2017).

	Orientation			Size			
Set	Trend	Plunge	Fisher Concentration	Location parameter, r_0	Exponent, k_r	Spatial Distribution	Intensity $P_{32}(r_0,\infty)$
1	280	20	10	0.25	2.6	Poissonian	1.1
2	20	10	15	0.25	2.6	Poissonian	2
3	120	50	10	0.25	2.6	Poissonian	0.75

[2] The bentonite bottom block rested on a bottom plate; this bottom plate, in turn, was placed on top of a sand filling (actually macam 2–4 mm) in the bottom of the borehole, as shown in Figure 2-6.

2.4 Deterministic fracture information

2.4.1 Large-scale fracture zones

Three, large-scale deterministic structures were identified as part of Task 8D, named wfracture_01, wfracture_02, and NNW4. Geometrical specifications of these geological structures were provided as CAD data, as shown in Figure 2-3.

2.4.2 Fracture interpretations in overcored boreholes KO0017G01 and KO0018G01

For Task 8D, a single fracture was associated with groundwater ingress to each of the overcored boreholes KO0017G001 and KO0018G01, as detailed in Table 2-2. For Task 8F, an updated description of the parameterisation of these two fractures was provided, as evaluated from the photos of the borehole surfaces and the mapped fractures, and given in Table 2-3. For KO0018G01, this updated description is consistent with the Task 8D description of the fracture, varying by only 5 cm depth and a few degrees in orientation. For KO0017G01, the depth and dip of the interpreted fracture was again consistent with measurements in Task 8D, although the strike was seen to vary by over 30 degrees. Extension of the fractures beyond the overcored borehole is largely unknown, other than:

- the fracture in KO0017G01 is not identified in the tunnel floor mappings. In addition, hydraulic responses indicate the fracture has good connectivity to the structure, wfracture_01, although this is not likely to be a direct connection,
- no good connection is found between the fracture in KO0018G01 and any other observations. Also, this fracture did not supply any water to the overcored borehole for the first couple of months.

Table 2-2. Fracture locations in boreholes KO0017G01 and KO0018G01 used in Task 8D. The "adjusted z-elevation" corresponds to the depth at which the estimated fracture plane would cross the central axis of the overcored borehole. Values are reproduced from the task description (Vidstrand et al. 2017).

Borehole	Diameter [mm]	Adjusted z – elevation [m]	Strike* [deg] RT90	Dip [deg] RT90
KO0017G01	300	−420.07	140	63
KO0018G01	300	−419.58	215	54

* Strike and dip refer to the orientation of a geologic feature. The *strike line* of a planar feature/fracture is a line representing the intersection of that feature with a horizontal plane. *Strike* (or strike angle) is the azimuth of this line, measured clockwise from North. The *dip* gives the steepest angle of descent of the planar feature/fracture, relative to the horizontal plane.

Table 2-3. Fracture locations in boreholes KO0017G01 and KO0018G01 for Task 8F. Values are reproduced from Fransson et al. (2017).

Borehole	Diameter [mm]	Adjusted z – elevation [m]	Strike [deg] RT90	Dip [deg] RT90
KO0017G01	300	−420.12	106	66
KO0018G01	300	−419.63	202	53

2.4.3 Additional fracture interpretations post-excavation of the bentonite

Additional fractures intersecting KO0018G01, and possibly contributing to the total inflow, have been identified post excavation of the bentonite parcels by studying photos of the surface of the bentonite and the markings of the fractures.

Only the images capturing the wet trace on the bentonite emplaced in KO0018G01 have been interpreted because the images for KO0017G01 covered only part of the bentonite section due to the poor condition of some of the bentonite parcels upon removal from the site.

Comparison of image grey-level and surface sample water content data show a relationship that supports the interpretation of the image features relating to wetting and hydration state. Features interpreted from the image and associated with the wetting process include:

- sinusoidal traces of dipping fractures,
- axial/vertical features suggestive of dripping down the outer bentonite surface,
- horizontal bands of darker bentonite.

Other parts of the bentonite block surfaces appear almost unaltered since emplacement.

For the most part features in the image are believed to relate to wetting, but the timing is uncertain. Wetting events during the experiment include:

- initial filling of the gap around the bentonite by pouring water down the gap (see Subsection 6.2.5 of Fransson et al. 2017),
- accidental wetting of the blocks by flooding of the central tube at day 37 (KO0017G01) and day 50 (KO0018G01) due to ponding at the tunnel surface (see Section 6.3 of Fransson et al. 2017),
- water transfer from the rock during the saturation period,
- water transfer from the rock during line-drilling and subsequent removal of the bentonite column.

Comparison with image logging of 76 mm borehole

Figure 2-10 shows a comparison of the features interpreted from the bentonite retrieved from the overcored hole and those picked from image logs of the 76 mm borehole KO0018G01. A summary of the features mapped is listed in Table 2-4, with the following observed:

- In general, borehole image interpretations and wetting profiles on the surface of the bentonite are in good agreement.
- Features in the top 0.5 m of the bentonite are difficult to isolate, perhaps due to greater wetting towards the top of the hole.
- Below 0.5 m, clear dipping fracture traces visible on the bentonite mostly correspond to image interpretations from the 76 mm borehole.
- There are small depth and orientation offsets between the dataset, typical of the limitations in mappings of the bentonite stack and borehole images.
- Fractures identified as open from borehole images are typically visible on the bentonite surface, suggesting pathways for groundwater ingress. In contrast, those mapped as sealed in borehole do not show a clear trace on the bentonite surface. The exception is a sealed fracture interpreted at 1.619 m depth which is visible on the bentonite, possibly caused by the overcored borehole intersecting an open area of the fracture not observed in the borehole.

Table 2-4. Fracture picks from KO0018G01 from BOREMAP/BIPS/Core, supplied by the Task Force.

Height above base plate [m]	Depth [m]	Interpretation	Aperture [mm]	Seen in BIPS	Visible in Bentonite
0.671	2.334	Open	0.5	1	Yes
0.834	2.171	Sealed	0.0	1	No clear feature
0.995	2.010	Open	0.5	1	Yes
1.030	1.975	Sealed	0.0	1	No clear feature
1.386	1.619	Sealed	0.0	1	Yes
1.899	1.106	Open	0.5	0	Yes
2.266	0.739	Open	0.5	1	Yes
2.665	0.340	Open	1.0	1	Uncertain
2.666	0.339	Open	1.0	1	Uncertain
2.681	0.324	Open	1.0	1	Uncertain
2.992	0.013	Open	0.5	0	Above bentonite
2.995	0.010	Open	0.5		Above bentonite

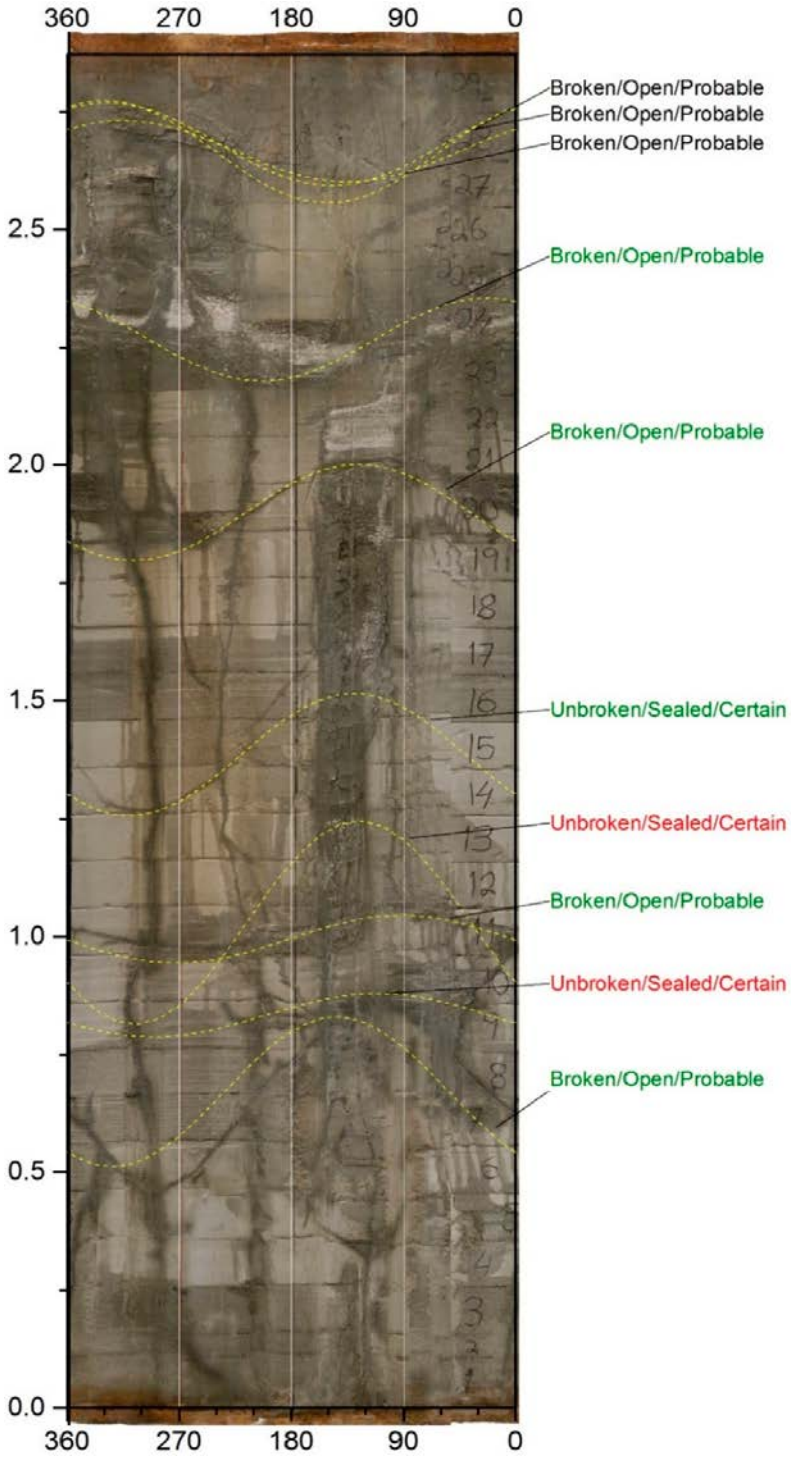

Figure 2-10. *Bentonite surface image of KO0018G01 with extrapolated fracture traces from core and image logging of 76 mm borehole, supplied by the Task Force. Traces labelled in green indicate a feature interpreted on the bentonite surface that coincides with a fracture interpreted from the pilot borehole image log (yellow). The statements certain/probable provide a qualitative indication of the confidence of the borehole mapping. Left axis shows height above base plate. Right axis shows the azimuth of the bentonite stack, where 0° corresponds to the orientation of the pore pressure sensor installed in block 7.*

2.5 Boundary conditions

Boundary conditions for the models are supplied by the Task Force as extracted from the current, official, hydrogeological model of the Äspö HRL, based on the SDM site Laxemar Deformation Zone Model. Due to its large scale, this regional scale model includes known discrepancies in tunnel geometries within the suggested BRIE model domain, as documented in the task description (Vidstrand et al. 2017). However, these discrepancies are minor, and as such the data are deemed suitable for defining the groundwater pressures on the outer boundary of the BRIE modelling domain.

Boundary conditions are unchanged from the Task 8D analysis (Baxter et al. 2014b), as summarised below.

A DarcyTools v3.3 sub-grid is used to extract values for pressure, salinity (from groundwater constituents), and velocities from the full regional Äspö HRL model (Äspömodel05) on a sub-grid covering approximately $(100\ \text{m})^3$, and incorporating the suggested model domain. The residual pressure P^R for this model is shown in Figure 2-11 for a horizontal slice through the TASO and TASD tunnels. The total pressure P^T is related to the residual pressure by the hydrostatic pressure

$$P^T = P^R - \rho_0\, g\, (z - z_0) \tag{2-1}$$

where the datum, $z_0 = 0$ m above sea level, is the reference altitude taken at the present day shoreline and ρ_0 is the fresh water density. The extracted data from model Äspömodel05 are supplied in a spreadsheet, as part of the task description (Vidstrand et al. 2017).

The salinity mass fraction, S, is specified as part of these boundary conditions, including spatial variation across the model domain. The salinity-density dependence is defined as:

$$\rho = 1\,000(1 + 0.0078 \cdot S) \tag{2-2}$$

All tunnels within the model domain are assumed open, with atmospheric boundary conditions applied.

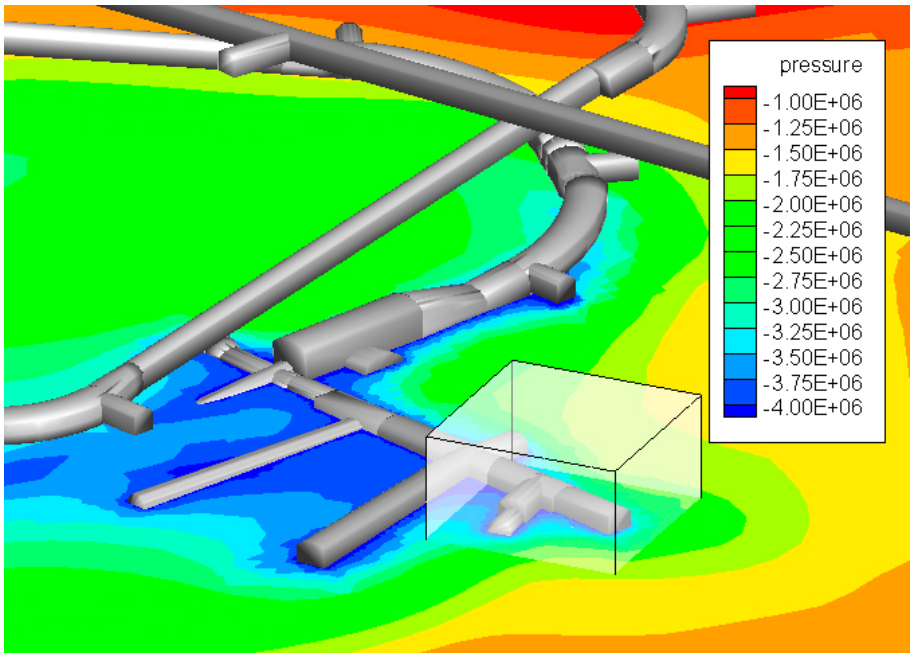

Figure 2-11. *Illustration of the pressure field [Pa], with reference elevation at the present day shoreline (0 m altitude). This figure is reproduced from the task description (Vidstrand et al. 2017).*

2.6 Initial conditions

Initial conditions for the inflow prediction to the five probe boreholes are identical to the previous Task 8D and are summarized below, further details are contained in Section 2.8 of Baxter et al. (2014b).

In Task 8F1, initial conditions for the inflow predictions are based on the "natural" conditions where:

- for pressure build-up measurement, all probing boreholes are packed off, assuming the packer to seal the upper 1 m of the borehole,
- for inflow measurement, each of the five probe boreholes is opened to the tunnel in turn.

An equivalent prescription of the initial conditions is made when considering inflows to the overcored boreholes KO0017G01 and KO0018G01.

For the second stage of the task, Task 8F2, initial conditions for modelling the resaturation of emplaced bentonite in the central overcored boreholes of the BRIE are taken from the modelling results of the first stage. In addition, the initial water content of the bentonite is 11.6 %, corresponding to an initial degree of saturation of 0.413 for the target void ratio of 0.78 (i.e. after swelling into the outer slot).

2.7 Material specifications

The material specifications used are taken from the task description (Vidstrand et al. 2017), being the same as those used in Task 8D, with values based on measurement, expert judgment and/or theory. Specifications for rock matrix, fractures and bentonite are detailed in Subsections 2.8.1 through 2.8.5 of Baxter et al. (2014b) respectively.

2.7.1 Processes considered

Both Task 8F1 and 8F2 models consider hydraulic processes, with brief details provided below:

- **Task 8F1:** models are developed using ConnectFlow, calculating single-phase fresh-water flow explicitly through the fractured bedrock. Simulations are conditioned against measurements for pressure build-up and the ingress of groundwater to the probe boreholes.
- **Task 8F2:** models are developed using ConnectFlow, performing groundwater flow calculations using an upscaled representation of the 8F1 bedrock and Richards' approximation. Calculations predict the resaturation profiles and times for bentonite emplaced in overcored 30 cm boreholes KO0017G01 and KO0018G01.

2.7.2 Parameters

The parameters necessary for modelling both Task 8F1 and 8F2 are detailed below.

Deterministic features

As part of Task 8C, three significant geological features were identified, named wfracture_01, wfracture_02 and NNW4. These are local to the BRIE experiment, intersecting the $(40\ m)^3$ proposed model domain from the task description (Vidstrand et al. 2017). The Task 8C prescription of these three deterministic fractures is shown in Figure 2-2 and Figure 2-3.

Subsequent to Task 8C, additional information regarding the geological structural model was established refining the geometry of structure wfracture_01 local to the TASO tunnel. This refinement requires the adjustment of large scale wfracture_01 to connect with these latest observations local to the TASO tunnel. The updated description of wfracture_01 is shown in Figure 2-12, where

- inflow data to the TASO tunnel suggests that the fracture wfracture_01 includes both the original 'global-scale' description of the fracture as well as the new 'local-scale' description as a splay (see Subsection 2.9.3 of Baxter et al. (2014b), Figure 2-12 a and Figure 2-12 b):
  - hydraulic properties for wfracture_01 were updated for Task 8D, obtained from hydraulic tests in a single borehole (KO0011A01), and yielding a transmissivity of 4 10^{-9} m^2/s. This is in comparison to the Task 8C parameterisation, which elicited a transmissivity of 2 10^{-8} m^2/s,
  - both the localised and large scale feature wfracture_01 are parameterised using the Task 8C description,
- the new local description of wfracture_01 intersects probe borehole KO0014G01. This is not observed in the borehole logs, and as such the new wfracture_01 description is truncated at −417.5 m (see Figure 2-12 c),
- hydraulic tests indicate possible isolation of borehole KO0014G01. Therefore, the new local description of wfracture_01 is extended vertically from −417.5 m to −420 m (see Figure 2-12 d).

For Task 8F1, the DFN representation of the fractured bedrock includes these three deterministic features, represented as flowing fractures, as shown in Figure 2-13. For Task 8F2, they form part of the upscaling process, generating equivalent rock permeabilities. The parameterisations of these three features are provided in Table 2-11 of Baxter et al. (2014b).

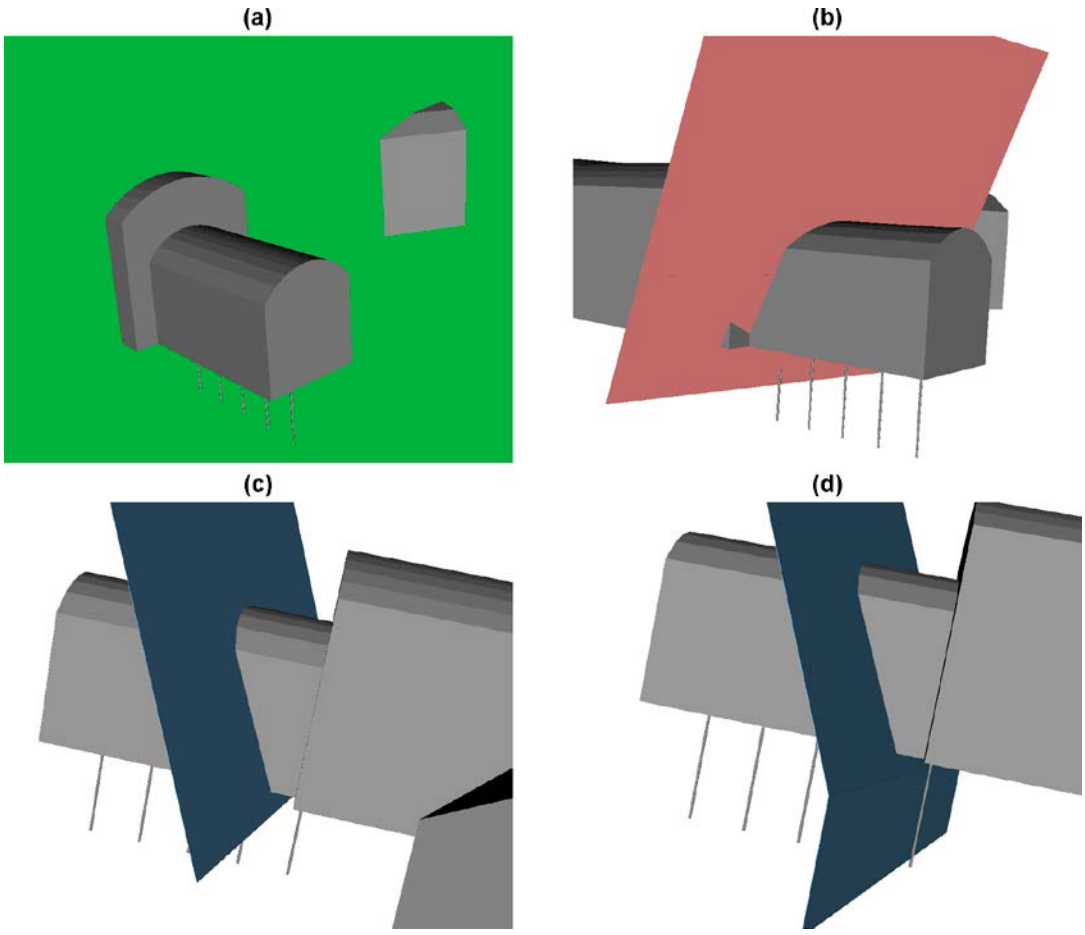

Figure 2-12. *(a) the original prescription of structure wfracture_01, taken from the task description for 8C; (b) the updated local description of wfracture_01, supplied as part of Task 8D; (c) truncation at −417.5 m of the updated local description of wfracture_01, avoiding intersection with probe hole KO0014G01; and (d) an extension of the updated local description of wfracture_01 to hydraulically isolate probe hole KO0014G01.*

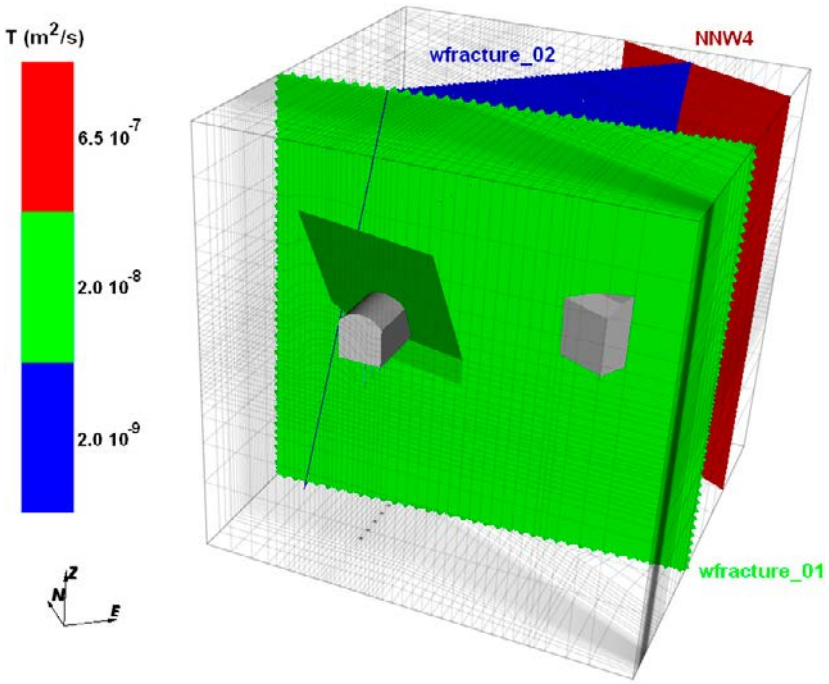

Figure 2-13. *Three large scale deterministic features, coloured by transmissivity, local to the TASO tunnel and within the model region defined. The local wfracture_01 prescription is also shown.*

Stochastic fracture statistics

Background fracture statistics for the bedrock local to the BRIE at the Äspö HRL were presented in Section 2.3. These include statistical distributions for:

- fracture orientation,
- fracture intensity,
- fracture distribution, and
- fracture size relationships.

Using this parameterisation for the fractured bedrock, multiple realisations of the DFN model are generated using the ConnectFlow software package.

From the task description (Vidstrand et al. 2017), it has been noted that no fractures were observed to intersect the entire tunnel periphery (except for the three deterministic geological features). Therefore, in order to avoid the DFN contradicting the physical understanding of the fractured bedrock local to the BRIE, the maximum side length of stochastic fractures is truncated at 10 m. In addition, for calculations to remain computationally tractable, a minimum fracture side length of 0.5 m is specified. Small fractures, shorter than this lower length limit, are unlikely to form hydraulically connected pathways through the bedrock, and as such there removal is not expected to significantly affect results. Instead, flows primarily occur through larger, more transmissive features.

Using the power-law size distribution for fractures, it is possible to rescale the fracture intensity according to truncation bounds on the fracture sizes using the following equation (Vidstrand et al. 2017):

$$P_{32}(r_{min}, r_{max}) = \frac{\left[r_{min}^{2-k_r} - r_{max}^{2-k_r}\right]}{r_0^{2-k_r}} * P_{32}(r_0, \infty) \qquad (2\text{-}3)$$

Applying Equation (2-3), with

- r_{min} = 0.28 m, the equivalent radius to a side length of 0.5 m,
- r_{max} = 5.64 m corresponding to a side length of 10 m,
- k_r is the power law exponent,
- r_0 is the location parameter, and

$P_{32}(r_0,\infty)$and the reduced fracture intensity (P_{32}) are detailed in Table 2-5 by set. These intensities formed the basecase DFN model for Task 8D before calibration of the fracture network was performed.

Table 2-5. Fracture intensities by fracture set (see Section 2.3), used as the Basecase for Task 8D fracture generation.

Set	Intensity $P_{32}(r_0,\infty)$	Intensity $P_{32}(0.28,5.64)$
1	1.1	0.85
2	2	1.55
3	0.75	0.58

Hydraulic attributes of the stochastically generated fractures also require specification. This is achieved through assigning transmissivities to individual fractures in the DFN model. For a given fracture, its transmissivity (T) can be determined from its size, with measured data shown in Figure 2-14. The central (dashed) line in this figure corresponds to the following power-law relation:

$$T = 7 \times 10^{-11} L^{1.7} \qquad (2\text{-}4)$$

where L is the fracture length. This empirical relationship is consistent with estimates derived from a variety of fracture scales at the Äspö site. The bounding lines in Figure 2-14 correspond to transmissivities defined using Equation (2-4), considering one order of magnitude each side.

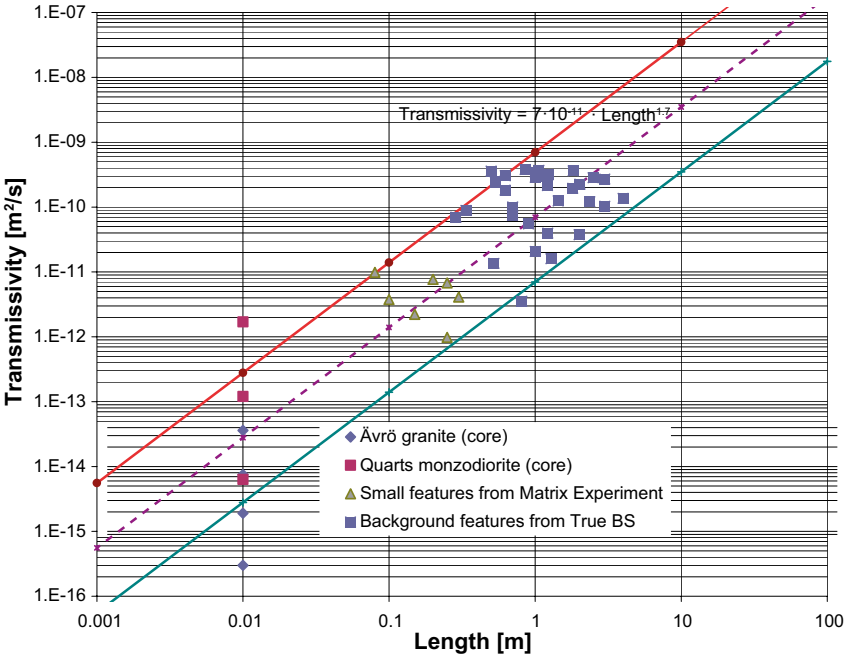

Figure 2-14. *Transmissivity correlation applied to stochastic fractures within the BRIE experiment.*

Porosities

The process of upscaling the fracture network yields a porosity for each element within the model domain. In addition, the porosity of the rock matrix is taken as $5\ 10^{-3}$, consistent with measurements reported in Subsection 2.8.1 of Baxter et al. (2014b).

Proposed relationships

Constitutive relationships detailing the capillary pressure and relative permeability functions are required for:

- the bentonite,
- the rock matrix, and
- the fractured rock.

The Task 8D description Baxter et al. (2014b) provides a reference case, used to form the basis of the constitutive relationships. These relationships are detailed in Subsections 2.7.3.1 through 2.7.3.3 for each of the model components listed above. To simplify the numerics, gas trapping mechanisms are not considered in any of the simulations performed.

Constitutive relations for bentonite

The capillary pressure (P_{cap}) of the bentonite uses a model suggested by van Genuchten (van Genuchten 1980),

$$P_{cap} = -P_o\left(\widetilde{S}^{-1/\lambda} - 1\right)^{1-\lambda} \tag{2-5}$$

where

$$\widetilde{S} = \frac{S_a - S_{ar}}{1 - S_{ar}} \tag{2-6}$$

and S_a is the saturation of the aqueous phase; S_{ar} is the residual saturation of the aqueous phase; and parameters λ and P_0 are empirical constants.

Within the bentonite, the intrinsic permeability is 6.4×10^{-21} m^2, and the Fatt and Klikoff (Fatt and Klikoff 1959) cubic-law representation of the relative permeabilities for the liquid phase is considered,

$$k_r = \tilde{S}^3 \tag{2-7}$$

Required parameters for the capillary pressure and relative permeability functions of the bentonite are detailed in Table 2-6.

Table 2-6. Parameterisation of the capillary pressure and relative permeability functions for the bentonite.

Parameter	Capillary Pressure	Relative Permeability
Functional description	Equation (2-5)	Equation (2-7)
Parameter λ [–]*	0.3	–
Parameter P_0 [MPa]*	9.23	–
Residual saturation S_{ar} [–]	0	0.01

*Value obtained from the task description.

Constitutive relations for the rock matrix

The capillary pressure of the rock matrix is modelled identically to the bentonite as in Equation (2-5).

Within the rock matrix, the intrinsic permeability is 1.0×10^{-21} m^2, and the relative permeabilities for the liquid phases use a van Genuchten function (van Genuchten 1980):

$$k_r = \sqrt{\widetilde{S}}\left(1-\left[1-\widetilde{S}^{1/\lambda}\right]^{\lambda}\right)^2 \tag{2-8}$$

Required parameters for the capillary pressure and relative permeability functions of the rock matrix are detailed in Table 2-7.

Table 2-7. Parameterisation of the capillary pressure and relative permeability functions for the rock matrix.

Parameter	Capillary Pressure	Relative Permeability
Functional description	Equation (2-5)	Equation (2-8)
Parameter λ [–]*	0.24	0.24
Parameter P_0 [MPa]*	0.6	–
Residual saturation S_{ar} [–]	0	0.01

*Value obtained from the task description (Vidstrand et al. 2017), and updated for Task 8D based on the relative humidities for core samples presented in Table 2-9 of Baxter et al. (2014b). These measurements are taken at relatively low saturations, and not necessarily applicable to the saturation state of the granite local to emplaced bentonite. As such, despite parameterisation of capillary pressure and relative permeability functions now based on data specific to the rock matrix local to the BRIE, caution is required when applying the van Genuchten model at high water saturations beyond the measurements considered.

Constitutive relations for fractured rock

The capillary pressure of the fractured rock is modelled identically to the bentonite, as in Equation (2-5). The parameters λ and P_0 for fractured rock are inferred from Figure 2-15, provided as part of the task description (Vidstrand et al. 2017). Here

$$\begin{aligned} \lambda &= 1 - 1/n \\ P_o &= \rho g/\delta \end{aligned} \tag{2-9}$$

and the mean hydraulic aperture for the fractures is approximately 3.8×10^{-6} m, calculated from the transmissivity correlation (2-4) and cubic law (3-3). For fractured bedrock, relative permeabilities for the aqueous and gas phases are modelled using the same functional form (van Genuchten) as the rock matrix in Equation (2-8).

Required parameters for the capillary pressure and relative permeability functions of the fractured rock are detailed in Vidstrand et al. (2017). The intrinsic permeabilities are calculated from upscaling the DFN model (see Section 3.1).

Table 2-8. Parameterisation of the capillary pressure and relative permeability function for the fractured rock.

Parameter	Capillary Pressure	Relative Permeability
Functional description	Equation (2-5)	Equation (2-8)
λ [–]*	0.56	0.56
P_0 [MPa]	4.905 10^{-3}	–
S_{ar} [–]	0	0.01

*Value are inferred from Figure 2-15, reproduced from the task description (Vidstrand et al. 2017) and using the relationships provided in Equation (2-9), along with mean hydraulic aperture of 3.8 μm.

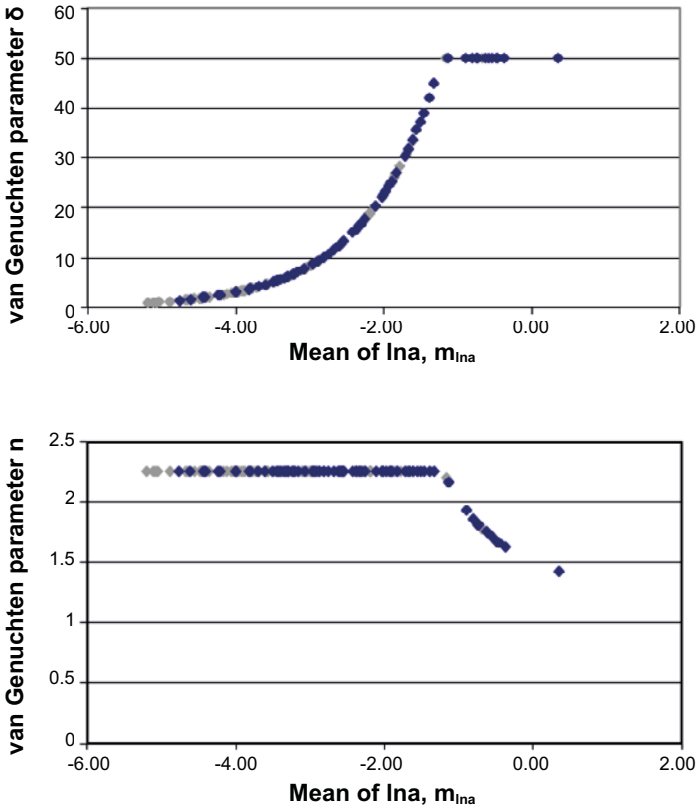

Figure 2-15. *Retention curves for van Genuchten capillary pressure (2-5) and relative permeability (2-8) functions for the fractured rock. The van Genuchten parameters δ and n are plotted for a range of mean hydraulic apertures of the fracture network (horizontal axis). Equation (2-9) relates the plotted parameters δ and n to the constitutive relations presented in Subsection 2.7.3. Graphs are reproduced from the task description (Vidstrand et al. 2017).*

2.8 Results of task 8D calibration

During Task 8D, a number of model variants were considered, with the intent to refine and calibrate the DFN to better represent the fractured rock local to the BRIE. A full description of the calibration process can be found in Chapter 5 of Baxter et al. (2014b). A brief summary of each of the model cases considered is given below:

- **Basecase**: based on the original statistics for stochastically generated fractures, interpreted from the task description (Vidstrand et al. 2017), and identical to Task 8C. Deformation zones are updated from Task 8C to include a new local scale hydrozone wfracture_01 (truncated from KO0014G01). This model case is considered in Subsection 5.1.1 of Baxter et al. (2014b).
- **Variant 1:** the deterministic component of the fracture network is specified identically to the Basecase. Stochastic models for fracture orientations, sizes, locations and transmissivity are also unchanged. The intensity of sampled fractures (P_{32}) is reduced to 75 % of the Basecase. This model case is considered in Subsection 5.1.1 of Baxter et al. (2014b).
- **Variant 2:** the deterministic component of the fracture network is specified identically to the Basecase. Stochastic models for fracture orientations, sizes, locations and transmissivity are also unchanged. The intensity of sampled fractures (P_{32}) is reduced to 50 % of the Basecase. This model case is considered in Subsection 5.1.1 of Baxter et al. (2014b).
- **Variant 3:** this model case is unchanged from Variant 2, with the exception of the transmissivity-size model used for stochastically generated fractures. For this variant, the correlated transmissivity model (defined as a one-to-one correlation between fracture size and transmissivity) is replaced with a semi-correlated representation. The semi-correlated model samples a normal deviate with mean defined by the correlated model and standard deviation of ½ an order of magnitude. This model case is considered in Subsection 5.1.2 of Baxter et al. (2014b).

- **Variant 4:** the stochastic fracture network for this variant is identical to Variant 3 above. The deterministic component of the DFN is modified from Variant 3 to consider an alternative geometric description of the locally defined feature wfracture_01, updated to fully isolate borehole KO0014G01. This model case is considered in Subsection 5.1.3 of Baxter et al. (2014b).
- **Variant 5:** this model case is unchanged from Variant 3, with the exception of conditioning the intersections with overcored boreholes KO0017G01 and KO0018G01. Stochastic fractures intersecting each of these holes are removed from the model and replaced with deterministic fractures. Note, wfracture_01 is defined according to Variant 3, and truncated at −417.5 m, the alternative description in Variant 4 is not used. This model case is considered in Subsection 5.1.4 of Baxter et al. (2014b).

The calibration phase of Task 8D1 identified the updated description of the stochastic fracture network defined through model Variant 5 as the most consistent representation of the bedrock local to the BRIE when compared to:

- fracture intersections with probe boreholes and traces mapped on the TASO tunnel,
- the distribution of transmissivities observed experimentally,
- pressure build-up in the five 76 mm probe boreholes KO0014G01, KO0015G01, KO0017G01, KO0018G01 and KO0020G01,
- inflows to each of the five 76 mm probe boreholes KO0014G01, KO0015G01, KO0017G01, KO0018G01 and KO0020G01, and
- the interpreted water-producing features observed in boreholes KO0017G01 and KO0018G01.

The Task 8F study uses this updated DFN prescription (i.e. Variant 5) for calculation of both inflows to the open overcored boreholes and the resaturation of emplaced bentonite, no consideration is given to the Basecase, and Variant 1–4 model definitions in Task 8F.

3 Approach to Task 8F

The adopted methodology for modelling Task 8F is detailed in this chapter, including:

- a discussion on the selected software used in this investigation, as well as a verification example, and
- details of the geometrical description of the model, including simplifications required for gridding the BRIE and subsequent mesh refinement used.

3.1 Software

The BRIE experiment investigates the hydraulic interaction between a fractured host rock and a bentonite buffer on the scale of 30 cm overcored boreholes. Modelling tools selected for this study need to be capable of representing the physics required for prediction of bentonite resaturation profiles and times. ConnectFlow is the software package identified that will be incorporated into the study of Task 8F, to:

- provide a discrete fracture network (DFN) representation of the groundwater flow through fractures in the host rock, and
- represent the resaturation process of the bentonite.

This is in contrast to previous modelling Amec Foster Wheeler have performed for the BRIE experiment which used TOUGH2 to simulate movement of the gas phase explicitly. The appropriateness of representing resaturation calculations using a single-phase rather than two-phase approach is considered in the Sensitivity Analysis Task (Carta et al. 2016). In the model formulations prescribed therein modelling results indicate Richards' (single-phase) approximation provides an adequate simplification to the physics represented; although if metrics such as the quantity of gas (air) being displaced are required, explicit representation of the gas phase through a two-phase flow formulation is necessary. For example, if gas entrapment was likely to occur, a greater difference between predictions based on Richards' and two-phase flow formulations may be likely. However, it was demonstrated in Task 8D (Baxter et al. 2014b) that the likelihood of gas entrapment to occur at the BRIE was low because:

- the permeability of the gas phase in bentonite may be several orders of magnitude higher than for the liquid phase, and
- the resaturation of the bentonite is characteristically heterogeneous, and as such entrapped gas is unlikely to form within the bentonite. Instead a preferential pathway for the gas phase to migrate to the open tunnel would exist.

The mesh refinement required of the BRIE models for prediction of resaturation at distinct sensor locations is such that the computational gain from simulating resaturation using a single-phase approach ensures that computational models will remain tractable.

3.1.1 ConnectFlow

ConnectFlow is a suite of software, developed by Amec Foster Wheeler for modelling groundwater flow and transport on a variety of scales. It consists of:

- a continuum porous media (CPM) module, referred to as NAMMU, and
- a discrete fracture network (DFN) module, referred to as NAPSAC.

The mathematical formulations adopted by ConnectFlow are presented in detail in (AMEC 2012a, b, c, d). For a high-level description the reader is referred to Joyce et al. (2010); summarised below for the aspects of the software directly applicable to modelling Task 8F.

The BRIE at the Äspö Hard Rock Laboratory (HRL) is located in a granitic bedrock, and the flow of groundwater is primarily through a series of interconnected, flow-conducting fractures. By applying

a DFN concept, it is possible to statistically represent the groundwater path from one fracture to another at the intersections between them. As discussed in Section 2.3, there are five properties used to characterise a fracture network. These are:

- the spatial distribution of fractures (e.g. Poisson, clustered),
- the fracture intensity, usually expressed as the fracture surface area per unit volume (P32), see Equation (2-3),
- the orientation of fractures (e.g. Fisher distributions for separate fracture sets),
- the size of fractures (e.g. log-normal, power-law distributions), and
- the hydraulic properties of fractures (e.g. transmissivity, transport aperture, etc).

The DFN concept is a powerful approach; able to model stochastically and deterministically (where sufficient characterisation has taken place) the individual flow conduits in fractured rock, and the available field data. The DFN models developed consist of fractures (represented as 2D planes) from two data sources:

- Deterministic features: usually large scale features (e.g. structures such as wfracture_01, wfracture_02 and NNW4), or local scale fractures interpreted from borehole intersections (e.g. the hydraulically active fractures observed to intersect overcored boreholes KO0017G01 and KO0018G01).
- Stochastic fractures: these are used to generate fractures within the bedrock which are not readily observed through intersection with an engineered feature (tunnel / boreholes / etc). A stochastic approach is adopted, sampling fracture characteristics from probability distribution functions (PDFs) for each fracture set. These statistical distributions are usually determined through field experiments such as borehole logging and hydraulic tests. Fracture networks resulting from sampled distributions are not expected to provide the exact geometric and hydraulic properties of features within the bedrock, rather providing one possible network of fractures that can statically describe the range of measurement. Uncertainties of a stochastic fracture network can be addressed by considering multiple realisations of the DFN model.

With regards to the emplaced bentonite, the representation of individual fractures intersecting a borehole is critical to understanding the potentially highly heterogeneous wetting of the buffer material. ConnectFlow utilises a continuum concept for modelling the resaturation processes, and as such it is necessary to convert the heterogeneous nature of the fracture network into equivalent continuous porous medium (ECPM) block properties. This process of calculating ECPM properties is called upscaling, implemented in ConnectFlow by calculating both a directional permeability tensor and fracture kinematic porosity for elements based on the fracture network. The upscaling methodology implements a flux-based approach, requiring several flow simulations to be performed through the DFN model on the scale of individual elements. A schematic of these flow calculations for a typical element within a 2D DFN model is shown in Figure 3-1.

A consequence of this upscaling methodology is possible over-prediction of block permeabilities. This over-prediction is caused by flows on the scale of individual elements occurring through fractures cutting the corner of the element, and is unrepresentative of flows through the in situ fracture network (see Figure 3-2). These over-predictions are especially significant in sparse heterogeneous fracture networks, where the flux through the network of interconnected fractures is affected by 'bottlenecks' through low transmissivity fractures, which is quite different to the flux through single fractures. To address this over-prediction, the upscaling methodology can be refined to simulate flow through a slightly larger domain than the element required for the ECPM properties, but then calculating the flux responses through the correct element size. The additional area around the element is referred to as a "*guard zone*", and is further discussed in Rhén et al. (2009).

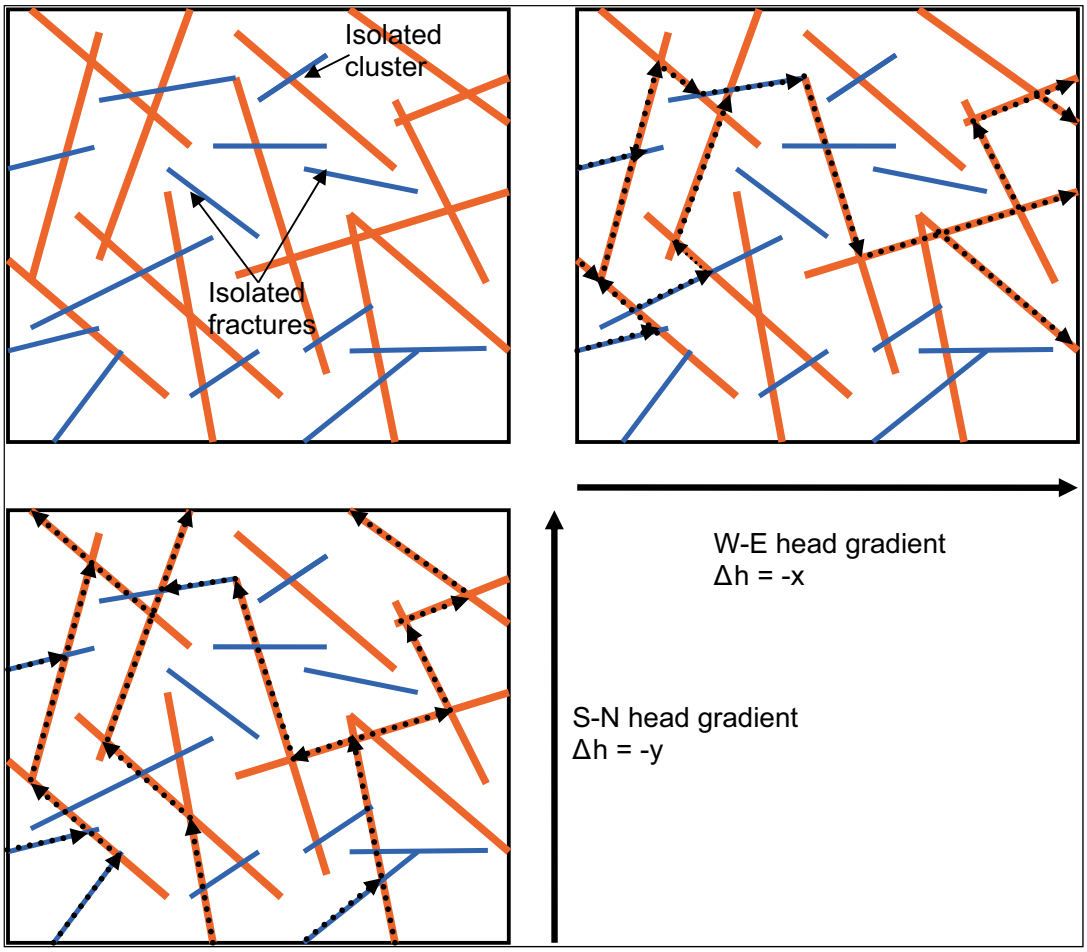

Figure 3-1. *A 2D illustration of flow through a network of fractures, reproduced from Joyce et al. (2010). Top left: illustrates a random network of fractures, with variable length and transmissivity (red fractures are highly transmissive, with blue fractures indicating low transmissivity). Top right: illustration of flow paths through the fracture network for a linear head-gradient decreasing along the x-axis. Bottom left: illustration of flow paths through the fracture network for a linear head-gradient decreasing along the y-axis.*

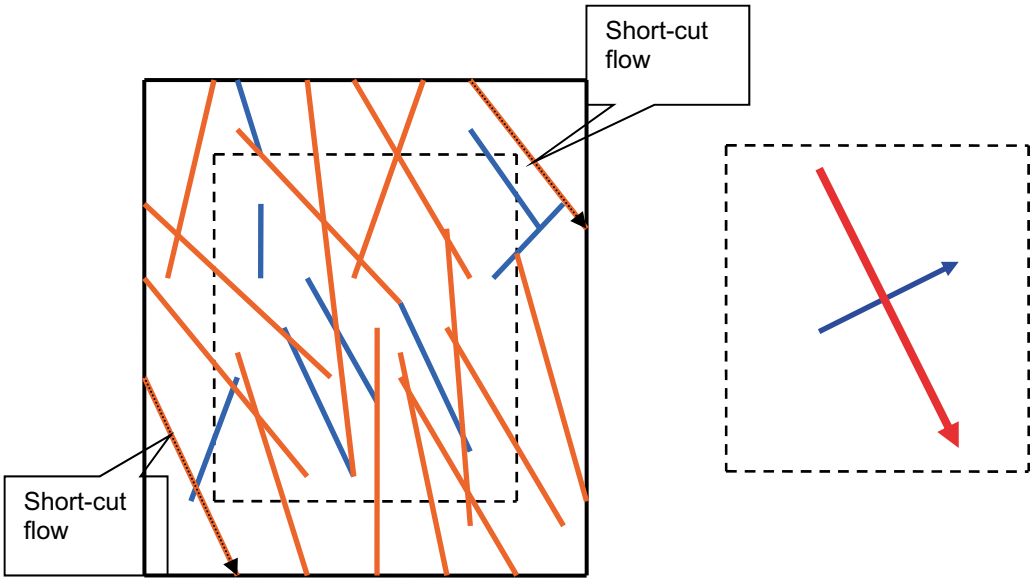

Figure 3-2. *2D illustration of how block-scale permeabilities can be overestimated. This figure is reproduced from Joyce et al. (2010).*

Calculating permeability tensors

Effective block permeabilities are calculated by simulating flux through the fracture network on the scale of individual elements. Within the DFN model, several groundwater flow-paths are possible due to the number and variety of connections observed across the network. Consequently, cross-flows occurring non-parallel to the head gradient can form. An anisotropic permeability tensor is used to account for these cross-flows, and for a 3D analysis, ConnectFlow uses six directional components to characterise a symmetric permeability tensor. For each head gradient direction, the DFN models are used to calculate the fluxes through each face of the block. The permeability tensor is then derived by a least-squares fit to these flux responses for the fixed head gradients (Jackson et al. 2000).

Calculating kinematic porosities (Hartley et al. 2012a)

The kinematic porosity, Φ, of individual elements is calculated by

$$\phi = \frac{\sum_f e_{tf} a_f}{V} \tag{3-1}$$

where V is the volume of the element, a_f is the area of each fracture in the block and e_{tf} is the transport aperture of the fracture. The transport aperture is related to the hydraulic aperture, e_{hf} by,

$$e_{tf} = 10 e_{hf} \tag{3-2}$$

as used in Hartley et al. (2012b), with similar relationships interpreted from tracer test programs, e.g. Hjerne et al. (2010). The hydraulic aperture for each fracture is calculated from the transmissivity, T_f, by the cubic-law:

$$e_{hf} = (12 \mu T_f / \rho g)^{1/3} \tag{3-3}$$

ConnectFlow verification

In the previous sub-tasks of Task 8, TOUGH2 was the tool selected used for the numerical simulation of the resaturation of the emplaced bentonite; based on a multiphase flow approach and capturing the air and water phases explicitly during hydration of the bentonite buffer. A parallel verification study carried out in AMEC (2012d) demonstrated good agreement between ConnectFlow and TOUGH2 when used to simulate the saturation process of bentonite buffers. Results from this study are presented in Figure 3-3, where saturation profiles are shown for six different locations

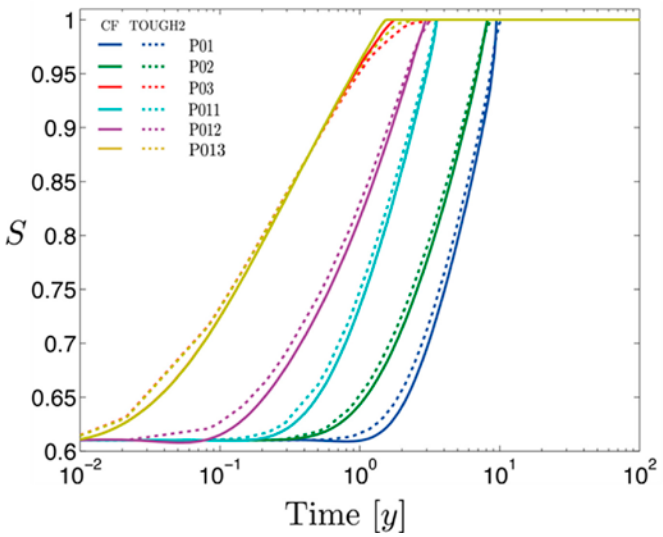

Figure 3-3. *Variation of saturation with time calculated by ConnectFlow and TOUGH2 simulations at six sensor locations (P01, P02, P03, P11, P12, P13) from one of the test cases analysed during the verification task (AMEC 2012d). This figure is reproduced from Figure 2-29 of AMEC (2012d).*

within a single buffer enclosing a container. Small deviations in the saturation rates observed are to be expected. Even though the same computational grid was used for both simulations, a different numerical solution scheme is adopted in TOUGH2 (i.e. Finite Difference) while the Finite Element method is implemented in ConnectFlow. In particular, the set of equations solved by ConnectFlow and TOUGH2 are different. TOUGH2 uses a multiphase calculation[3], whilst ConnectFlow solves Richards' equation (van Genuchten 1980, Richards 1931, Celia et al. 1990).

3.2 Model description

The mesh used for modelling Task 8F is based on the previous modelling (Task 8D), with the exception of the refinement local to the overcored boreholes, which has been greatly increased.

3.2.1 Geometrical description and mesh refinement

The primary investigation area for the BRIE is in the vicinity of the TASO tunnel of the Äspö HRL. The size of the implemented model domain differs between subtasks, as described below:

- Task 8F1. The model domain is defined as specified in the task description (Vidstrand et al. 2017), with bounding coordinates presented in Table 2-1 of Baxter et al. (2014b). The model domain forms a (40 m)3 block, as shown in Figure 3-4, and incorporates both TASO and TASD tunnels. Tunnel floors are located at an elevation of −417.0 m, with the five probe boreholes extending a further 3 m (to an elevation of −420.0 m).
- Task 8F2. In this subtask, the resaturation of bentonite emplaced in the central overcored boreholes is modelled. Here, the numerical requirements are significantly greater, with extensive refinement necessary local to the resaturation front. In order for computations to remain tractable, the volume of the model domain has been reduced from that used in Task 8F1 above and the mesh has been greatly refined in the region close to the bentonite/host rock interface, providing localised refinement to the two central overcored boreholes KO0017G01 and KO0018G01. The model domain used for Task 8F2 is shown in Figure 3-5, extending 15 m in the axis of the tunnel, 12 m lateral to the tunnel and 6.25 m vertically and discretized in to 8 node hexahedra finite elements using linear basis functions.

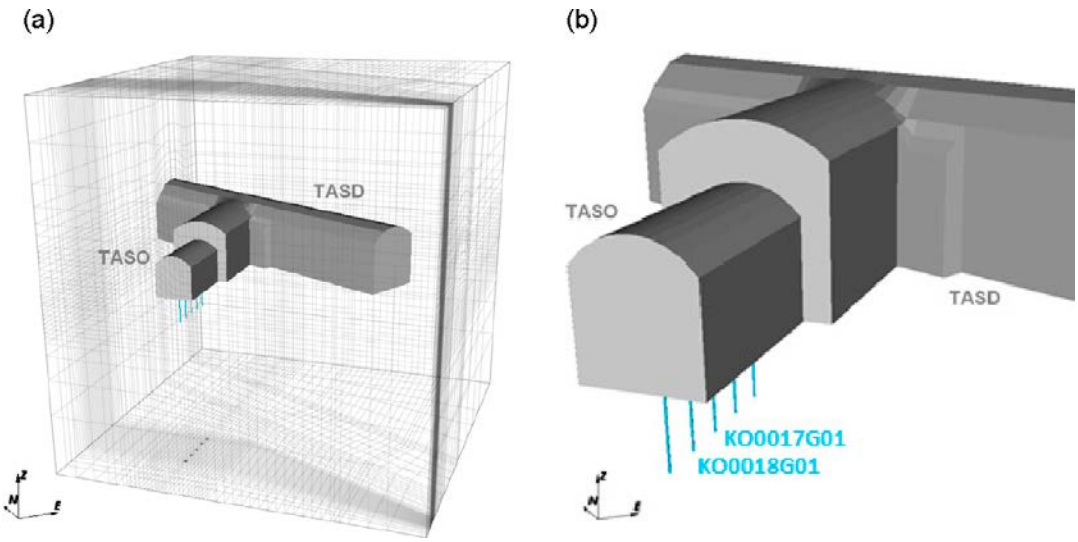

Figure 3-4. *(a) Location of BRIE experiment with the TASO and TASD tunnel at the Äspö Hard Rock Laboratory in Sweden. (b) The five boreholes for investigation are shown in blue.*

[3] For this verification test, the TOUGH2 simulation was constructed so as to approximate Richards' equation (i.e. high relative gas permeability and allowing the gas phase to exit the model through the container boundary).

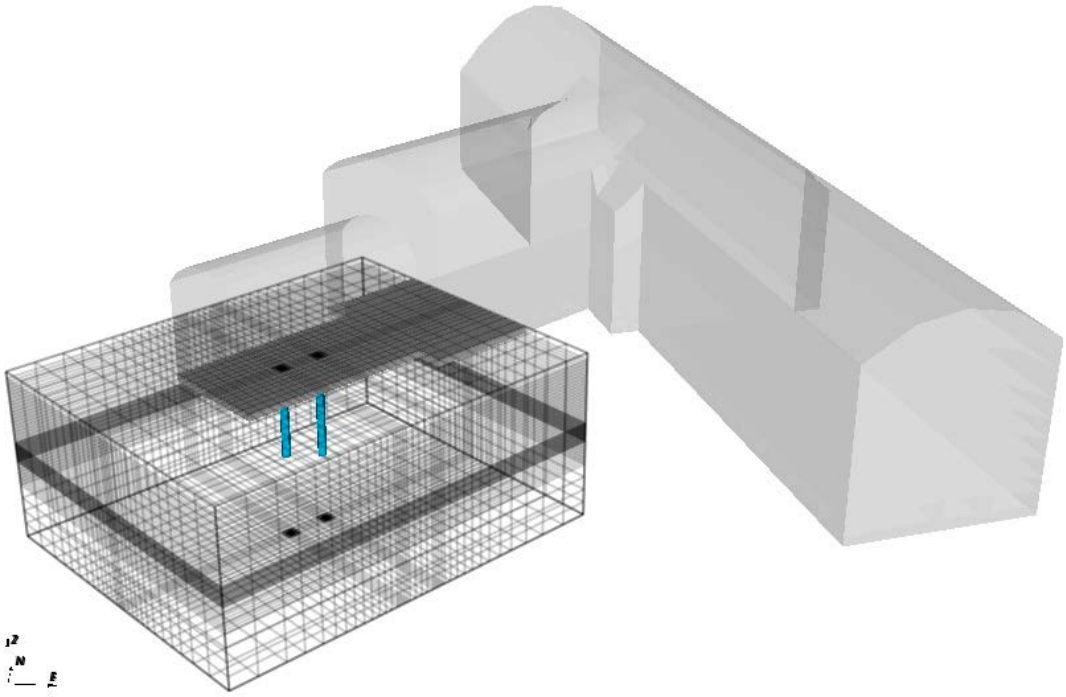

Figure 3-5. *A local region to the two overcored central boreholes, selected for mesh refinement necessary for hydration calculations.*

3.2.2 Numerical model

The models developed for numerical simulation of Task 8F1 and Task 8F2 are quite different, as summarised below.

- Task 8F1. For this subtask, the fractured bedrock is represented explicitly; created from a combination of the large scale deterministic features identified local to the BRIE and the stochastically generated background fractures sampled from parameters outlined in Chapter 2. Steady-state flow solutions are considered, consistent with stabilised measurements of pressure build-up and inflows. To consider uncertainties in the sampled background fracture network, one hundred realisations of the stochastic DFN component are considered.
- Task 8F2. For this subtask, ConnectFlow is used to model the transient resaturation of bentonite emplaced within the central overcored boreholes of the BRIE. The numerical formulation of ConnectFlow utilises a continuum approach, and the mesh must be refined sufficiently to capture the saturation front within the bentonite. The properties (permeability and porosity) of individual elements within the grid are calculated from upscaling the complete DFN models from Task 8F1 (see Subsection 3.1.1). The central overcored boreholes have a diameter of 0.3 m, with KO0018G01 3 m deep, and KO0017G01, 3.5 m deep. The bentonite emplaced within the ConnectFlow mesh is discretised 16 times azimuthally (i.e. 16 wedges) and 16 times radially, with elements 0.12m to 0.25m tall (the shortest elements are located close to the sensor's locations).

4 Post-excavation data sampling

In this chapter, a review of the additional data available after excavation of the BRIE is presented. In particular, the methodologies used for sampling the experimental data are detailed, including:

- water content measurements for both overcored boreholes KO0017G011 and KO0018G01, and
- confirmatory analysis of groundwater ingress (i.e. fracture locations) to the bentonite buffer.

4.1 Dismantling of the BRIE

After dismantling of the BRIE experiment, the removed bentonite stacks from the two overcored boreholes were sampled following a general scheme defined in Fransson et al. (2017). Samples 30 mm wide were taken in five radial directions, at six radial positions and at three levels in each block (see Figure 4-1 a_1 and a_2) resulting in 90 samples collected from each investigated bentonite block. In total, 13 blocks from KO0017G01 and 12 blocks from KO0018G01 were analysed following this scheme (see Figure 4-1 b); although two of the blocks, Block 1 in KO0017G01 and Block 2 in KO0018G01, were slightly shorter (height 50 mm) than the other blocks and have been sampled at two levels only (Fransson et al. 2017).

A second, more detailed, sampling scheme (see Figure 4-1 c) was subsequently defined to increase the radial resolution local to the main fracture of interest (Fransson et al. 2017). This refined scheme collected samples at 20 radial directions, four radial positions and at the mid-level in each analysed block (Fransson et al. 2017). Three blocks from KO0017G01 and two blocks from KO0018G01 were analysed in this way.

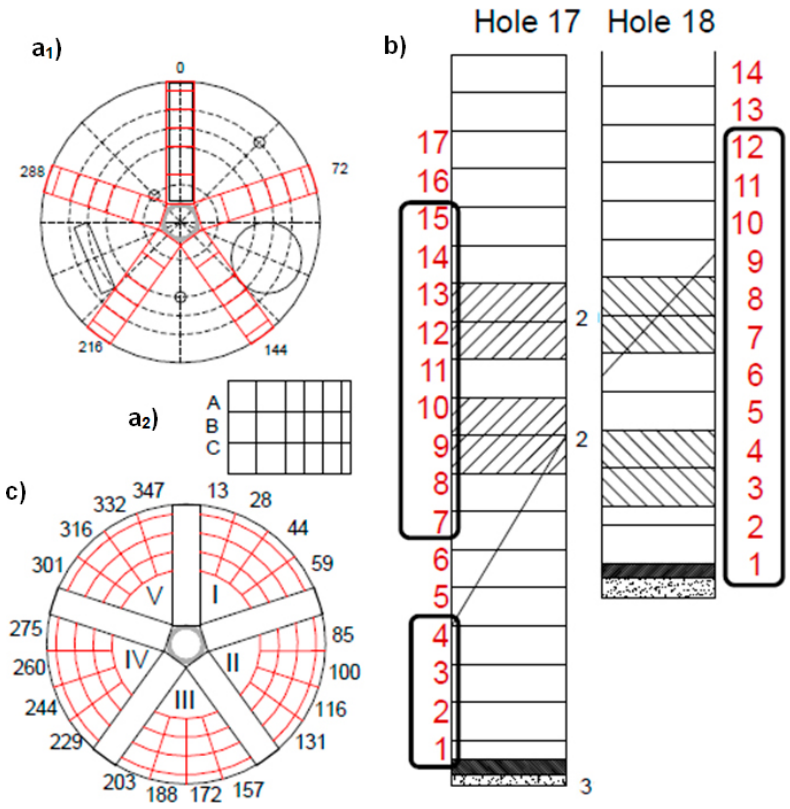

Figure 4-1. *Sampling scheme for KO0017G01 and KO0018G01. The shaded blocks indicate the instrumented blocks. Taken from Fransson et al. (2017), Figure 6-22 therein.*

4.2 Water content

The water content measurements for the bentonite buffer are visualised for both overcored boreholes KO0017G01 and KO0018G01 (see Figure 4-2 and Figure 4-3 respectively) using data points and the default Tecplot inverse distance interpolation method[4].

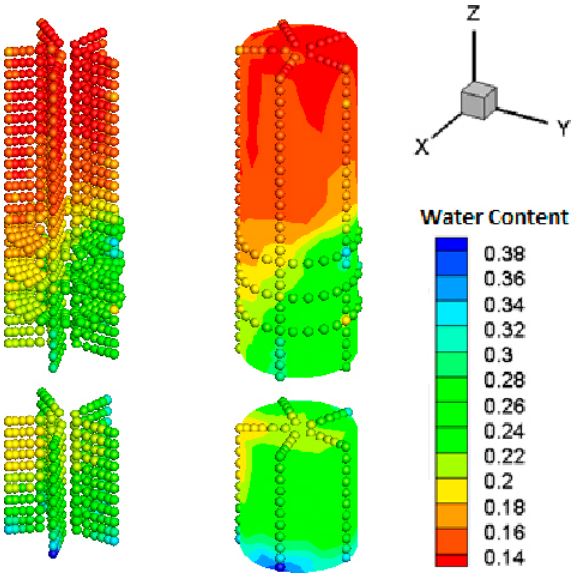

Figure 4-2. *Scatter plot of volumetric water content [dimensionless] and surface plot of interpolated water content in KO0017G01.*

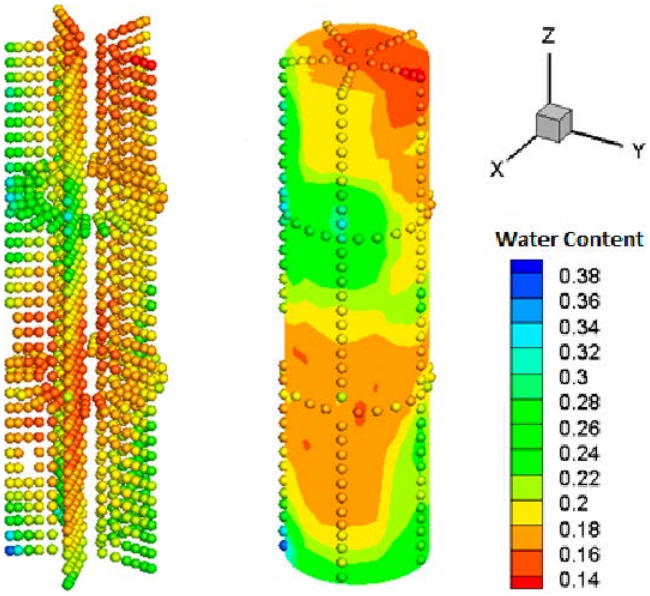

Figure 4-3. *Scatter plot of volumetric water content [dimensionless] and surface plot of interpolated water content in KO0018G01.*

[4] The inverse-distance interpolation averages the values at the data points from one set of zones (the source zones) to the data points in another zone (the destination zone). The value at each source zone data point is weighted by the inverse of the distance between the source data point and the destination data point (raised to a power) as: $\varphi_d = \frac{\sum \omega_s \varphi_s}{\sum \omega_s}$ (summed over the selected points in the source zone) where φd and φs are the values of the variables at the destination point and the source point, respectively, and ωs is the weighting function, defined as: ωs = D–E, where D is the distance between the source point and the destination point and E is the exponent, (3.5 in this case) [from 21-11.2 of Tecplot 360 2013 User's Manual Release 1].

In both the boreholes, the driest region is located at the top of the hole and the wetter region at the bottom. The water content does not uniformly decrease along the hole, but rather indicates localised regions of hydration that could indicate the presence of water-producing fractures. The water content measurements from KO0018G01 were typically smaller than those from KO0017G01.

4.2.1 Comparison of relative humidity sensors and water content measurements

In addition to the water content measurements taken after excavation of the BRIE; during the experiment bentonite parcels were instrumented at both a 'wet' section dominated by fracture flow and a 'dry' section potentially dominated by matrix flow. Each of these sections consists of two instrumented blocks – one upper block and one lower block.

The upper blocks contained three relative humidity-sensors, whereas the lower blocks contained two total pressure sensors and a pore pressure sensor. Data from these twelve relative humidity sensors are compared to the water content measurements taken at similar locations within the bentonite parcels by using the same relation detailed in Fransson et al. (2017) and given in Equation (4-1), comparing relative humidity of the bentonite and its water content (see Figure 4-4). This study has been completed to check the consistency and to estimate an uncertainty of the available data.

$$RH(w) = \begin{cases} 59 + 367(\mathrm{w} - 0.12), & \mathrm{w} < 0.21 \\ 92 + 114(\mathrm{w} - 0.21), & \mathrm{w} \geq 0.21 \end{cases} \tag{4-1}$$

Table 4-1 and Table 4-2 compare the relative humidity evaluated from the water content of the samples of the bentonite blocks closest to the sensor with the final time measurements taken from the relative humidity sensors. Both boreholes are considered, with the value of the relative humidity evaluated from the water content data typically very close (i.e. < 3 % difference) to the data collected by the sensors. The maximum difference observed is never more than 6.5 %.

Table 4-1. Distance of the closest bentonite samples to each of the six relative humidity sensors in KO0017G01. The water content evaluated from the sensor corresponds to the final measurements.

KO0017	WBR001	WBR002	WBR003	WBR004	WBR005	WBR006
Distance from sensor [m]	1.48E−02	3.04E−02	2.88E−02	1.61E−02	4.70E−02	5.76E−02
Water Content data [%]	2.08E−01	1.74E−01	2.22E−01	1.52E−01	1.51E−01	1.39E−01
RH data from sensor [%]	9.16E+01	7.89E+01	9.98E+01	6.82E+01	6.77E+01	6.67E+01
RH from WC [%] Eq (4-1)	9.12E+01	7.87E+01	9.34E+01	7.06E+01	7.03E+01	6.61E+01
Percentage difference	0.40 %	0.28 %	6.42 %	−3.56 %	−3.94 %	0.91 %

Table 4-2. Distance of the closest bentonite samples to each of the six relative humidity sensors in KO0018G01. The water content evaluated from the sensor corresponds to the final measurements.

KO0018	WBR007	WBR008	WBR009	WBR010	WBR011	WBR012
Distance from sensor [m]	1.89E−02	4.36E−02	5.77E−02	1.06E−02	2.60E−02	5.22E−02
Water Content data [%]	1.74E−01	1.73E−01	2.08E−01	1.79E−01	1.64E−01	2.04E−01
RH data from sensor [%]	8.10E+01	7.74E+01	9.33E+01	7.77E+01	7.32E+01	8.71E+01
RH from WC [%] Eq (4-1)	7.87E+01	7.85E+01	9.15E+01	8.05E+01	7.51E+01	8.99E+01
Percentage difference	2.86 %	−1.52 %	1.96 %	−3.70 %	−2.59 %	−3.19 %

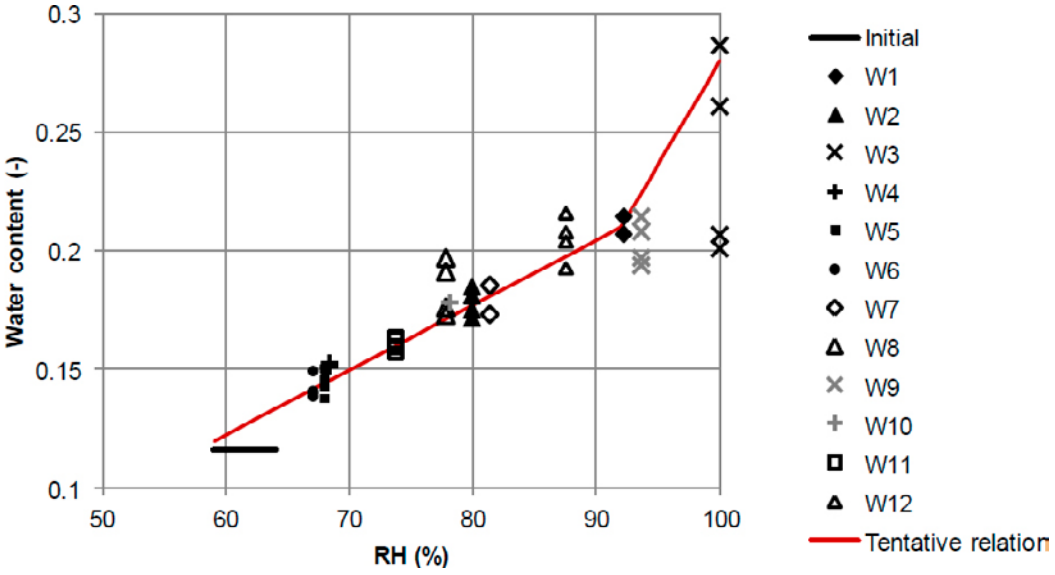

Figure 4-4. *Adoption of a tentative retention relation given in Equation (4-1) used for translation of water content data into RH data. This figure is reproduced from Fransson et al. (2017).*

4.3 Fracture position

For Task 8D, two fractures interpreted from optical measurements are identified as pathways for groundwater ingress. These correspond to a fracture in KO0017G01, intersecting at the central-lower part of the borehole and a fracture located at the bottom of KO0018G01. Table 4-3 summarises the parameterisation for these two fractures. In addition, characterisation of the BRIE included hydraulic tests (see Subsection 5.3.7 of Fransson et al. 2017), including measuring flows during packer[5] and nappy tests[6] for the 300 mm overcored boreholes. Table 4-4 summarises these data, and also includes measurements for the 76 mm boreholes. Confirmatory analysis is performed, comparing the locations of the inflow measurements to the overcored boreholes with the wettest regions of the bentonite identified from water content measurements performed post-excavation of the BRIE. If the inflows are not consistent with the resaturation profiles, it would indicate fracture interpretations in the overcored boreholes are insufficient to accurately predict the resaturation profiles.

In Figure 4-5, the location of the wettest iso-surfaces (i.e. an iso-surface displays a constant value of a variable as a surface on a plot) in KO0017G01 suggests the presence of a nearly vertical fracture intersecting the borehole (on one-side of the hole). This restricted geometric intersection has not been identified previously from fracture interpretations and could be a consequence of either a partial intersection with a fracture or varying hydraulic properties of the fracture along the two sides of the hole (e.g. partial sealing of the fracture). The wet region at the bottom of the hole is likely a consequence of the installation procedure; where 6.85 litres of formation water was poured through the sand filling and 1.05 litres was poured into the outer slot. For overcored borehole KO0018G01, water content in Figure 4-6 indicates the presence of a second fracture, located higher up the drillhole.

[5] Packer tests were performed by sealing off the top 1 m of each borehole with an inflatable packer (bladders) and measuring the subsequent pressure build up in each packed-off hole. Thereafter, one borehole at a time was opened and the outflow was measured, i.e. yielding the inflow for atmospheric pressure at the borehole top (Vidstrand et al. 2017).

[6] Nappy tests are performed by placing absorbent sheets (nappies) along the deposition hole or tunnel wall. Flow measurements are obtained by dividing the increase of weight of these nappies by the corresponding time.

Table 4-3. Fracture locations in boreholes KO0017G01 and KO0018G01. Table is reproduced from the task description (Vidstrand et al. 2017).

Borehole	Diameter [mm]	Adjusted z-elevation [m]	Strike [deg] RT90	Dip [deg] RT90
KO0017G01	300	−420.07	139.5	62.8
KO0018G01	300	−419.58	214.7	54.1

Table 4-4. Compilation of flow for boreholes KO0017G01 and KO0018G01. Reproduced from Table 5-14 of Fransson et al. (2017).

	KO0017G01	KO0018G01
Flow (76 mm) borehole	0.25 ml/min (0.5–2.97 m, 400 min), Phase 1	No flow observed
Flow PFL (Posiva Flow Logging method)	~ 0.5 ml/min (< 30 ml/h or 0.5 ml/min, uncertain)	No flow observed
Flow (300 mm) borehole (this is the value used as comparison)	0.12–0.25 ml/min (2.1–3.5 m, 400 min), Phase 3	0.01–0.03 ml/min (2.1–3.1 m, 400 min), Phase 3
Flow nappy test	~ 0.1 ml/min (2.25–3.25 m) Possibly water was entering in the lower part of the borehole (along pegmatite vein)	No flow observed

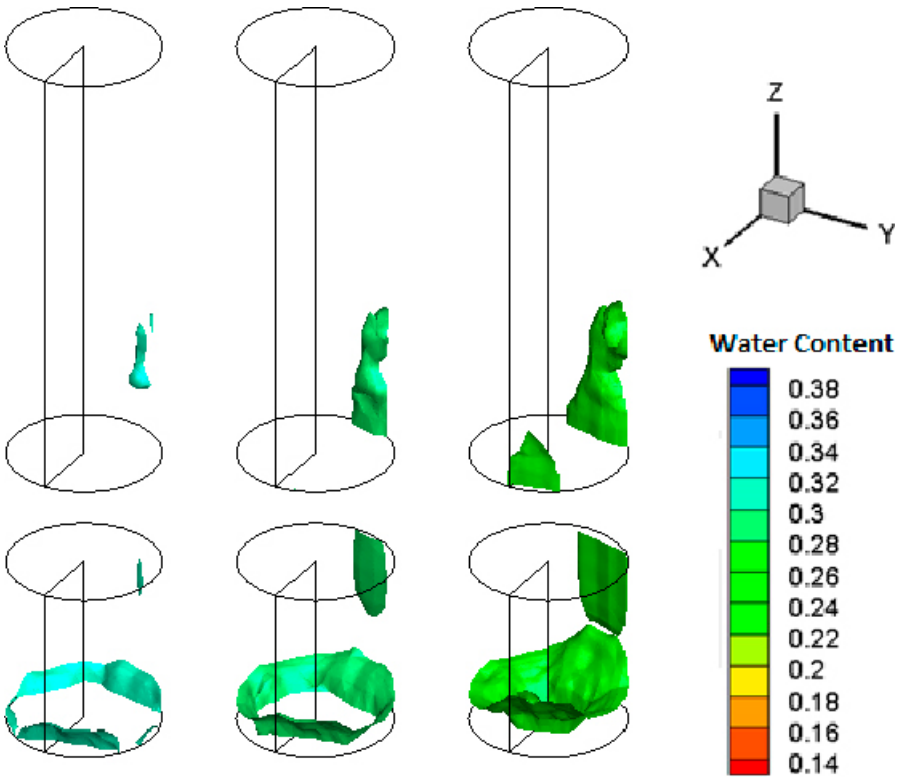

Figure 4-5. *Iso-surfaces of volumetric water content [dimensionless] in KO0017G01 for three different values of water content: 0.31 (left), 0.29 (mid) and 0.27 (right). Note the gap in the water content measurements is a consequence of damage to the bentonite stack whilst retrieving from the deposition hole.*

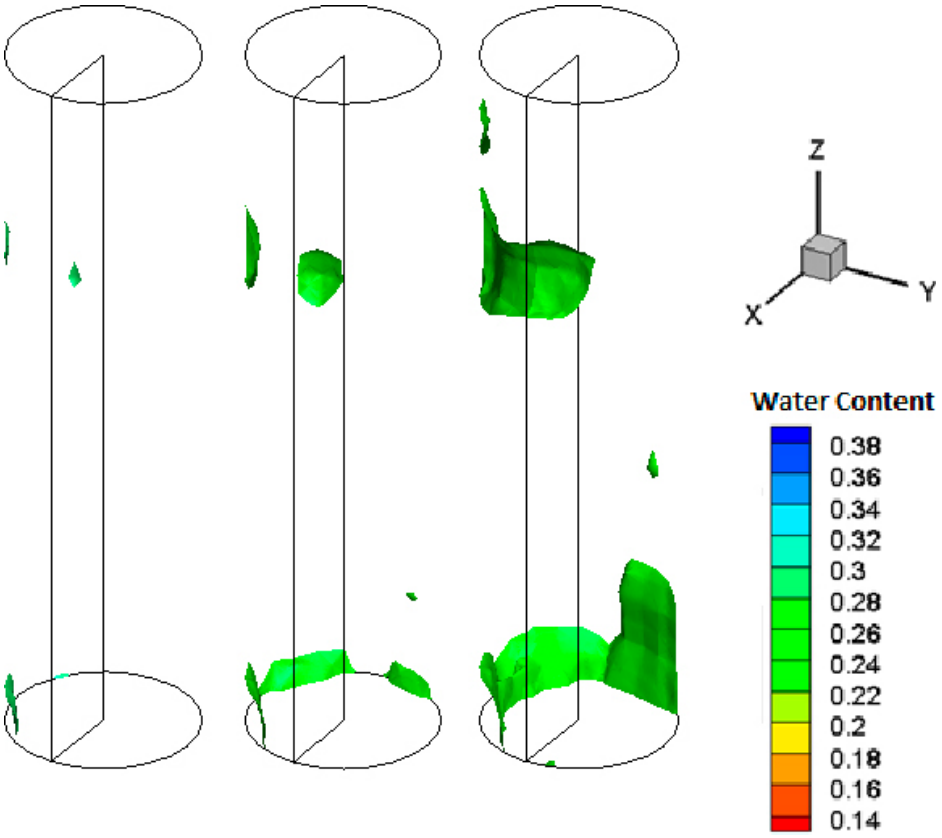

Figure 4-6. *Iso-surfaces of volumetric water content [dimensionless] in KO0018G01 for three different values of water content: 0.29 (left), 0.27 (mid), 0.25 (right).*

5 Basecase model (based on Task 8D description)

In this chapter, the Task 8D model description is used to evaluate relative humidity evolution at the twelve sensors in KO0017G01 and KO0018G01. This model will form a basecase for future conditioning of material properties and fracture locations (Chapters 6 and 7) to refine the resaturation process. Inflows under open hole conditions are evaluated for 100 realisations of the stochastic DFN to ensure the models adhere, in a statistical sense, to observations. Subsequent resaturation simulations are performed for the optimal realisations based on inflow.

Upon completion of the BRIE, relative humidity measurements taken at the twelve sensor locations within the bentonite installations were provided to the modelling groups participating in the EBS Task Force. In this chapter, the models developed for Task 8D for predictive modelling of the resaturation of emplaced bentonite are compared with this new experimental data. The Task 8D models form an optimal description of the BRIE based on the information available pre-completion of the experiment. As such, they form a basecase model for this study, allowing further conditioning based on the latest experimental data available post-excavation of the bentonite. Simulations are identical to those developed for Task 8D with the exception of:

- the deterministic fractures identified in KO0017G01 and KO0018G01 are updated to the latest understanding,
- the computational grid has been substantially refined local to the sensors, and
- resaturation profiles are calculated using ConnectFlow rather than TOUGH2.

5.1 Inflows

Inflows to the two overcored boreholes have been evaluated for 100 realisations of the stochastic fracture network (see Figure 5-1 and Figure 5-2), generated using the results of the Task 8D calibration (5^{th} variant) of the background network's specifications. In these models, the stochastic fractures intersecting the reamed boreholes are removed from the fracture network, and replaced with the deterministic specification of fractures obtained from geological mappings. As such, the variability seen in Figure 5-1 and Figure 5-2 is solely due to the way these near-field deterministic fractures are embedded/connected to the heterogeneity of the wider fracture network. Only realisations which yield a good agreement between the evaluated inflow and observations (i.e. the modelled inflows lie in between the uncertainty limits of the experimental data) (see Table 4-4) are selected for simulation of the subsequent resaturation of emplaced bentonite.

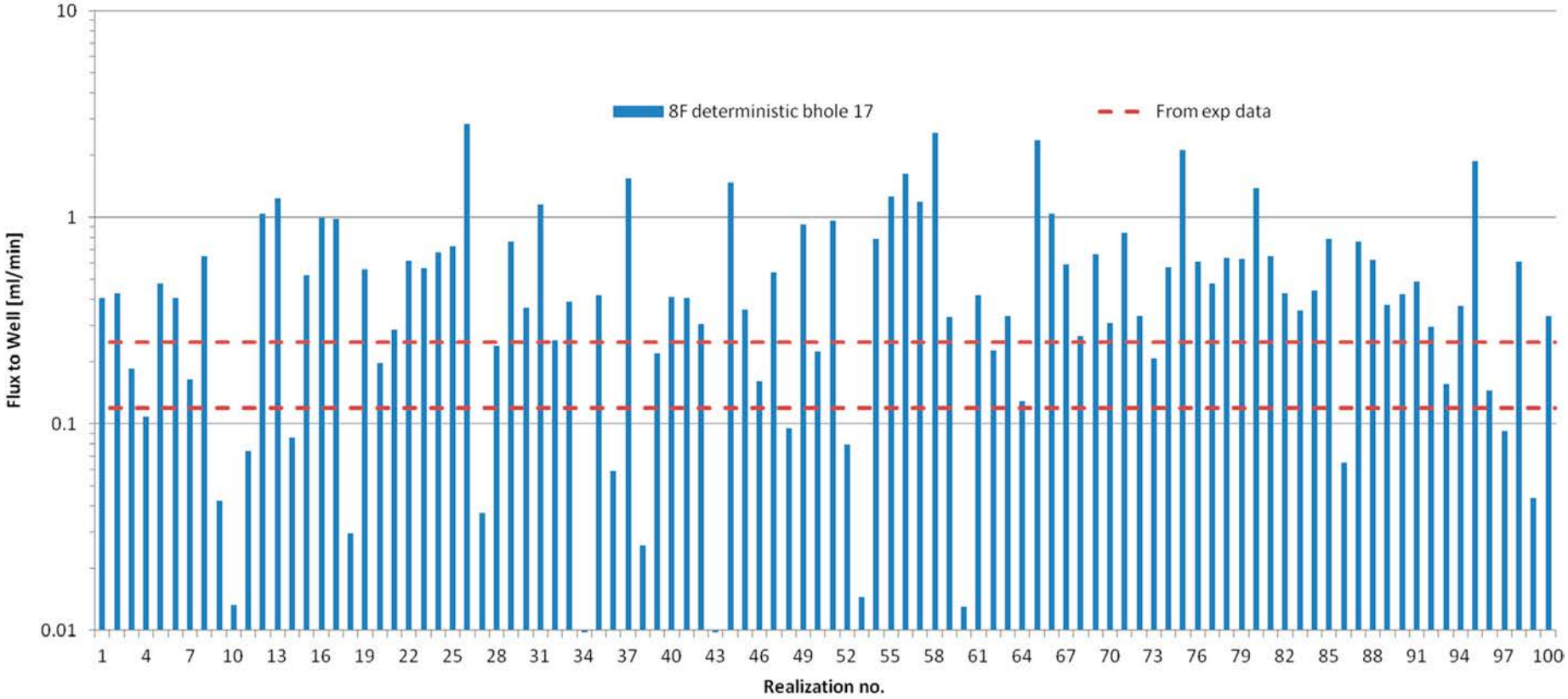

Figure 5-1. *Inflow in KO0017G01 evaluated for 100 different realizations of the fracture network created by using the 5th variant of the background network specifications. The red dashed lines limit the experimental band of values found during the experimental phase (from 0.12 to 0.25 ml/min in KO0017G01). The realizations which have been further investigated are those falling between the dashed lines.*

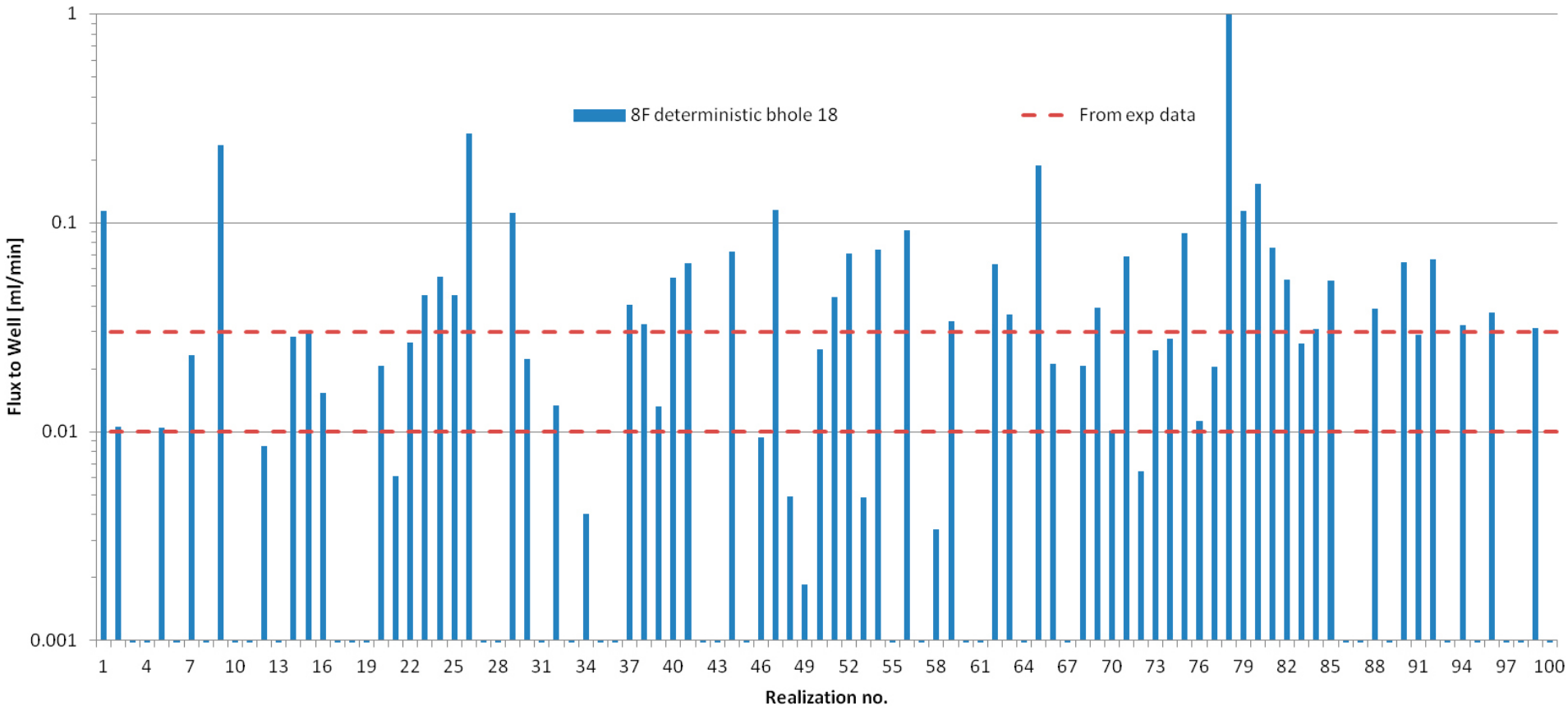

Figure 5-2. *Inflow in KO0018G01 evaluated for 100 different realizations of the fracture network created by using the 5th variant of the background network specifications. The red dashed lines limit the experimental band of values found during the experimental phase (from 0.01 to 0.03 ml/min in KO0018G01). The realizations which have been further investigated are those falling between the dashed lines.*

5.2 Resaturation

Two instrumented bentonite packages were emplaced in overcored boreholes KO0017G01 and KO0018G01 for 400 and 500 days respectively. Six relative humidity sensors, denoted WBR001 through WBR006 are installed in KO0017G01 and six sensors WBR007 through WBR012 are installed in KO0018G01 (cf. Figure 2-7 and Figure 2-8).

For all sensors other than WBR003, the experimental data show an initial localised peak in relative humidity. This is a consequence of the installation process of the bentonite, as described in Section 2.2, which includes the filling of the outer slot with water. Relative humidity recorded by sensor WBR003 does not show this behaviour as it is located closest to the intersecting fracture (see Figure 6-7 of Baxter et al. 2014b), and as such the surrounding bentonite resaturates on a timescale that disguises this effect.

The resaturation profiles evaluated for this basecase model have been compared to the data acquired from the relative humidity sensors. In Figure 5-3 the resaturation profiles at the three sensor locations in the wet section of KO0017G01 are shown. The hydration process at point WBR001 (black line in the graph) and at WBR003 (green line in the graph) are in good agreement with the sensor data, but simulation of the hydration process at point WBR002 is too fast. This could be caused by a range of issues, including the incorrect position of the assumed deterministic fracture intersecting the borehole, or incorrect parameterisation of one of the materials (e.g. heterogeneity in the rock matrix, or bentonite).

When comparing the hydration process evaluated by the model against the experimental data in the dry section of the bentonite, (see Figure 5-4), it is noticeable that the hydration process is too rapid at all sensor locations. In the experimental data, after the initial localised peak, the relative humidity is shown to increase very slowly and to have a noticeable change only 250 days after installation.

The model results shown use realisation 3 of the DFN (for inflows see Figure 5-1). The authors have previously demonstrated (see previous modelling of the BRIE (Baxter et al. 2014b)) that once fracture realisations have been both screened for inflow magnitude and constrained by fracture intersections with the hole, the variability in the evolution of relative humidity between realisations is relatively small. Therefore, in this study, we restrict ourselves to the first realisation that satisfies the inflow measurements under open conditions, in the knowledge that the model calibration performed thereafter has the flexibility to adjust the geometric properties of fractures intersecting the hole to ensure the relative humidity profiles during resaturation are adequately matched. In other words, this study (Task 8F) aims to improve the understanding of the capability of the current models to adequately represent the experimental resaturation profiles of the BRIE, within the framework of a single realisation of the current conceptual / numerical models; and to identify limitations and potential improvements to the existing numerical models. It does not consider sensitivity of the modelling results to either parameter uncertainty (considered previously in Carta et al. 2016) or stochastic uncertainty of the DFN model (considered previously in Baxter et al. 2014a, b).

The following chapters consider conditioning of both the material properties for the bentonite and rock matrix, as well as the geometric and hydraulic properties of the fracture intersecting the overcored boreholes, to improve the correlation between the simulated and observed relative humidity at each of the twelve sensors. In all cases realisation 3 of the underlying stochastic DFN model is used.

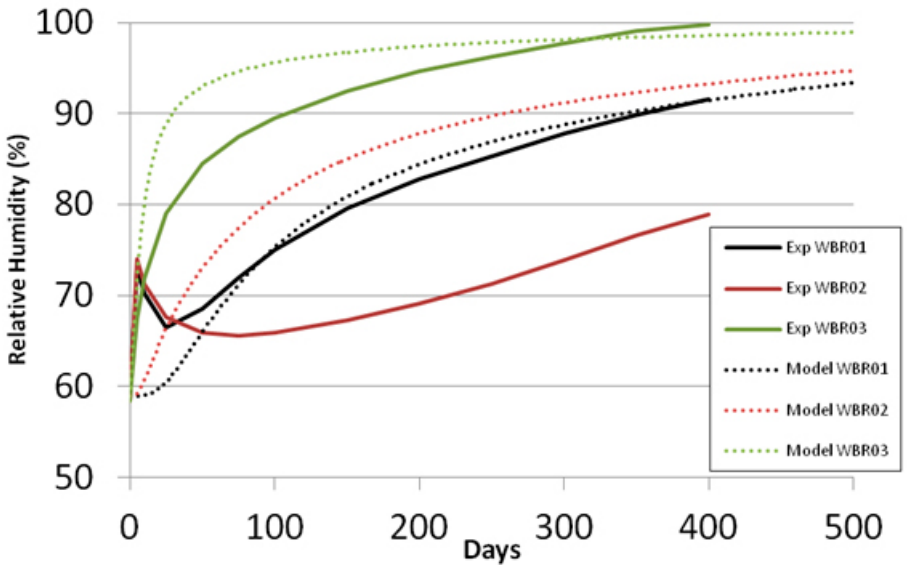

Figure 5-3. *Resaturation profiles evaluated in the base case at the sensor locations in the wet section of KO0017G01. The dotted lines are the results from the model while the continuous lines are the experimental data.*

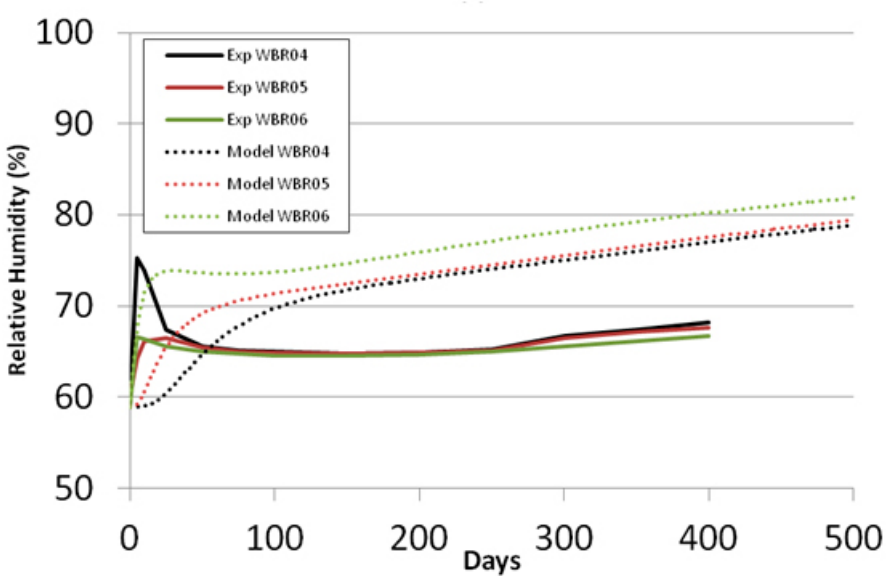

Figure 5-4. *Resaturation profiles evaluated in the base case at the sensor locations in the dry section of KO0017G01. The dotted lines are the results from the model while the continuous lines are the experimental data.*

6 Conditioning in the absence of fractures

In this chapter resaturation of the bentonite in the absence of fractures is considered. This corresponds to a case where the rock matrix supplies all of the groundwater to the emplaced bentonite and the resulting hydration is homogeneous. By considering the absence of fractures, material properties for the bentonite can be conditioned to improve the simulated resaturation in the dry sections of the overcored boreholes. In particular, the following properties of the bentonite are considered:

- Changes to the cubic law for relative permeability.
- A sensitivity study of the propagation of the pressure front through the bentonite.

As discussed in Chapter 5, the initial resaturation rate of the bentonite evaluated by the basecase model is too fast, especially in regions of the bentonite far from the sources of groundwater ingress. In this chapter, a series of model variants are considered with alternative parameterisation of the bentonite, with the aim of slowing the rate of resaturation. All fractures intersecting the overcored boreholes have been removed from the DFN, and simulations are therefore analogous at early times to the experimental data in the dry section of the bentonite.

The numerical formulation of the relative permeability in the bentonite and the diffusivity of the pressure front through the bentonite have both been varied; within model variants constrained to either the prescribed range (Vidstrand et al. 2017) or compatible with experimental values which have been reported in the literature (Harrington and Horseman 2003).

The wetting process in the dry section of the bentonite has been studied for three model variants considering:

- changes to the cubic law for relative permeability (Section 6.1),
- a sensitivity study of the bentonite's specific storage coefficient, directly influencing the propagation of the pressure front through the bentonite (Section 6.2), and
- a combination of both of the above (Section 6.3).

6.1 Relative permeability

The Task Description Report (Vidstrand et al. 2017) suggests the relative permeability in the liquid phase (k_r) of the bentonite is

$$k_r = \tilde{S}^n \tag{6-1}$$

where the basecase model implements the Fatt and Klikoff (Fatt and Klikoff 1959) cubic-law representation of the relative permeabilities (i.e. an exponent of 3). The Task Description Report (Vidstrand et al. 2017) recommends the exponent n lies in the interval $2 \leq n \leq 4$ and as such, three model variants are considered:

- The basecase expression of the relative permeability in the aqueous phase.
- A model variant considering an increased value of the exponent ($n = 4$).
- A model variant considering a reduced value of the exponent ($n = 2$).

The modelling results at point WBR004, located in the dry section of KO0017G01, are presented in Figure 6-1. Changing the value of the exponent in the expression has a large effect at short times post installation, a smaller exponent implies a quicker hydration process and a larger exponent implies a slower one.

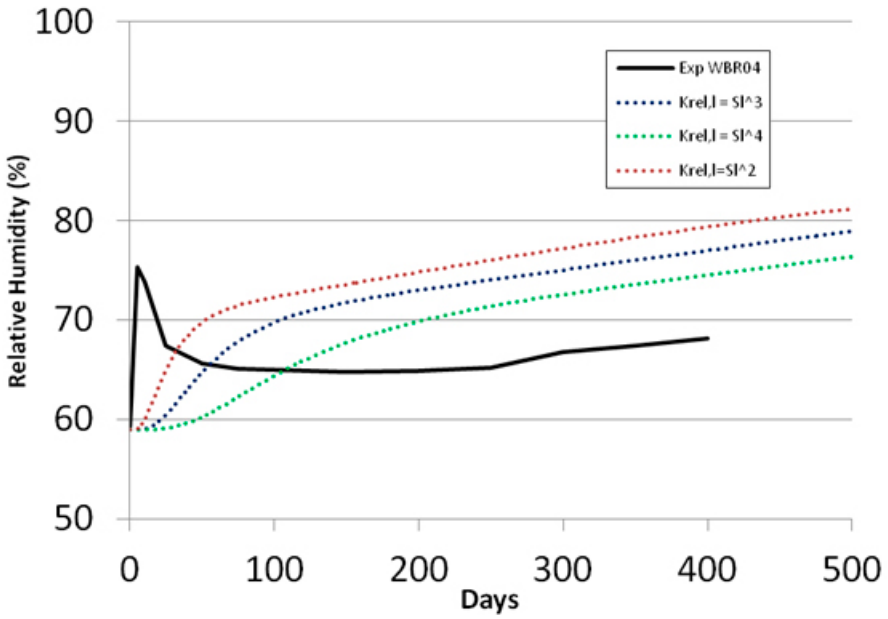

Figure 6-1. *The evolution of relative humidity calculated at sensor location WBR004 within the bentonite during the first 400 days post installation. Results are presented for three model variants, where no fractures have been modelled, and characterised by a different expression of the relative permeability in the liquid phase: $k_r = \tilde{S}^2$ (dotted red); $k_r = \tilde{S}^3$ (dotted blue); $k_r = \tilde{S}^4$ (dotted green). Measurements from the BRIE experiment are coloured black.*

6.2 Propagation of the pressure front through the bentonite

The physical processes which drive the propagation of the pressure front through the bentonite are equivalent to the processes which occur when water flows through an aquifer. The governing equation for unsaturated groundwater motion in a porous medium, as implemented in ConnectFlow, is given below:

$$\left(\frac{S}{g}S_w + n\rho\frac{\partial S_w}{\partial P}\right)\frac{\partial P}{\partial t} = \frac{\partial}{\partial x_i}\left[\rho k_{ij}\frac{k_r(S_w)}{\mu}\left(\frac{\partial P}{\partial x_j} + \rho g\frac{\partial z}{\partial x_j}\right)\right] \qquad (6\text{-}2)$$

where S[1/m] is the specific storage coefficient controlling the diffusion of the pressure front through the material , n is the porosity, S_w is the saturation for the wetting phase, ρ[kg/m^3] is the density, g[m/s^2] is the gravitational acceleration, k_r is the relative permeability, k_{ij}[m^2] is the intrinsic permeability tensor, μ[kg/s · m] is the dynamic viscosity and P[P_a] is the pressure.

It is noteworthy that the specific storage coefficient for the bentonite is dependent on both the net stress and suction, and as such should not be expected to be homogeneous. However, to implement this dependency in the models would require development of coupled hydraulic-mechanical models which are beyond the scope of this study. As such, models presented in this section only consider a constant value for the specific storage coefficient of the bentonite.

SKB (Harrington and Horseman 2003) performed long term gas injection tests on cylinders of pre-compacted saturated MX80 bentonite in which the specific storage coefficient had been evaluated under different geometrical constraints of the apparatus (Harrington and Horseman 2003). Two of these tests were undertaken using a custom-designed constant volume and radial flow (CVRF) apparatus and a third test was performed using an apparatus which radially constrained the specimen during gas flow. Inverse modelling of the first two tests "gives an average permeability of 1.7×10^{-21} m^2 and a specific storage in the range 1×10^{-6} to 9×10^{-6} m^{-1}. These values of specific storage are exceptionally small, as one might anticipate for a fully-saturated constant volume system

(Harrington and Horseman 2003). The fitted permeability and specific storage of the third test are 8.7×10^{-21} m^2 and 3.8×10^{-4} m^{-1} respectively. "Specific storage is clearly substantially larger than the range established for the CVRF conditions, showing that axial swelling has a very profound effect on storage" (Harrington and Horseman 2003).

Installation of the BRIE precluded the axial swelling of the bentonite by retaining pillars, but the bentonite was partially allowed to swell in the radial direction because of the presence of a small air gap between the bentonite parcel and the rock. This probably resulted in a non-homogeneous bentonite specific storage coefficient in the radial direction, and with an average value potentially larger than the one prescribed by the task description. Although the nature of this swelling is specific to the BRIE installation procedure, it is anticipated that limited swelling of the bentonite may also occur during the emplacement of waste within a GDF.

To evaluate this effect, the resaturation of emplaced bentonite is reconsidered for the following cases:

- The basecase value (2×10^{-6} m^{-1}) of the bentonite specific storage coefficient.
- A model variant considering a value of 1.64×10^{-5} m^{-1} for the bentonite specific storage coefficient.
- A model variant considering a value of 6.4×10^{-5} m^{-1} for the bentonite specific storage coefficient.

It is shown in Figure 6-2 that the evolution of relative humidity is greatly affected by the value of the bentonite specific storage coefficient. While its value increases the velocity of the hydration process slows down. The resaturation profile evaluated by the model reaches a best agreement with the experimental data for a value of the bentonite specific storage coefficient of 6.4×10^{-5} m^{-1}.

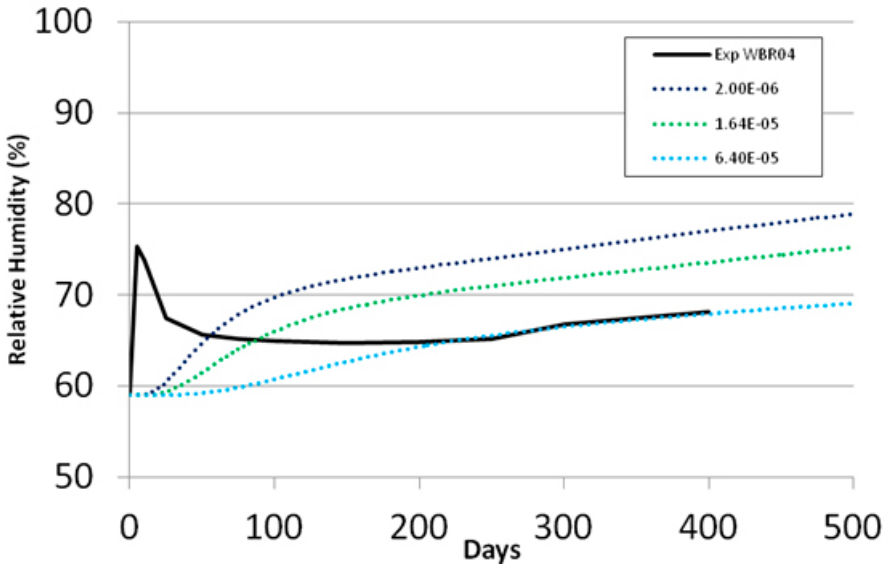

Figure 6-2. *The evolution of relative humidity calculated at sensor location WBR004 within the bentonite during the first 400 days post installation. Results are presented for three variants of a model where no fractures have been modelled, and characterized by a different value of the bentonite specific storage coefficient: 2.0×10^{-6} (dotted blue); 1.64×10^{-5} (dotted green); 6.4×10^{-5} (dotted light blue). Measurements from the BRIE experiment are coloured black.*

6.3 Conditioning of the parameters describing the bentonite

The wetting process in the dry section of the bentonite has been further studied for three different combinations of the parameters considered in Sections 6.1 and 6.2:

- Variant 1: model parameterisations considering liquid relative permeability in bentonite, kr = $\tilde{S}^4$ and bentonite specific storage coefficient = 6.4×10^{-5} m^{-1}.
- Variant 2: model parameterisations considering liquid relative permeability in bentonite, kr = $\tilde{S}^2$ and bentonite specific storage coefficient = 6.4×10^{-5} m^{-1}.
- Variant 3: model parameterisations considering liquid relative permeability in bentonite, kr = $\tilde{S}^3$ and bentonite specific storage coefficient = 6.4×10^{-5} m^{-1}.

The evolution of the relative humidity calculated at the sensor locations in the dry section of KO0017G01 are presented in Figure 6-3 (basecase) through Figure 6-6.

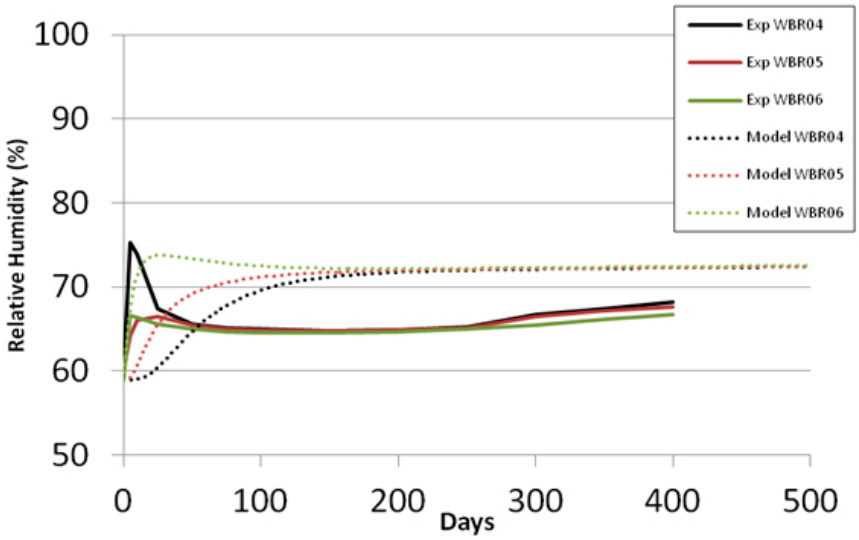

Figure 6-3. *The evolution of relative humidity calculated at the three sensor locations in the dry section of the bentonite during the first 400 days post installation in KO0017G01. The no-fracture model results, which have been evaluated by using the basecase parameters, are presented as dotted lines while measurements from the BRIE experiment are continuous lines.*

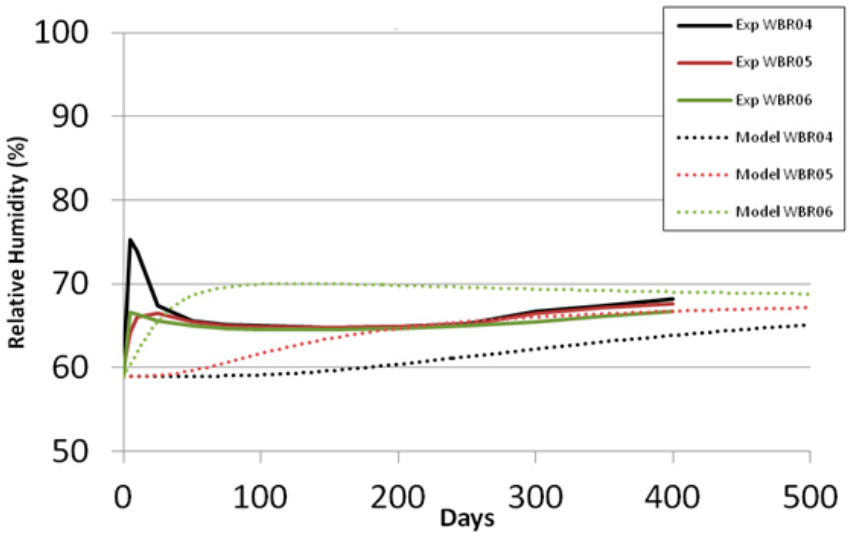

Figure 6-4. *The evolution of relative humidity calculated at the three sensor locations in the dry section of the bentonite during the first 400 days post installation in KO0017G01. The no-fracture model results, which have been evaluated by using the Variant 1 parameters, are presented as dotted lines while measurements from the BRIE experiment are continuous lines.*

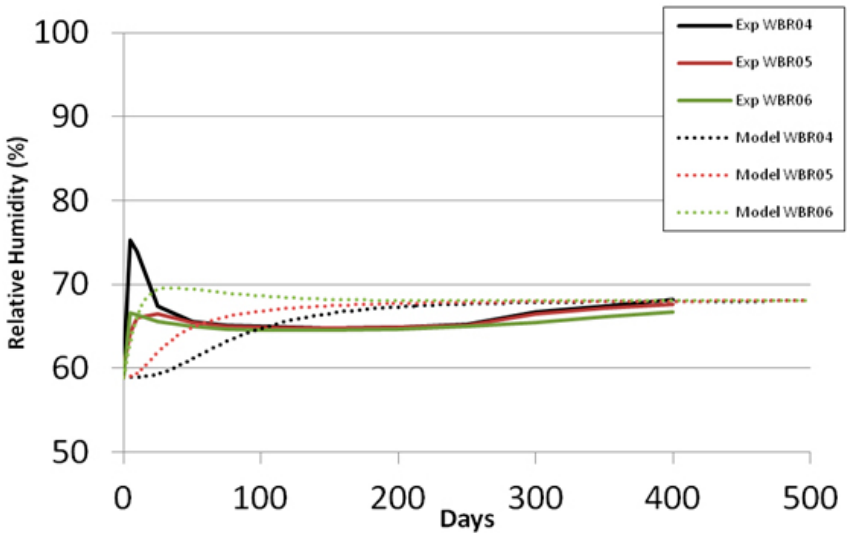

Figure 6-5. *The evolution of relative humidity calculated at the three sensor locations in the dry section of the bentonite during the first 400 days post installation in KO0017G01. The no-fracture model results, which have been evaluated by using the Variant 2 parameters, are presented as dotted lines while measurements from the BRIE experiment are continuous lines.*

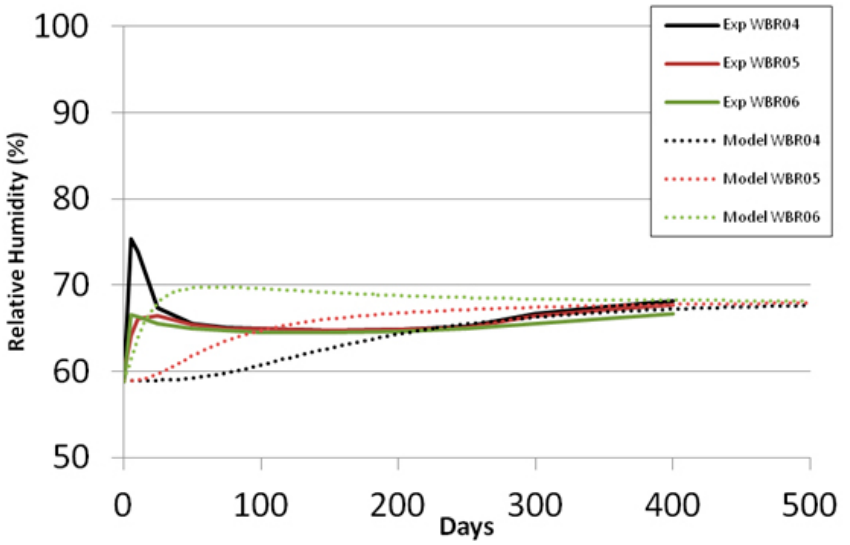

Figure 6-6. *The evolution of relative humidity calculated at the three sensor locations in the dry section of the bentonite during the first 400 days post installation in KO0017G01. The no-fracture model results, which have been evaluated by using the Variant 3 parameters, are presented as dotted lines while measurements from the BRIE experiment are continuous lines.*

All three variants present a substantial improvement of the resaturation profiles when compared to the basecase parameterisation. In conclusion:

- the hydration process in Variant 1 is potentially too slow, with the resaturation at point WBR004 slower than the expected data,
- the initial hydration in Variant 2 is too fast and, at later times, the modelled resaturation rate is too small,
- variant 3 shows relatively good agreement with the experimental data, especially in the long term, even if the behaviour between experimental data and modelled results does not perfectly match at early times post installation.

It is noted that even if the early resaturation peaks in the experimental data are a consequence of the installation process of the bentonite, which includes filling of the outer slot with water, it is likely, because of the quantities of water involved, that this process does not significantly affect the resaturation rate at longer times. The parameters used in Variant 3 provide the optimal solution of those considered and are therefore used in the following chapter to predict the hydration process in the dry region of the bentonite parcel emplaced in KO0018G01 and in the wet regions of the bentonite parcel emplaced in both of the holes.

6.4 Conclusions from calibration in the absence of fractures

As discussed in Chapter 5, the initial resaturation rate of the bentonite predicted by the basecase model is significantly faster than measurements from the relative humidity sensors indicate. This is especially evident in locations furthest away from the hydraulically active fractures intersecting the deposition holes. In this chapter, a number of model variants detailing alternative parameterisation of the bentonite have been considered, with the aim of slowing the rate of resaturation predicted by the simulations at the relative humidity sensors located in the drier regions of the bentonite. Calibrating the bentonite properties to these specific sensors (i.e. in the absence of fractures) reduces uncertainties in the geometric and hydraulic description of fractures intersecting the deposition hole in model predictions.

Calibration of the bentonite has considered the following aspects of the bentonite:

- The relative permeability of the model.
- The specific storage coefficient of the bentonite.

Of the model variants considered, the best model predictions for resaturation in the drier regions of the bentonite came from simulations implementing a cubic law for the relative permeability of the liquid phase in the bentonite, and a specific storage coefficient of 6.4×10^{-5} m^{-1}. In this case, model predictions yielded good agreement with the sensor measurements, especially towards the end of the experimental period considered.

Finally, it is noted that the calibration of the model parameterisation to the six relative humidity sensors in the drier regions of the bentonite is restricted to the two bentonite aspects detailed above. However, if the calibration process was extended to consider additional properties of the bentonite, or the surrounding rock matrix, it is highly likely that alternative parameterisation could be identified that yields an equally successful calibration. This non-uniqueness of model parameterisation is discussed further in Chapter 9.

7 Conditioning the local fractures

In this chapter a new model is developed incorporating the conditioned bentonite parameterisation from Chapter 6, and considering variants of the deterministic fractures identified within the two overcored holes. Two alternative models for the fractures are considered:

- the deterministic fractures, as identified from image logs and deposition hole mappings, and updated as part of Task 8F, and
- the deterministic fractures, as identified from image logs and deposition hole mappings, originally provided as part of Task 8D.

Based on the findings of Chapter 6, this chapter considers the resaturation of the bentonite using the deterministic local fractures intersecting KO0017G01 and KO0018G01. The terminology used to identify the different sets of deterministic fractures is as follows:

- Original fractures, these are the fractures described in Table 2-2, and previously used during Task 8D (Baxter et al. 2014b).
- Updated fractures, these are the fractures described in Table 2-3 and reproduced from Vidstrand et al. (2017).

7.1 Fractures interpreted from image logs (Task 8F)

Using the updated fractures defined for Task 8F, the relative humidity evolution in the wet section of KO0017G01 is in good agreement to the experimental data (Figure 7-1). The main discrepancy in the model resaturation is a slight under prediction of the relative humidity at sensors WBR002 and WBR003. This could be a consequence of not including in the models the initial ingress of water due to filling of the outer slot with formation water during emplacement of the bentonite stack (as measured by the sensors and illustrated by the initial peak in relative humidity).

The evolutions of the relative humidities calculated at sensor locations within the dry section of bentonite in hole KO0017G01 are also in good agreement with measurements (see Figure 7-2). These results are also very similar to those evaluated in the model with all fractures removed (see Chapter 6), and suggest that the underlying assumptions for this conditioning process are valid.

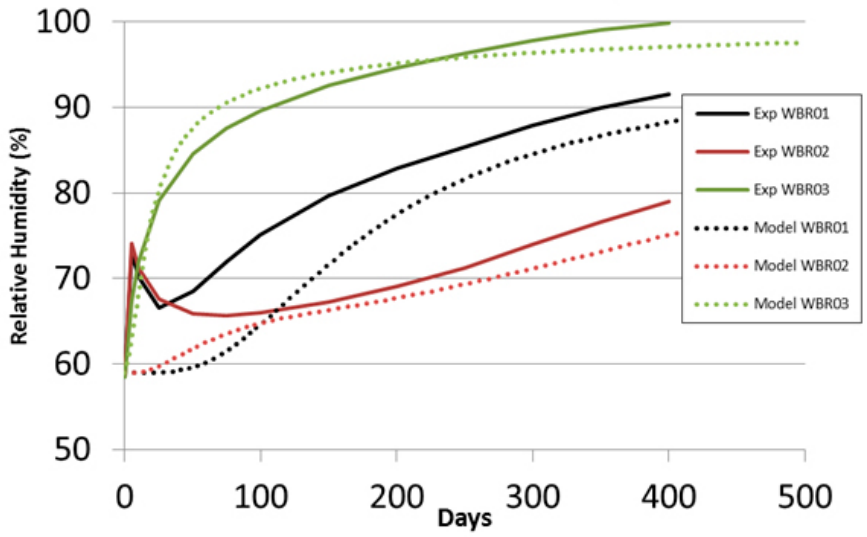

Figure 7-1. *The evolution of relative humidity calculated at sensor locations within the wet section of bentonite in KO0017G01 during the first 400 days post installation (dotted lines). Results are presented against experimental data for sensors WBR001 through WBR003 (continuous lines). The set of the deterministic fractures implemented in the model is the updated specification.*

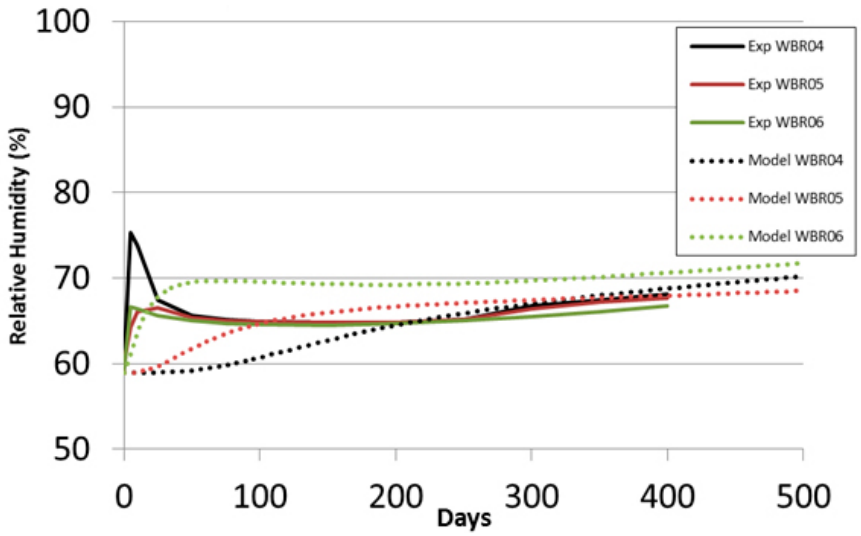

Figure 7-2. *The evolution of relative humidity calculated at sensor locations within the dry section of bentonite in KO0017G01 during the first 400 days post installation (dotted lines). Results are presented against experimental data for sensors WBR004 through WBR006 (continuous lines). The set of the deterministic fractures implemented in the model is the updated specification.*

From characterisation of inflows to the central overcored boreholes, the resaturation of bentonite emplaced in KO0018G01 was expected to resaturate at a slower rate than KO0017G01 (inflows were typically a factor of 10 less in KO0018G01). As such, the bentonite package in KO0018G01 was left in situ for a further 100 days before excavation (i.e. 500 days after installation). Six relative humidity sensors, denoted WBR007 through WBR012 were installed in the bentonite, as shown in Figure 2-6 through Figure 2-8. The evolution of relative humidity within the bentonite evaluated by the model and the experimental data for the six sensor locations is shown in Figure 7-3 and Figure 7-6.

The evolution of relative humidity calculated at the sensor locations within the dry section of bentonite in KO0018G01 during the first 500 days post installation are shown in Figure 7-3 and indicate only small discrepancies from the experimental data. The evolutions of relative humidity calculated at sensor locations within the wet section of bentonite in KO0018G01 are shown in Figure 7-4. The major discrepancy with experimental results is the overly fast resaturation predicted at sensors WBR007 and WBR008 when compared to measurements.

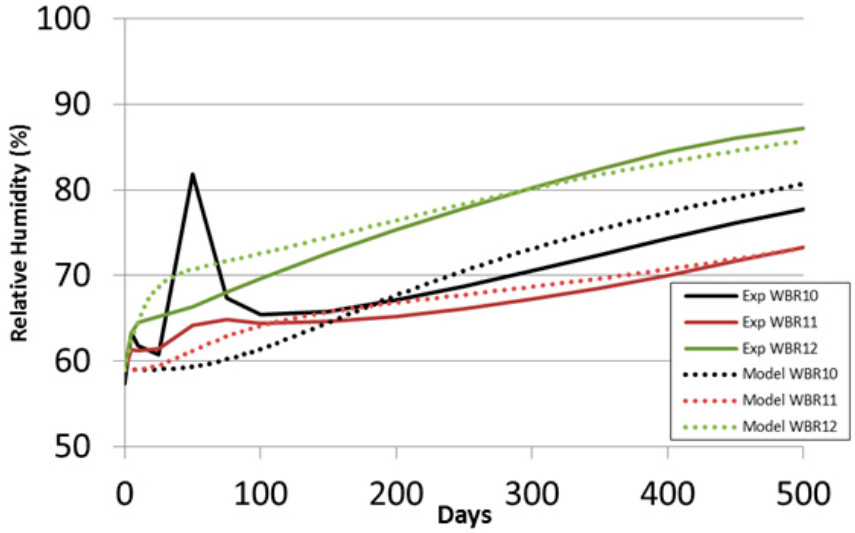

Figure 7-3. *The evolution of relative humidity calculated at sensor locations within the dry section of bentonite in KO0018G01 during the first 500 days post installation (dotted lines). Results are presented against experimental data for sensors WBR010 through WBR012 (continuous lines). The deterministic fractures implemented in the model are the updated set delivered as part of Task 8F.*

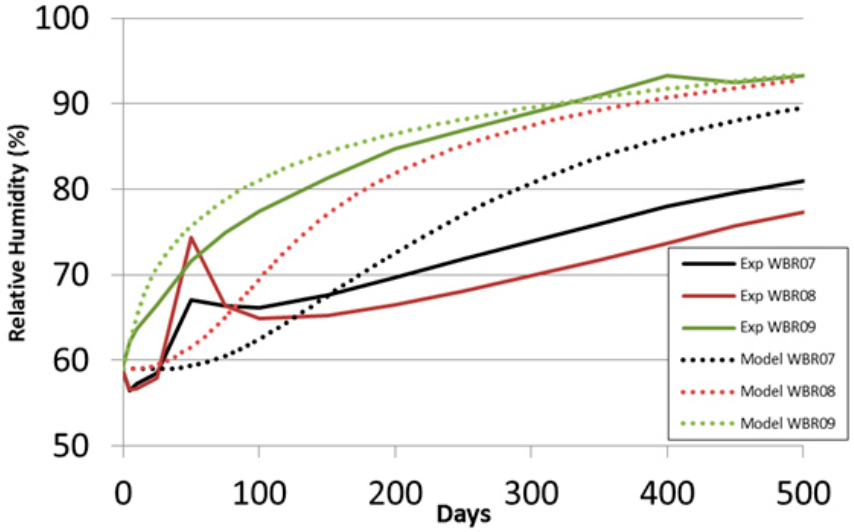

Figure 7-4. *The evolution of relative humidity calculated at sensor locations within the wet section of bentonite in KO0018G01 during the first 500 days post installation (dotted lines). Results are presented against experimental data for sensors WBR007 through WBR009 (continuous lines).*

7.2 Fractures interpreted from image logs (Task 8D)

Sensitivities of bentonite resaturation to the location of the deterministic fractures interpreted from the image in the overcored boreholes are detailed in this section by reverting back to the Task 8D specifications of these individual fractures. Changes in the specification between Task 8D and Task 8F for the single fractures intersecting overcored boreholes KO0017G01 and KO0018G01 are detailed in Subsection 2.4.2, with changes to the specifications small, and consisting of either displacing the fracture by a few centimetres or rotating the fracture by a few degrees. However, although these changes are small in the context of the interpretations, they may be significant to the resulting resaturation profiles at the twelve relative humidity sensors. The evolutions of the relative humidity using the Task8D specification of the deterministic fractures are presented in Figure 7-5 and Figure 7-6 for the wet sections of holes KO0017G01 and KO0018G01 respectively.

The agreement between the evolution of relative humidity evaluated by the model and the experimental data in the wet region of the bentonite emplaced in KO0018G01 is very good. For KO0017G01, the hydration process at sensor locations WBR002 and WBR003 is also reproduced by the model. The only resaturation profile that still shows some differences between experimental data and the results from the simulation corresponds to sensor WBR001.

Although the resaturation profiles in the wet section of the bentonite in KO0018G01 have improved significantly when compared to the previous study (see Figure 6-8 and 6-9 of Baxter et al. 2014b), they are still not as consistent with experimental data as the equivalent section in KO0017G01. The wetting profiles at sensor locations WBR007 and WBR008 are slightly too fast, while the wetting profile at WBR009 matches very well the experimental data.

Comparison of model predictions using Task8F and Task8D specification of deterministic fractures identifies the following:

- For the sensor located at the wettest point in KO0017G01 and KO0018G01 (sensors WBR003 and WBR009 respectively), little difference is seen between the two specifications of the local fractures.
- For sensor WBR001 in KO0017G01, the model simulations using Task 8F fractures are in slightly better agreement with experimental results than when simulations adopt the Task 8D specification. However, it is noted that in both cases the models underpredict the measured resaturation.
- For sensors WBR002 (KO0017G01), and WBR007 and WBR008 (KO0018G01) simulations utilising Task 8D local fractures are more consistent with the sensor data than equivalent models including the Task 8F local fractures.

The evolution of the relative humidity in the dry sections of both bentonite parcels is minimally affected by this relatively small change in the position of the deterministic fractures and the resaturation profiles are nearly identical to those shown in Figure 7-2 and Figure 7-3.

From the above comparisons, it is deemed that the Task 8D fracture description provides a slight improvement to the consistency of models to sensor data when compared to models based on the Task 8F description. As such, the Task 8D model will be used throughout the remainder of this report to provide long term predictions of the evolution of the bentonite buffer.

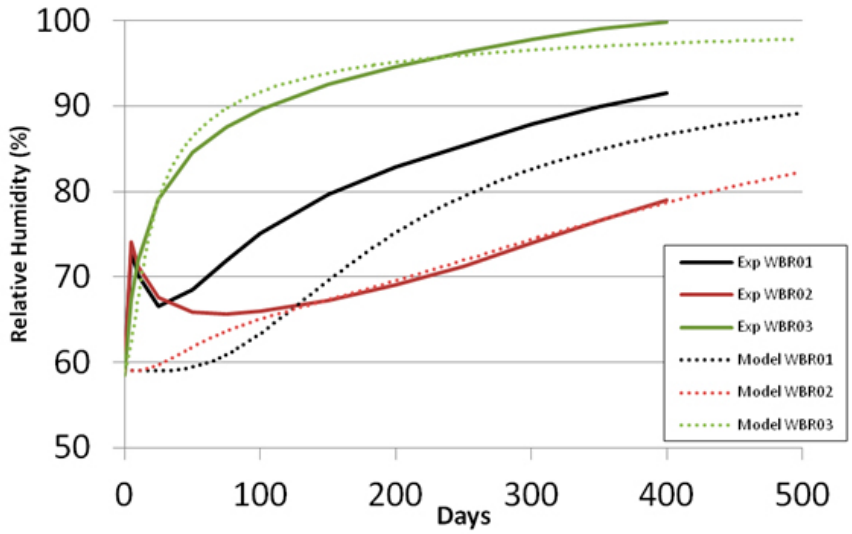

Figure 7-5. *The evolution of relative humidity calculated at sensor locations within the wet section of bentonite in KO0017G01 during the first 400 days post installation (dotted lines) evaluated by using the previous Task 8D deterministic fractures. Results are presented against experimental data for sensors WBR001 through WBR003 (continuous lines).*

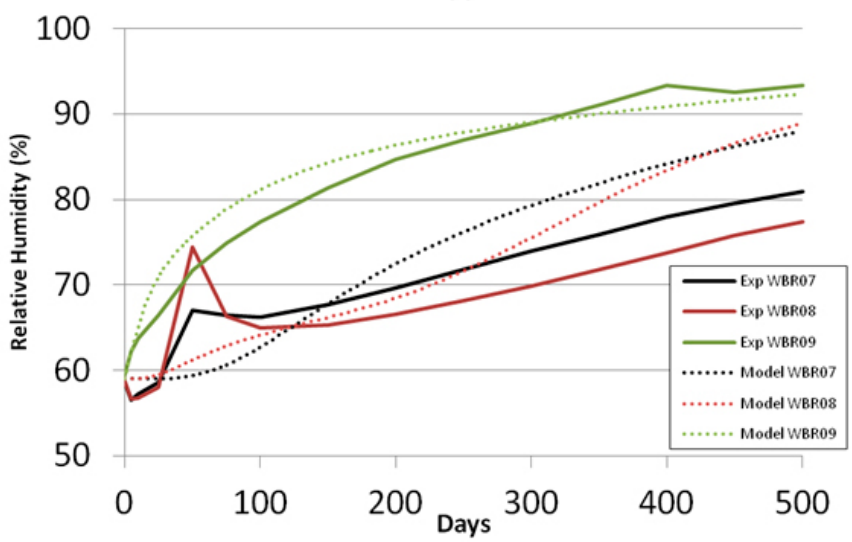

Figure 7-6. *The evolution of relative humidity calculated at sensor locations within the wet section of bentonite in KO0018G01 during the first 500 days post installation (dotted lines) evaluated by using the previous Task 8D deterministic fractures. Results are presented against experimental data for sensors WBR007 through WBR009 (continuous lines).*

7.2.1 Horizontal saturation contour plots

Contour plots of saturation within the bentonite stacks emplaced in KO0017G01 and KO0018G01 are requested by the task description (Vidstrand et al. 2017). These are shown in Figure 7-7 and Figure 7-8 as a series of horizontal slices, taken at elevations detailed in Table 7-1, and corresponding to instrumented bentonite blocks. Computed results, presented in terms of saturation, correspond to the model variant in which Task 8D deterministic fractures have been modelled and are shown at different times: 100 days; 150 days; 200 days and 250 days.

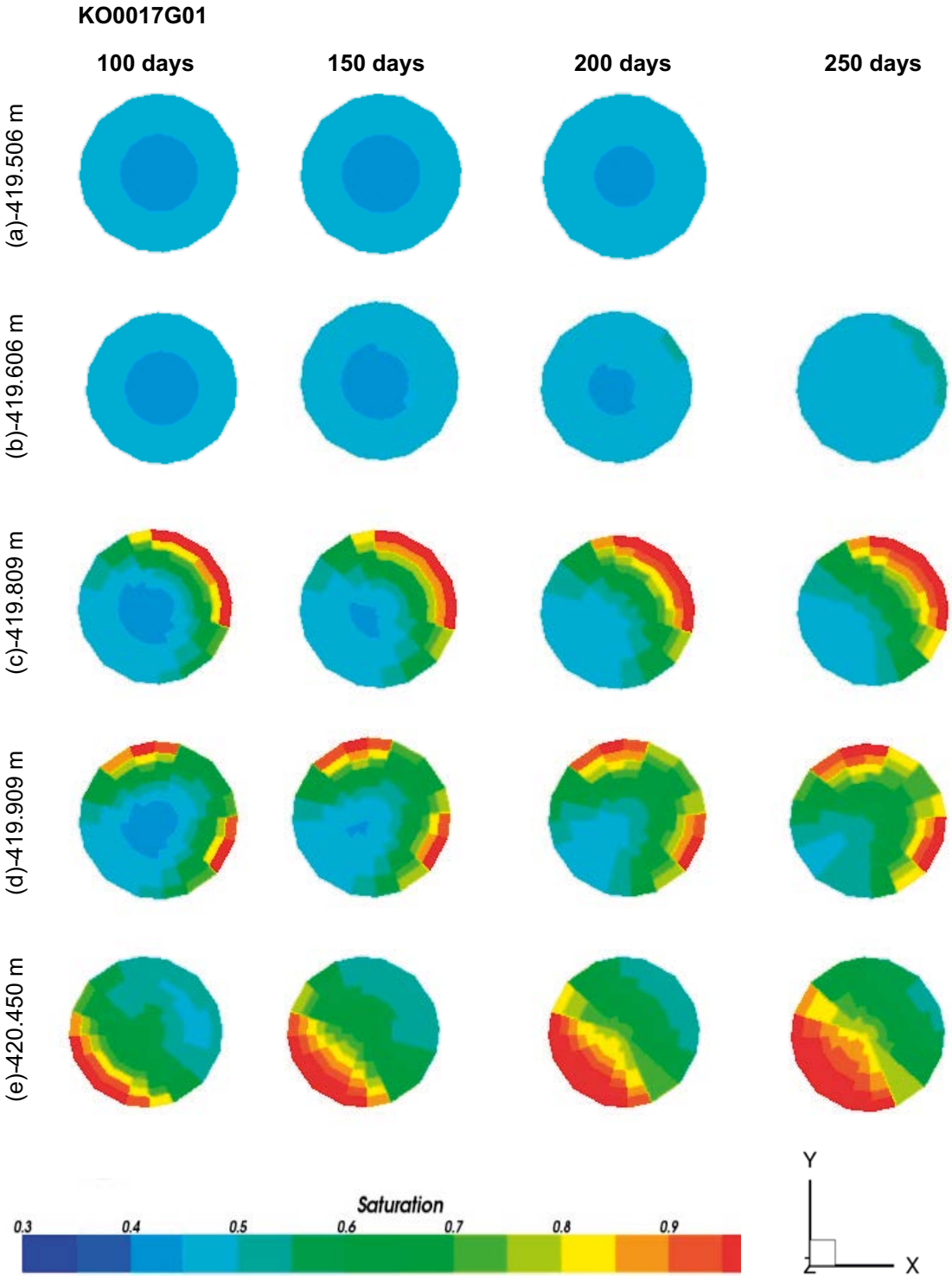

Figure 7-7. *Liquid saturation of the bentonite, contoured over several horizontal slices taken at elevations shown in Table 7-1. Results correspond to 100, 150, 200 and 250 days after installation of the bentonite package in borehole KO0017G01.*

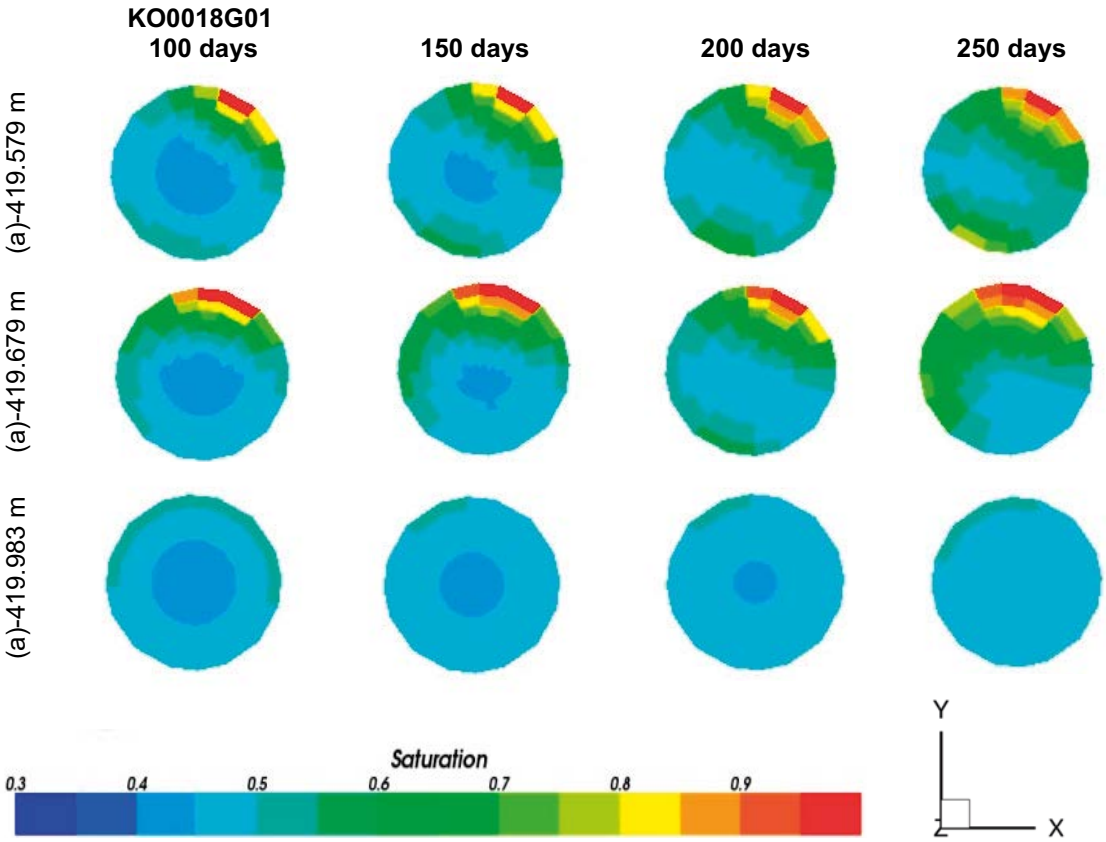

Figure 7-8. *Liquid saturation of the bentonite, contoured over several horizontal slices taken at elevations shown in Table 7-1. Results correspond to 100, 150, 200 and 250 days after installation of the bentonite package in borehole KO0018G01.*

For KO0017G01, the orientation of the water producing feature is clearly observed through the hydration profiles. The resaturation front at shallow depths progresses from the North-East, whereas towards the bottom of the hole the bentonite resaturates from the South-West. This is consistent with the fracture orientation, striking 140°.

For overcored borehole KO0018G01, resaturation in the investigated sections is primarily from the North-East. This is consistent with the mid-section of the fracture, oriented to strike 215º and suggests that the location of the slices does not span to the top or bottom of the fracture intersection. The water inflow in overcored borehole KO0018G01 is much lower than the one in overcored borehole KO0017G01, as is shown in the evolution of resaturation across these slices.

Table 7-1. Depths for requested saturation contour plots, reproduced from task description (Vidstrand et al. 2017).

KO0017G01	KO0018G01*
−419.506 m	−419.579 m
−419.606 m	−419.679 m
−419.809 m	−419.983 m
−419.909 m	
−420.618 (−420.450) m**	

*Liquid saturation at an elevation of −420.083 m is requested in KO0018G01 by the task description (Vidstrand et al. 2017). Due to approximations made during meshing the domain, this elevation is beyond the bottom of the bentonite package modelled. No alternative elevation is considered.

**Liquid saturation at an elevation of −420.618 m is requested in KO0017G01 by the task description (Vidstrand et al. 2017). Due to approximations made during meshing the domain, this elevation is beyond the bottom of the bentonite package modelled. Therefore, an alternative elevation of −420.45 m is considered, located towards the bottom of overcored borehole KO0017G01.

7.2.2 Water content

Models for the resaturation of the emplaced bentonite in each of the overcored boreholes have been conditioned based on the evolution of relative humidity at each of the twelve sensor locations. Using the model which employs the Task 8D specification of the deterministic fractures, it is possible to predict the water content throughout the bentonite at the time of excavating the BRIE; comparing model results to the extensive measurements performed. Scatter plots are shown in Figure 7-9 and Figure 7-10, comparing the water content measured in the bentonite with model predictions after 400 days of emplacement (KO0017G01) and 500 days (KO0018G01).

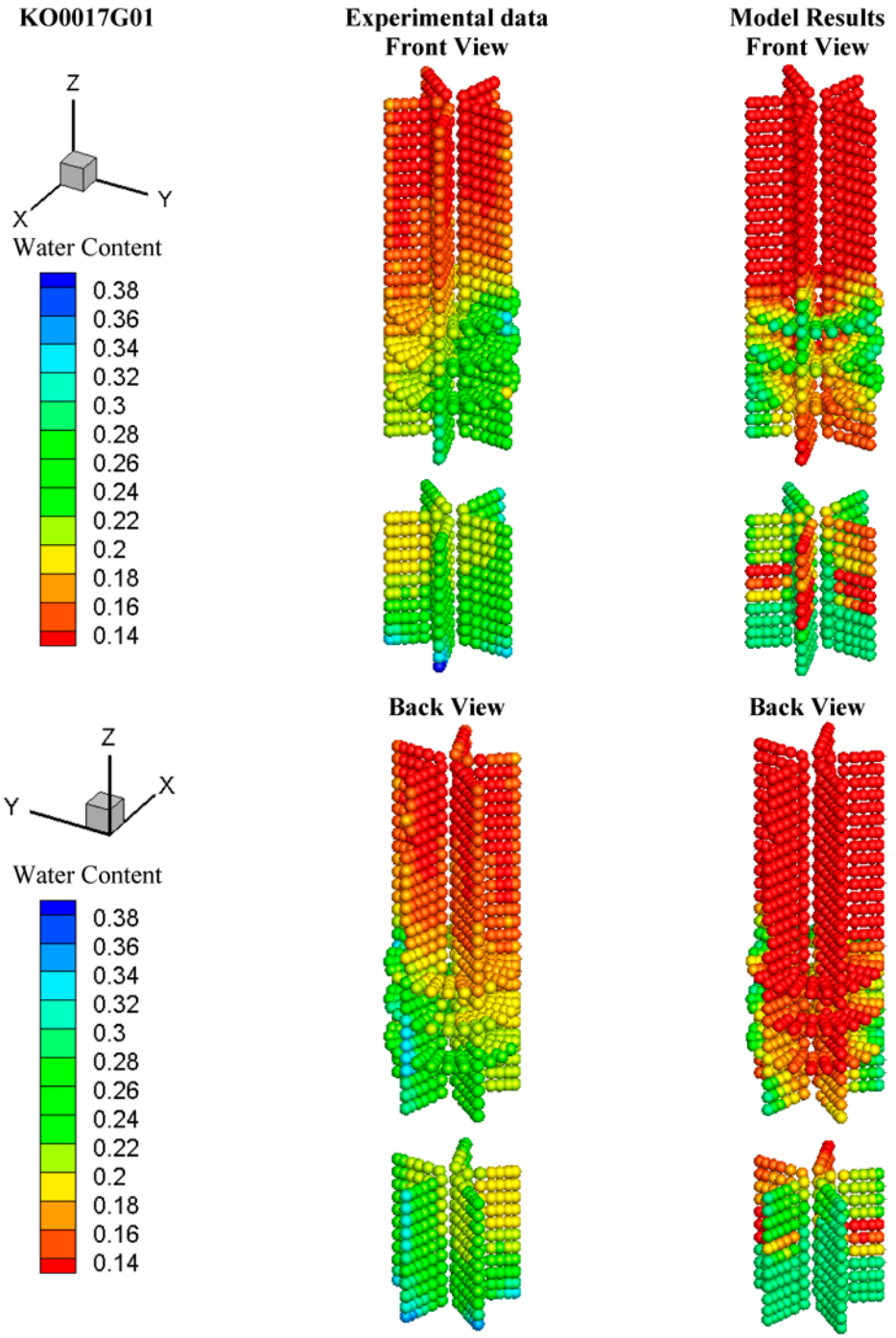

Figure 7-9. *Scatter plot of water content in borehole KO0017G01 from experimental data and model (based on Task 8D specifications) results.*

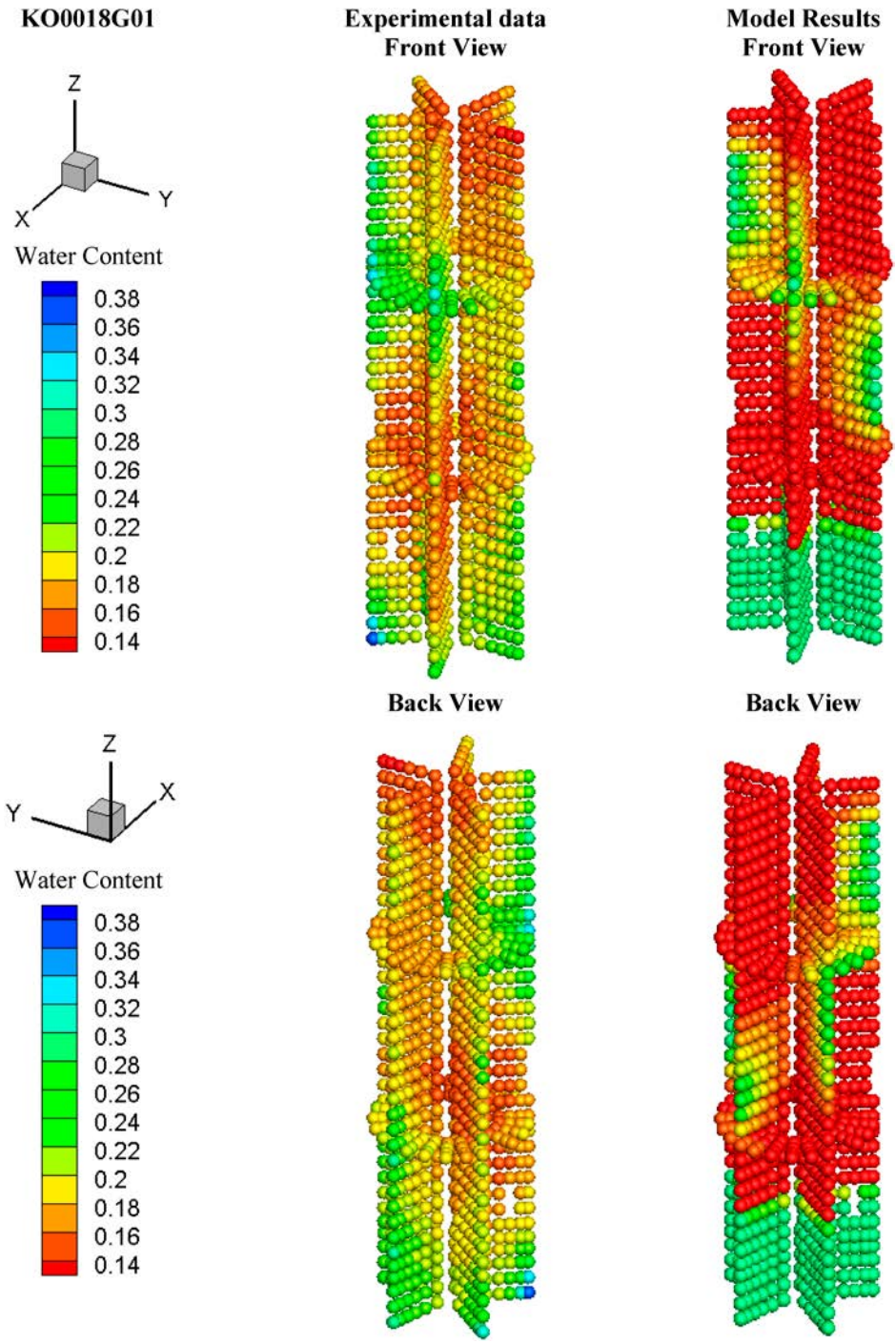

Figure 7-10. *Scatter plot of water content in borehole KO0018G01 from experimental data and model (based on Task 8D specifications) results.*

Model results are consistent with the experimental data, indicating regions of enhanced resaturation due to the presence of the fractures. However, the models often predict that the drier regions of the bentonite are too dry and the wetter regions of the bentonite are too wet (i.e. the model predictions for water content are more heterogeneous than the measurements suggest). This is possibly a consequence of not fully representing the installation procedure of the BRIE, which included a homogeneous wetting phase of the bentonite through addition of water in the outer slot of the overcored boreholes. It is anticipated that further representing the installation procedure and this addition of water would further refine the conditioning of the models (e.g. material properties, fracture locations, and initial conditions) and improve predictions of the water content throughout the bentonite.

8 Long term prediction

In Chapters 5, 6 and 7, simulations consider the early-time evolution of the bentonite buffer on timescales consistent with the duration of the experiment (e.g. spanning up to 500 days). Chapter 8 provides long term predictions by extending the duration of the simulation to two hundred years. The conditioned model selected is based on the Task 8D specification of the deterministic fractures, as found most consistent with sensor data in the previous chapters. In particular, the variation of pressure and saturation with time in the host rock local to the overcored boreholes is presented.

8.1 Pressures in the host rock local to the overcored boreholes

Contour plots of liquid pressure are presented in Figure 8-1 and Figure 8-2, based on the seventh realisation of the upscaled fracture network model utilising the Task 8D specification of the deterministic fractures. Simulation results focus on the near field of KO0017G01 and KO0018G01 during the first one hundred years post-installation (as requested by the task description). The figures presented correspond to:

- a vertical cross-section incorporating both overcored boreholes, and oriented parallel with the TASO tunnel central line, as shown in Figure 8-1 at 0, 0.1, 0.5, 1, 10, and 100 years,
- a horizontal cross-section positioned at an elevation of −418.5 m, and cutting through both overcored boreholes, as shown in Figure 8-2 at 0, 0.1, 0.5, 1, 10, and 100 years.

Within the bentonite, the liquid pressure evolves from an initial value of approximately −70 MPa to −1 MPa, observed at locations of saturated conditions. The location of the fracture intersections with each of the overcored boreholes is visible from the pressure evolution. Negative liquid pressures are also observed in the rock matrix local to the bentonite stacks.

8.2 Saturation in the overcored borehole near field

Contour plots of liquid saturation in host rock local to the overcored boreholes are shown in Figure 8-3 and Figure 8-4 for two slices through the seventh realisation of the upscaled fracture network model. These slices are defined consistently with those shown in Section 8.1.

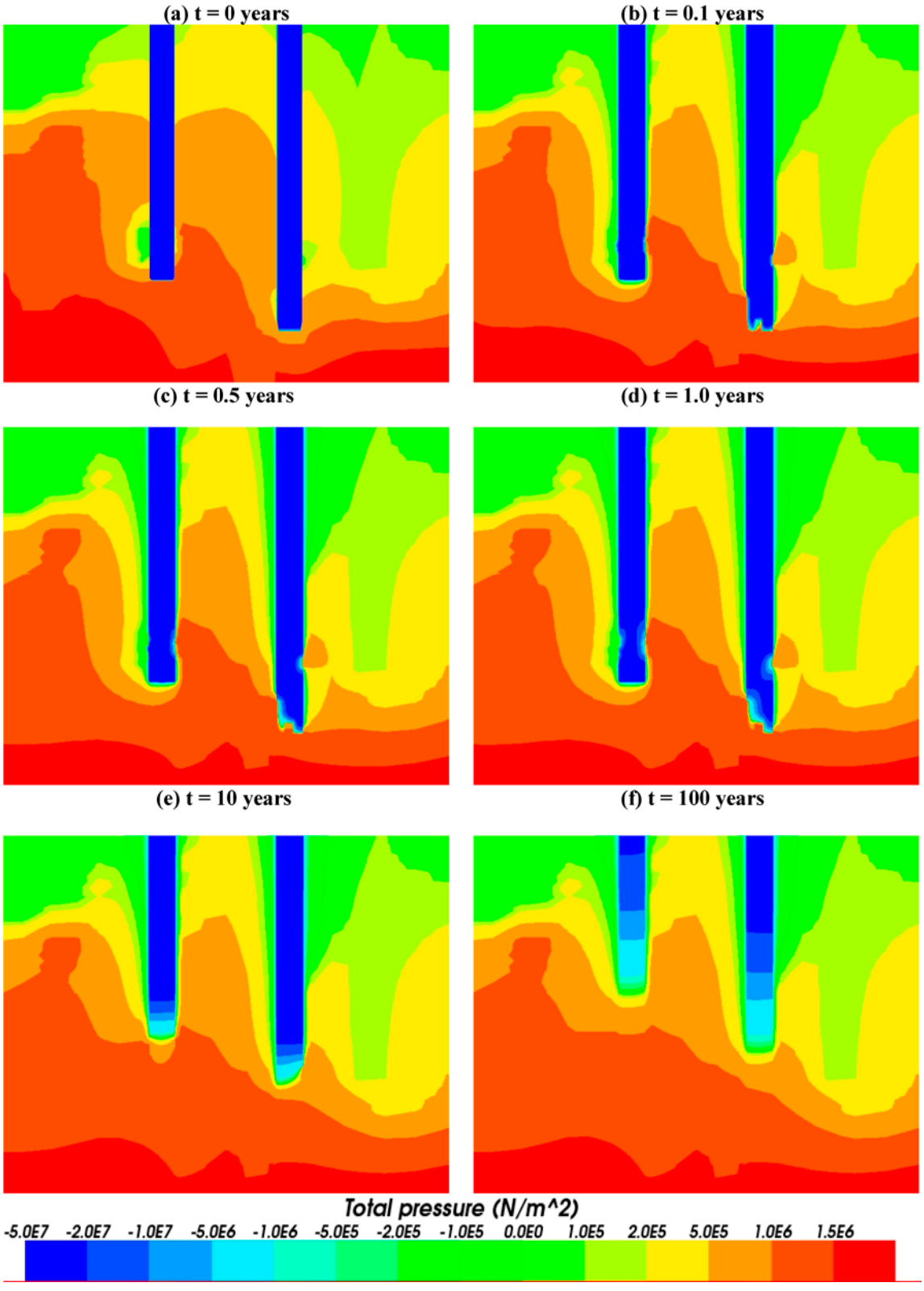

Figure 8-1. *Evolution of liquid pressure [MPa] for a vertical slice, oriented to include the two overcored boreholes KO0017G01 and KO0018G01. Results are shown for the seventh realisation of the upscaled stochastic fracture network.*

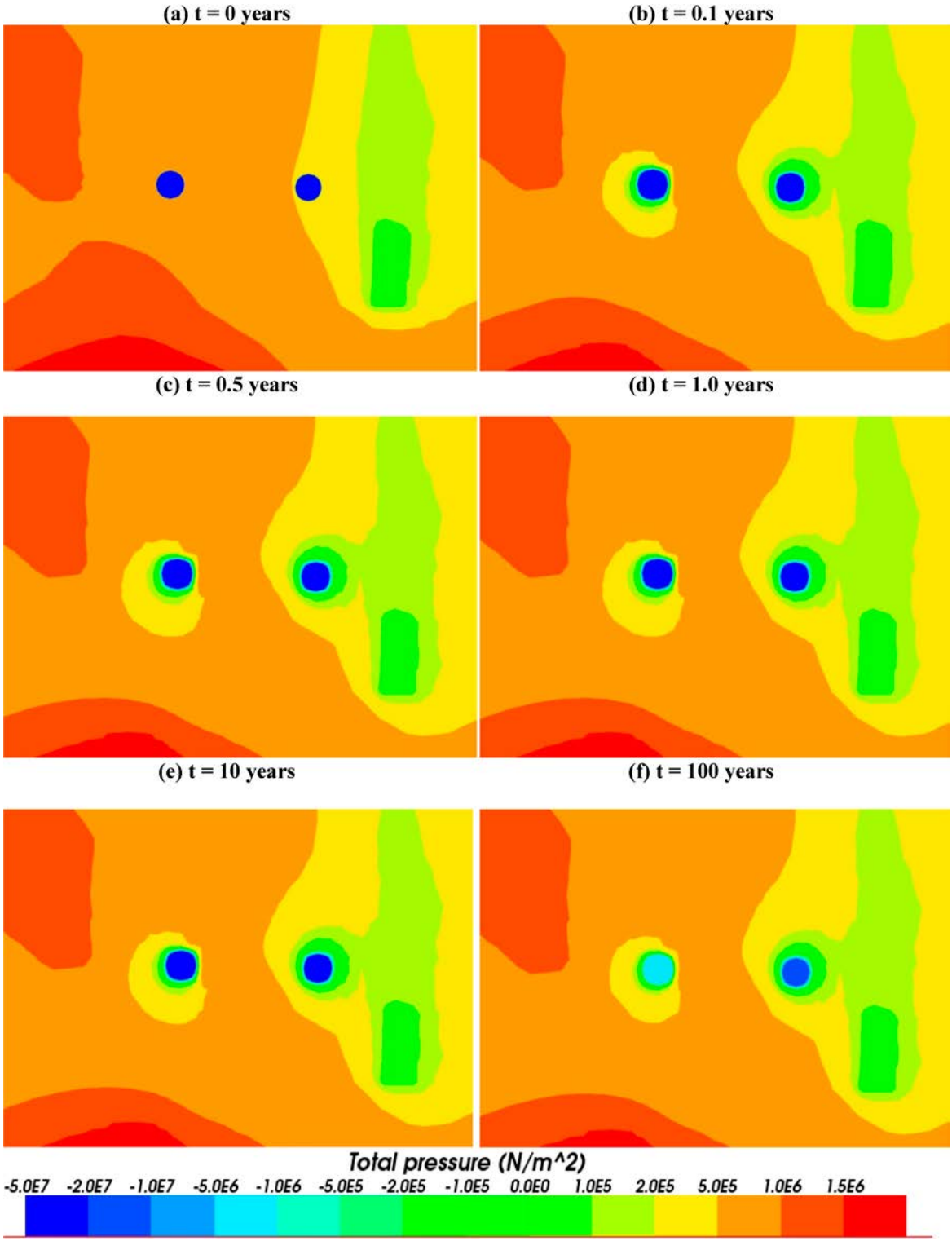

Figure 8-2. *Evolution of liquid pressure [MPa] across a horizontal slice, taken 1.5 m below the TASO tunnel at an elevation of −418.5 m. Results are shown for the seventh realisation of the upscaled stochastic fracture network.*

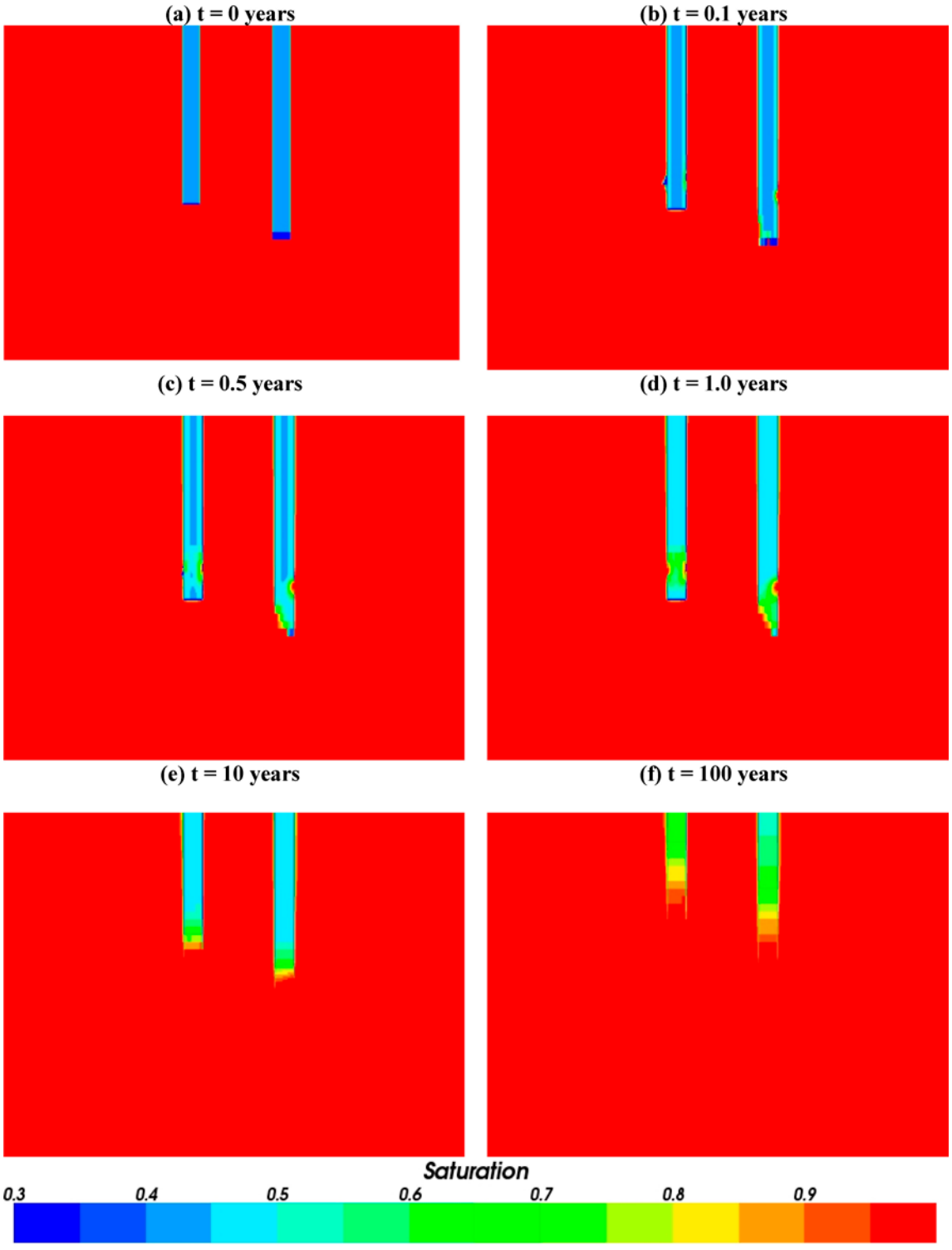

Figure 8-3. *Evolution of liquid saturation for a vertical slice oriented to include the two overcored boreholes KO0017G01 and KO0018G01. Results are shown for the seventh realisation of the stochastic fracture network.*

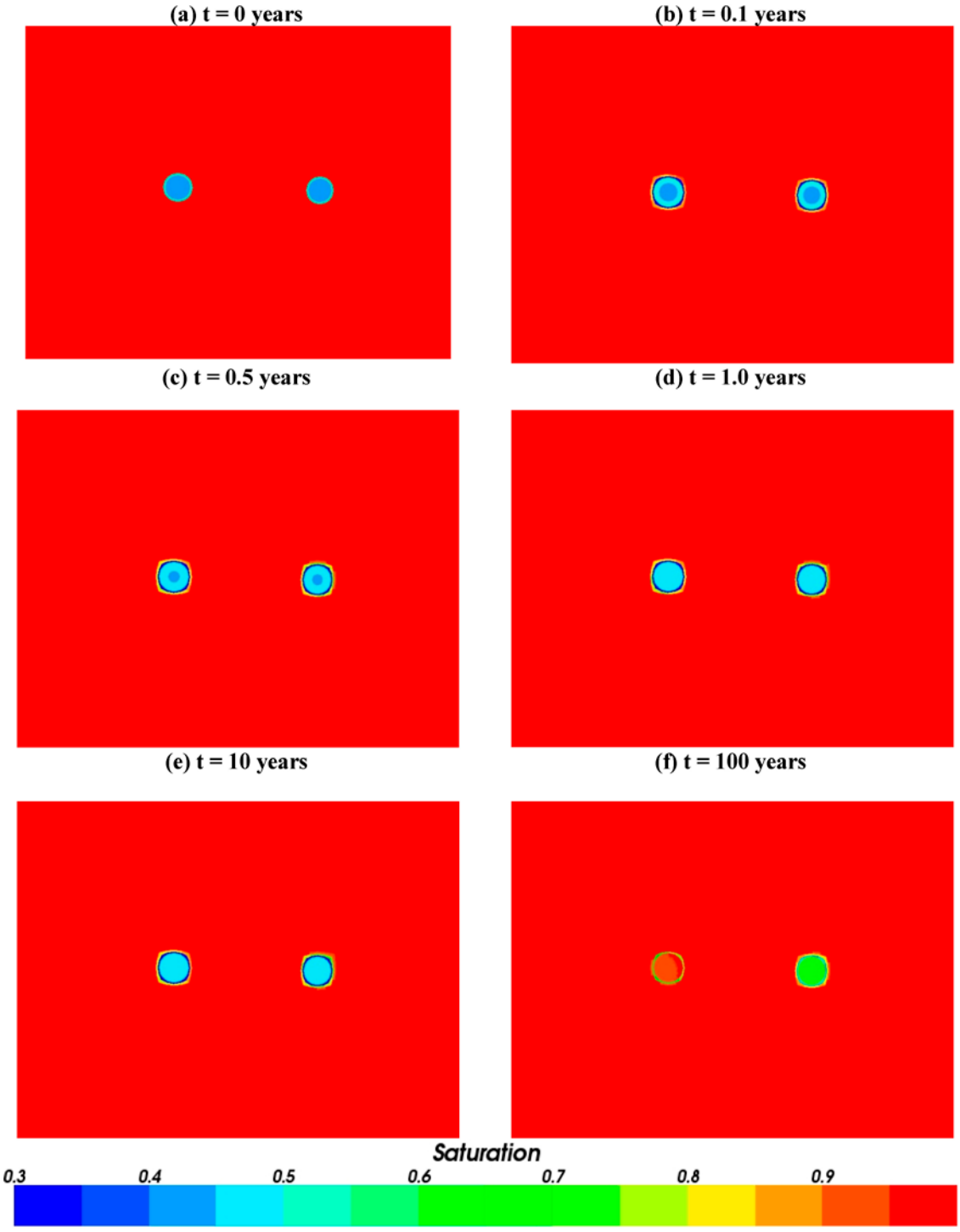

Figure 8-4. *Evolution of liquid saturation across a horizontal slice, taken 1.5 m below the TASO tunnel at an elevation of −418.5 m. Results are shown for the seventh realisation of the stochastic fracture network.*

8.3 Pressure evolution within the bentonite

Liquid pressure within the bentonite is extracted from the model at 24 separate locations in each of the overcored boreholes KO0017G01 and KO0018G01. A schematic of these locations, and the nomenclature used are shown in Figure 8-5. Corresponding figures for the evolution of liquid pressure at each of these locations is presented in Figure 8-6 and Figure 8-7, corresponding to each of the boreholes considered. Results in this section are presented for the seventh realisation of the upscaled stochastic fracture network.

In both boreholes, the saturation rate is dominated by the fracture intersections, providing groundwater towards the bottom of each overcored borehole. Consequently, the liquid saturation within the bentonite (and therefore the liquid pressure) increase most rapidly towards the bottom of the holes. Resaturation towards the top of the holes is likely dominated by groundwater entering the bottom of the bentonite stack and migrating towards the TASO tunnel, with limited contribution from the rock matrix.

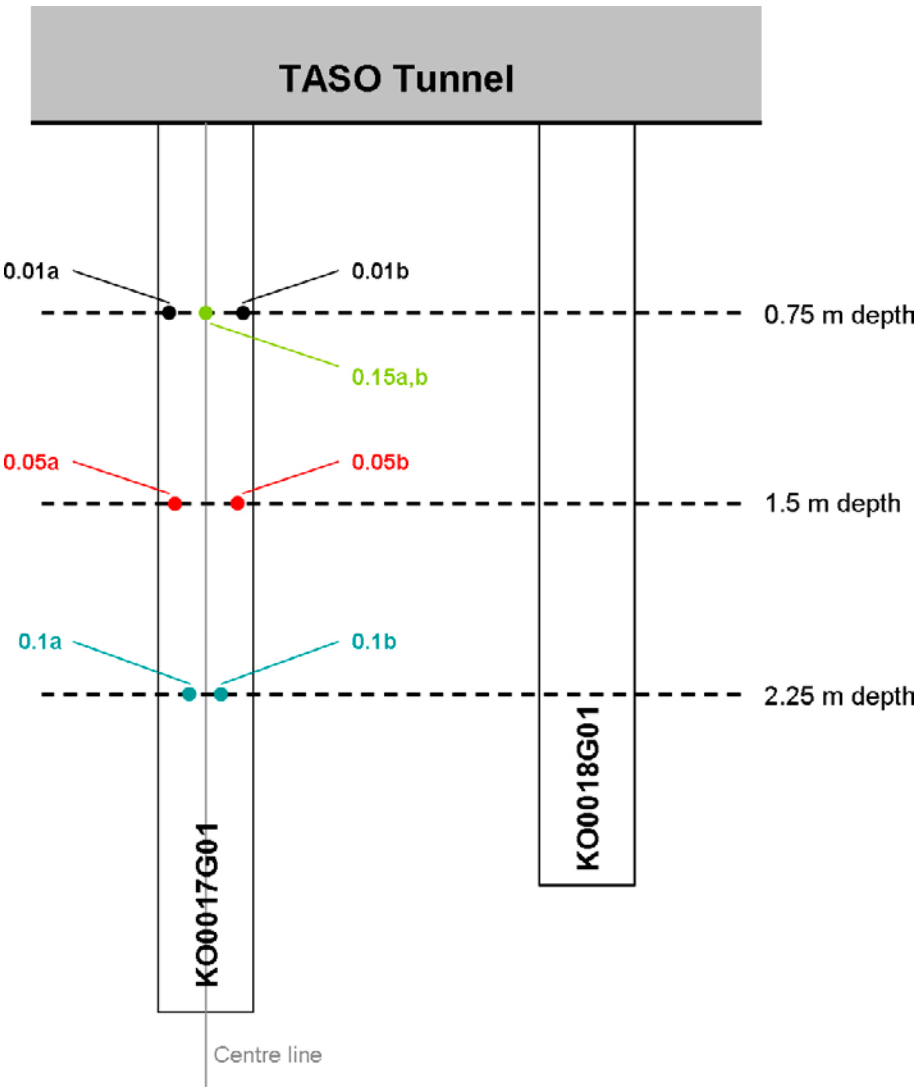

Figure 8-5. *Schematic illustrating monitored points within the bentonite, 0.01 m, 0.05 m, 0.1 m and 0.15 m from the deposition borehole wall. All points are evaluated at all depths for the two overcored boreholes considered. Pressure evolutions within the bentonite at these locations are shown in Figure 8-6 and Figure 8-7.*

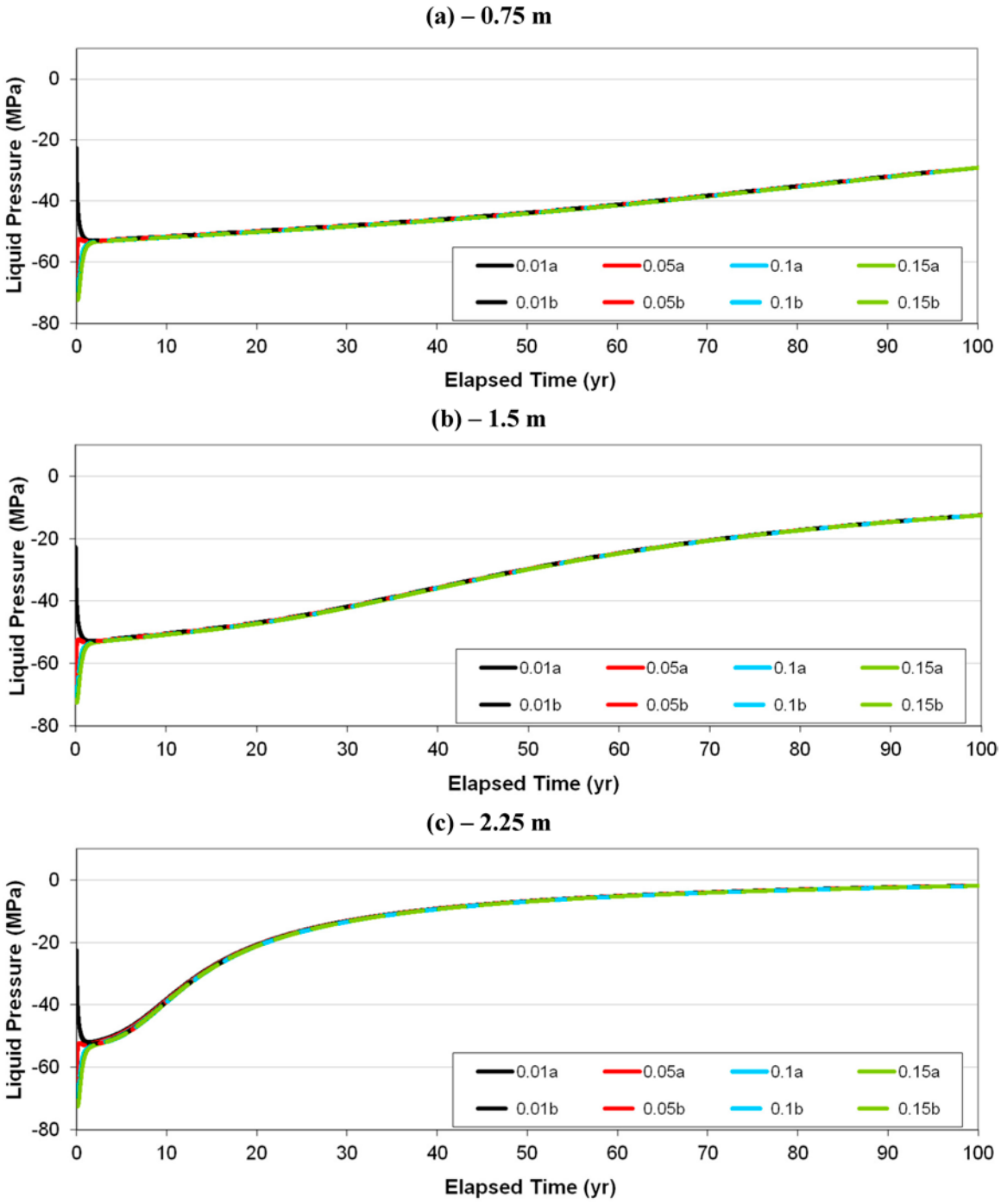

Figure 8-6. *Liquid pressure [MPa] calculated within the bentonite 0.01 m, 0.05 m, 0.1 m, and 0.15 m from the deposition borehole wall. Results are shown for a slice oriented to intersect both the boreholes, with "a" and "b" distances denoting direction from the edge of the overcored borehole. The pressure curves shown correspond to the seventh realisation of the upscaled stochastic fracture network. Figures (a, b, c) are for borehole KO0017G01 at depths of 0.75 m, 1.5 m and 2.25 m respectively.*

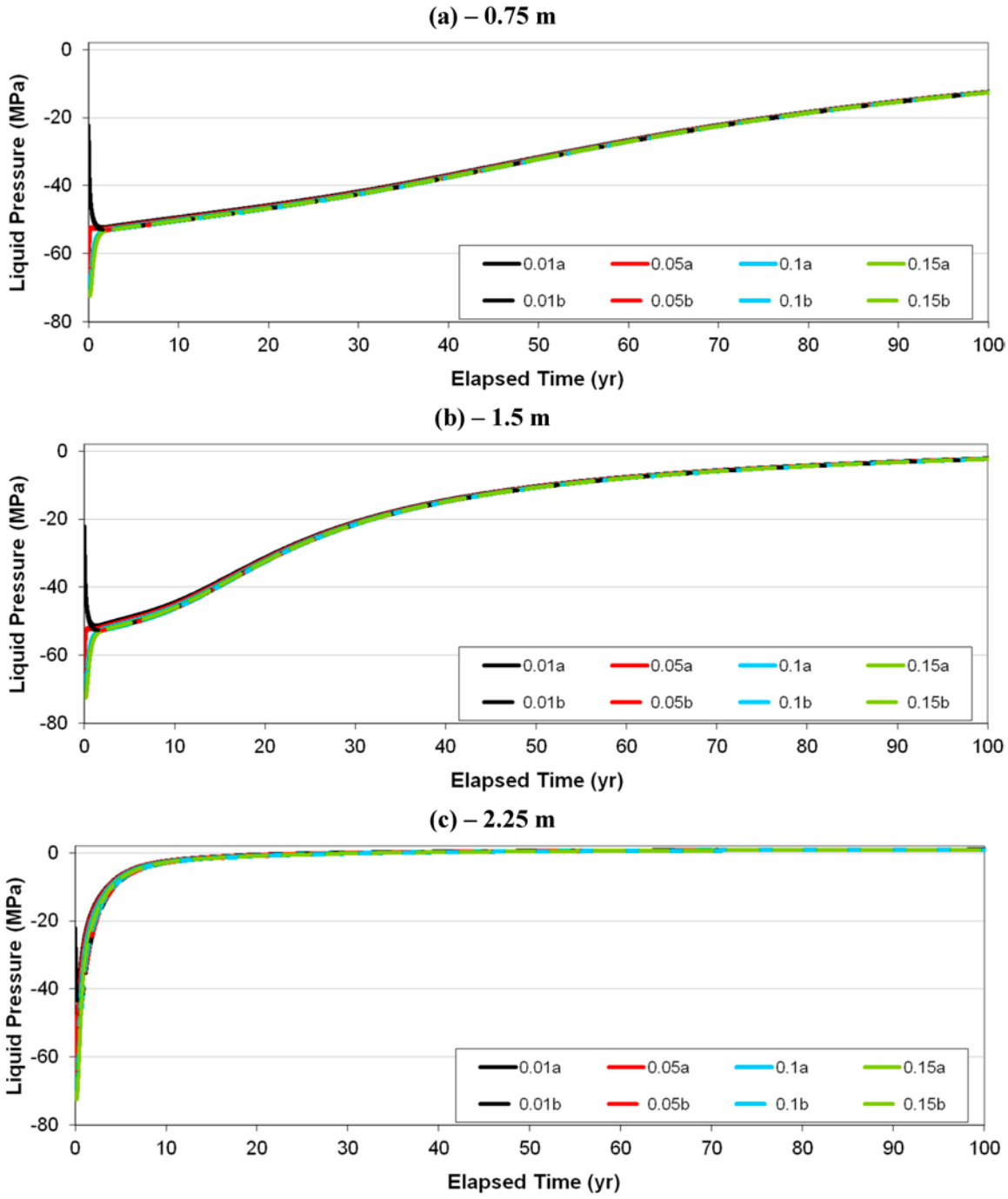

Figure 8-7. *Liquid pressure [MPa] calculated within the bentonite 0.01 m, 0.05 m, 0.1 m, and 0.15 m from the deposition borehole wall. Results are shown for a slice oriented to intersect both the boreholes, with "a" and "b" distances denoting direction from the edge of the overcored borehole. The pressure curves shown correspond to the seventh realisation of the upscaled stochastic fracture network. Figures (a, b, c) are for borehole KO0018G01 at depths of 0.75 m, 1.5 m and 2.25 m respectively.*

There is a difference in the initial liquid pressure between the points located in the outermost region of the bentonite (0.01a and 0.01b) and all others (see Figure 8-8). The initial pressure at these two locations is set to be approximately equal to −20 MPa, whilst the initial pressure at the other location is of the order of −70 MPa. This discrepancy reflects the fact that the pressure is a continuous variable, and that the discontinuity at the bentonite/host rock interface cannot be represented by assigning two different values for the pressure at the same node. In this instance, the pressure assigned at these interface nodes is that of the rock matrix (approximately atmospheric pressure), whilst the second outermost points are assigned the value of the initial bentonite pressure (~ −70 MPa).

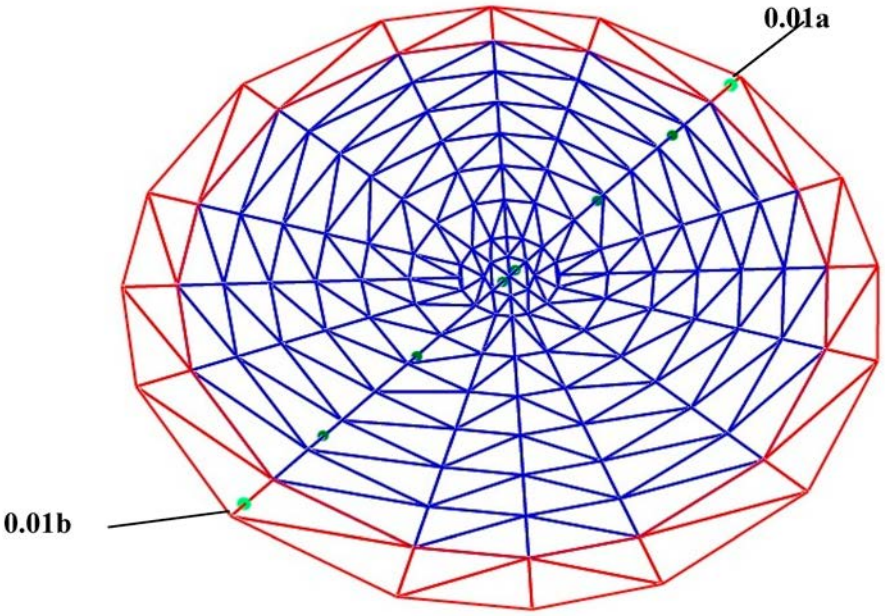

Figure 8-8. *Location of the studied points within the modelled grid representing the bentonite. The red region is the outermost bentonite ring, which represents the bentonite/host rock interface.*

This numerical construct is analogous to the installation conditions for the bentonite buffer, where water is poured into the outer slot resulting in elevated saturation at the outer surface of the bentonite.

An alternative model description would assign the pressure value at the interface to be identical to the pressure inside the bentonite, but in this case, the same effects would be observed in the first elements outside of the bentonite.

8.4 Pressure evolution within the bedrock

Liquid pressure within the fractured bedrock is extracted from the model at 27 separate locations local to overcored boreholes KO0017G01 and KO0018G01. A schematic of these locations, and the nomenclature used are shown in Figure 8-9. Corresponding figures for the evolution of liquid pressure at each of these locations is presented in Figure 8-10 and Figure 8-11, corresponding to the host rock local to each of the boreholes considered. Results in this section are presented for the seventh realisation of the upscaled stochastic fracture network.

Desaturation of the rock, local to the emplaced bentonite results in negative liquid pressures down to −2 MPa. Desaturation is greatest closest to the bentonite, as expected. Liquid pressures are slow to return to in situ pressures, with negative pressures still prevalent 0.01 m from the bentonite after 100 years.

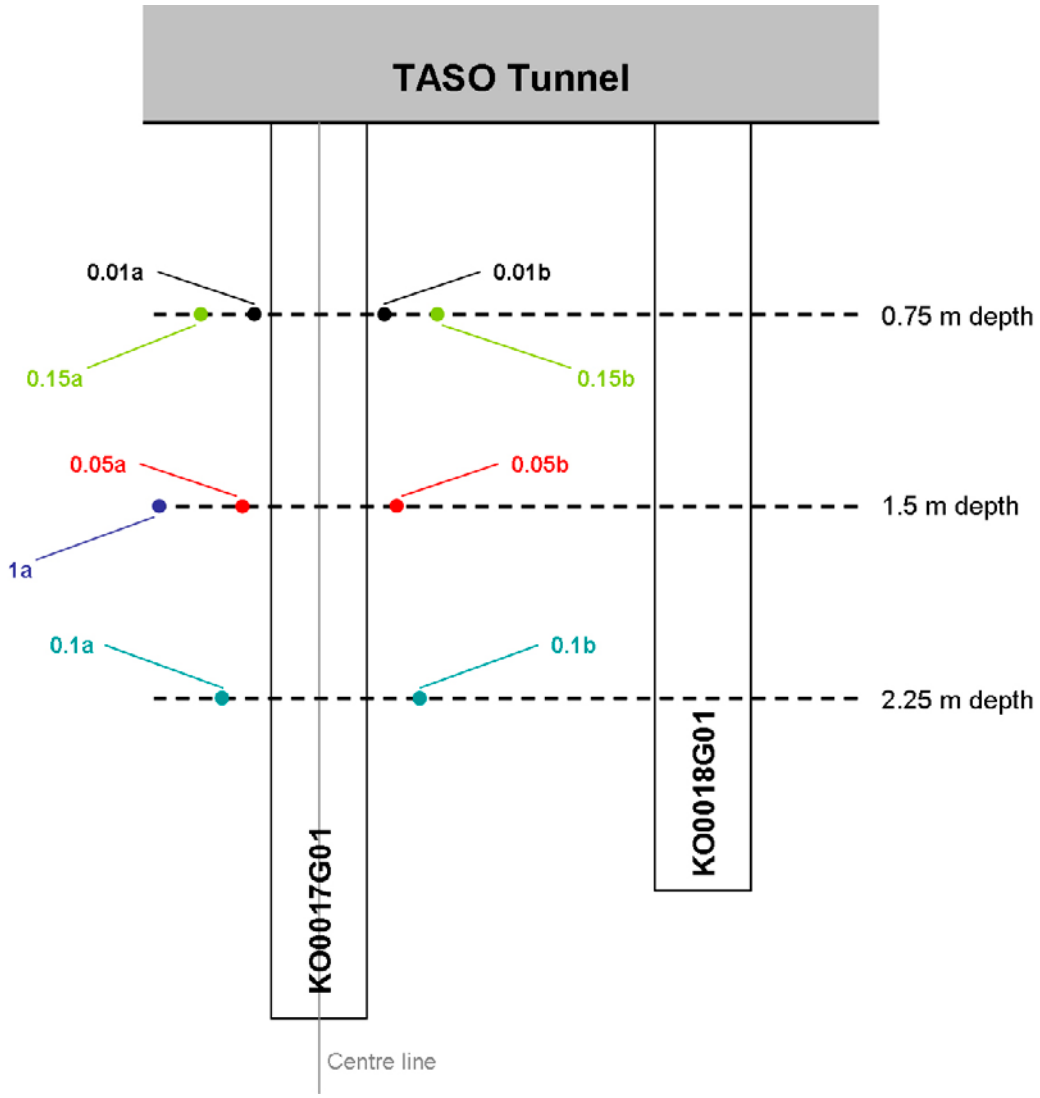

Figure 8-9. *Schematic illustrating monitored points within the bedrock, for pressure evolutions shown in Figure 8-10 and Figure 8-11.*

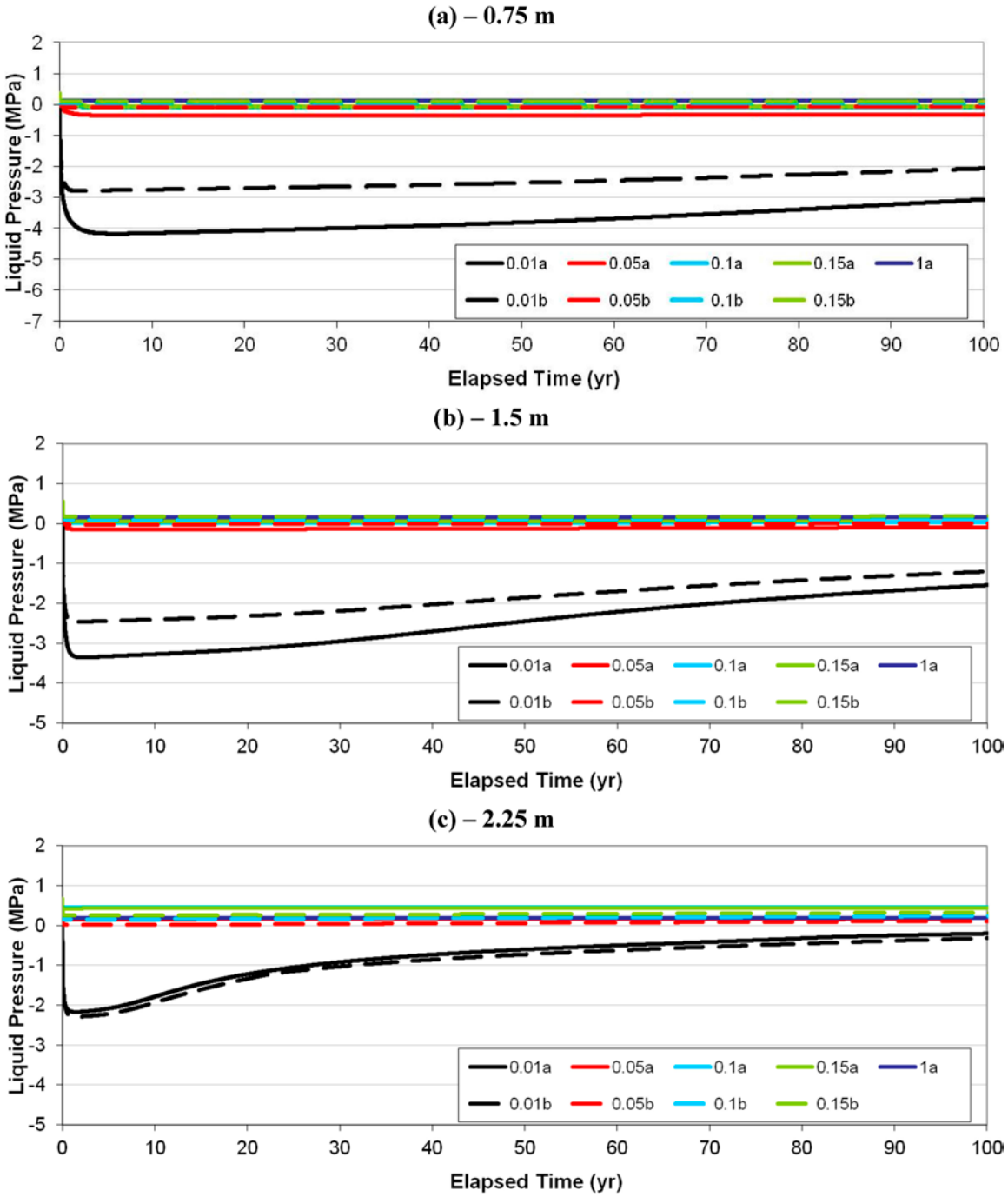

Figure 8-10. *Liquid pressure [MPa] calculated within the bedrock 0.01 m, 0.05 m, 0.1 m, 0.15 m, and 1.0 m from the deposition borehole wall. Results are shown for a slice oriented to intersect the two over-cored boreholes, with "a" and "b" distances denoting direction from the edge of the overcored borehole. The pressure curves shown correspond to the seventh realisation of the stochastic fracture network. Figures (a, b, c) are for borehole KO0017G01 at depths of 0.75 m, 1.5 m and 2.25 m respectively.*

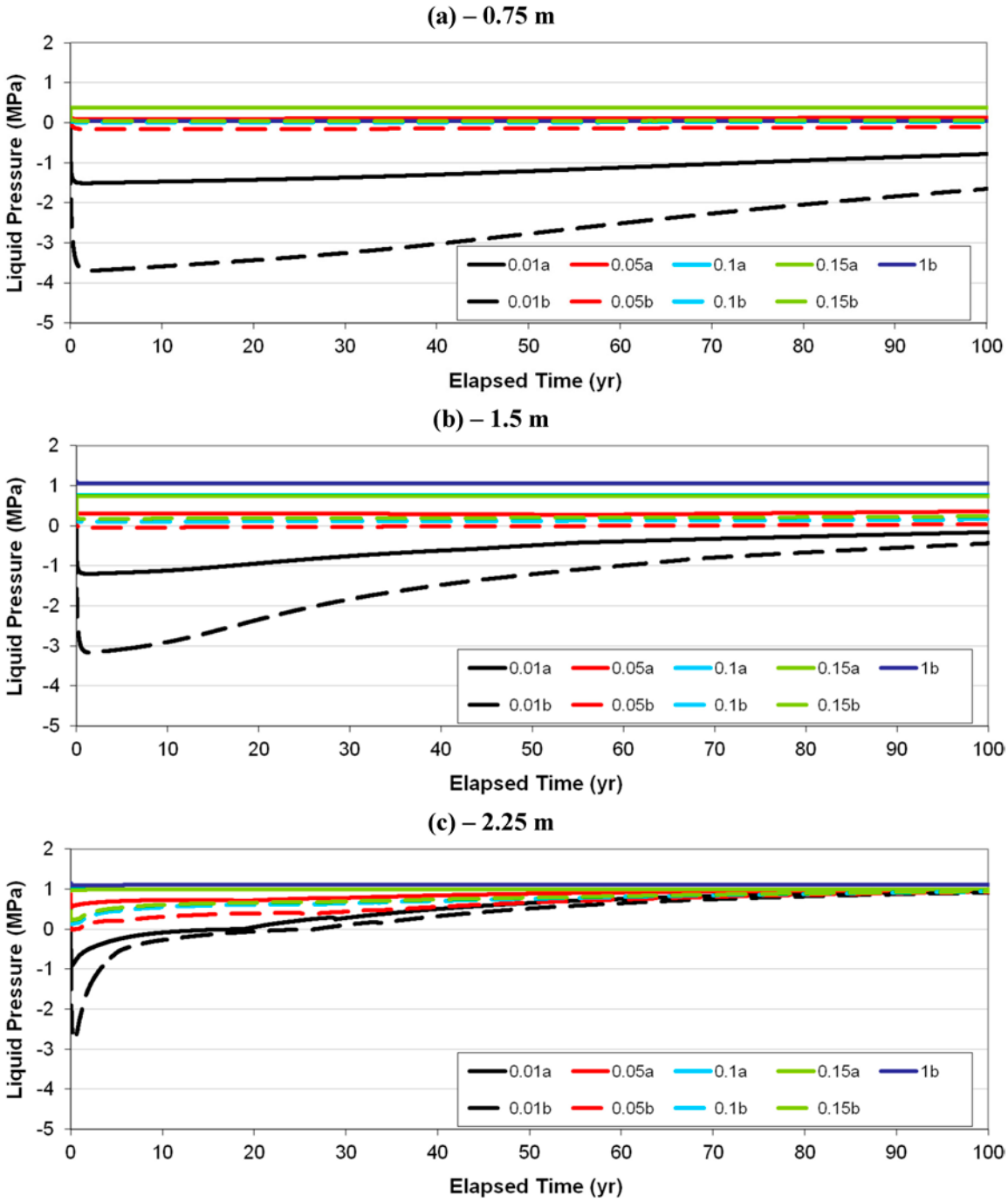

Figure 8-11. *Liquid pressure [MPa] calculated within the bedrock 0.01 m, 0.05 m, 0.1 m, 0.15 m, and 1.0 m from the deposition borehole wall. Results are shown for a slice oriented to intersect the two overcored boreholes, with "a" and "b" distances denoting direction from the edge of the overcored borehole. The pressure curves shown correspond to the seventh realisation of the stochastic fracture network. Figures (a, b, c) are for borehole KO0018G01 at depths of 0.75 m, 1.5 m and 2.25 m respectively.*

9 Discussion and conclusions

To manage the safe disposal of higher-activity wastes, a multiple barrier concept is utilised to isolate the wastes from the biosphere. Commonly, a bentonite buffer forms part of an engineered barrier system (EBS) surrounding the emplaced disposal container in some concepts for high heat generating wastes. Radioactive Waste Management (RWM) is considering using bentonite in its illustrative generic designs of the UK GDF.

Although models developed in this report are specific to the Äspö Hard Rock Laboratory (HRL), the tools, conditioning techniques and methodologies developed are generic, and directly applicable to any future work carried out on UK specific issues for the simulation of bentonite hydration in a fractured host rock.

This report has demonstrated the feasibility of using a physically realistic approach to simulate the rock bentonite interface through modelling Task 8F and the BRIE. This approach explicitly represents the heterogeneity of the fractured bedrock necessary to predict resaturation times and profiles of emplaced bentonite. In addition, methodologies have been developed for conditioning models of the bentonite using additional site measurements as they become available post-excavation of the BRIE experiment. In summary, the developed approach has identified:

- that the saturation of bentonite is highly heterogeneous, and accurate representation of the surrounding fractured bedrock, especially of the fractures intersecting the boreholes, is critical to understand the hydration of emplaced bentonite,
- the ability of the ConnectFlow software to simulate the heterogeneous hydration of the bentonite, and
- that the physical properties of the bentonite are an important parameter in the prediction of the resaturation times of the emplaced bentonite.

The data available from BRIE form a comprehensive data set for understanding and refining generic methodologies developed to represent the interaction between the groundwater flow from the rock, and the resaturation of the bentonite material. In addition, participation in Task 8F has built confidence in the ability to model the resaturation processes by developing models based directly on experimental observation.

9.1 Evaluation of conceptual models and modelling approach

The following discussion covers quantitative and qualitative analysis of the Task 8F modelling performed in this report, responding to the key questions identified in the task 8F description from the Task Force (Vidstrand et al. 2017).

9.1.1 Quantitative results

What is the range of predicted inflows into an open overcored borehole?

After conditioning of the DFN model, a large number of the hundred realisations of the stochastic DFN model provide hydraulic connections to both overcored boreholes KO0017G01 and KO0018G01. Inflows to open overcored boreholes for these realisations are:

- KO0017G01: 0.02 ml/min – 2.25 ml/min.
- KO0018G01: < 0.01 ml/min – 2.42 ml/min.

Simulated inflows to each of the deposition holes typically span two-orders of magnitude and, although the fractures intersecting the deposition holes are specified deterministically, the wider fracture network is still sampled from statistical distributions and the variability in model predictions illustrate the inherent stochastic uncertainties in the wider fracture network. From the 100 realisations considered, the 7th, the 32nd, the 39th and the 50th realisations simulate inflows within both the bounds estimated from measurements (0.12 ml/min – 0.25 ml/min for KO0017G01, and 0.01 ml/min – 0.03 ml/min for KO0018G01).

What is the range of predicted times needed to re-wet the bentonite to a saturation of 95 %?

From models conditioned to both fracture observations in the deposition holes, as well as the short-term (less than 2 year) responses measured at the twelve relative humidity sensors; long-term predictions of the resaturation of emplaced bentonite have been performed for 100 years post emplacement (as requested by the Task Force). This timescale was selected to capture the major resaturation processes of bentonite emplaced on the scale of the BRIE. However, for the latest variant of the model, 95 % liquid saturation may not be reached throughout the entire bentonite stack within 100 years. Further simulations to 200 years predict the bentonite emplaced in KO0018G01 reaches 95 % liquid saturation 195 years after emplacement. However, KO0017G01 is still to reach 95 % liquid saturation after 200 years. In this hole, the 95 % resaturation front has propagated up the deposition hole (from the fracture) 1.63 m.

9.1.2 Qualitative discussion

What are the key features and properties of the natural and engineered systems that need to be known for deposition hole screening?

Posiva and SKB are currently cooperating regarding the harmonisation of repository requirements including the requirements on the repository host rock. One such requirement for the hydraulic acceptance criteria for deposition hole positions currently requires the total inflow to open deposition holes to be below 0.1 l/min to ensure proper installation of the bentonite buffer. Although the distribution of inflows to the deposition holes is significant for resaturation of emplaced bentonite, itdoes not currently form a requirement for deposition hole acceptance.

The effect of inflow distributions to a deposition hole on the resultant resaturation of emplaced bentonite was first observed in the Task 8C modelling (Baxter et al. 2014a). The bentonite has very low permeability, and consequently the time taken for 95 % liquid saturation to be reached over the entire bentonite stack will be significantly longer if inflows are concentrated towards the bottom of the hole compared to an even distribution over a number of fractures intersecting along the length of the hole.

The Task 8D study noted that the background permeability of the rock matrix is also significant to understanding the resaturation times and profiles of emplaced bentonite, with predictions very sensitive to changes in the rock matrix parameterisation. Consequently, characterisation of the rock matrix local to the deposition holes is also required.

Finally, in this study the effects of bentonite parameterisation have been considered. Specifically, understanding the diffusion of the pressure front through the bentonite is critical to understanding the resaturation times.

What information and data from the BRIE experiment are most valuable for the overall system understanding, and model development?

When calculating resaturation rates and profiles of bentonite emplaced within an overcored borehole in the BRIE, the following aspects are critical for accurate predictions:

- The groundwater flow at Äspö, is predominately through a series of interconnected fractures. Characterisation of geometric and hydraulic properties of the fracture network is important to resaturation, providing:
  - a global scale analysis, required for fracture statistics of the background fracture network; and
  - a local scale analysis, required for conditioning individual overcored boreholes, and their hydraulic connections to the wider fracture network.
- Rock matrix permeability, measured at in situ stress conditions is critical to understanding resaturation rates. This is particular true for the driest region of the bentonite, whereas the behaviour of the wet regions might be dominated by the presence of local fractures.
- Bentonite properties for relative permeability and migration of the pressure front are significant for understanding the response of the bentonite buffer to groundwater ingress.

How does the conceptualization of the natural and engineered systems influence model predictions, and interpretation of the expected system behaviour?

The BRIE at Äspö Hard Rock Laboratory is located in granitic bedrock, with groundwater flow primarily through a series of interconnected, flow-conducting fractures. By applying a DFN concept, it is possible to represent:

- the groundwater pathway statistically between interconnected fractures in the rock mass, and
- the inflow locations interpreted within individual overcored boreholes deterministically.

This DFN model can then be upscaled to equivalent block permeabilities and porosities, providing a highly heterogeneous description of the fractured rock for use in resaturation calculations.

An alternative approach, representing the host rock using homogeneous permeability values, was considered as part of the Task 8C modelling (Baxter et al. 2014a). That representation was insufficient to fully capture the heterogeneous processes that occur during bentonite resaturation and the model systematically over predicted the resaturation rate of the bentonite.

9.1.3 Comparison to experimental results

The models developed as part of this report are compared to the BRIE experimental results for resaturation of bentonite emplaced in the central overcored boreholes. To refine model predictions, the fractured bedrock is conditioned based on characterisation of the fracture network local to both the TASO tunnel and central overcored boreholes, as well as inflow and relative humidity measurements in the dry section of borehole KO0017G01 and KO0018G01.

The models conditioned to the twelve relative humidity sensors provide substantially improved relative humidity evolutions at these points when compared to the experimental results and model predictions from Task 8D (Baxter et al. 2014b). Using these conditioned models; additional predictions of the water content (based on several hundred measurements) performed following dismantling of the BRIE, can be made (see Section 7.2.2). Model predictions indicate good agreement matching the general behaviour of the resaturation of the bentonite. The extent of resaturation within the bentonite buffer is in places underpredicted; possibly a consequence of:

- not representing the installation procedures of the experiment within the modelling (the outer slot of the overcored boreholes were filled with water), or
- an indication that the conditioned model parameters could be further refined (e.g. the rock matrix permeability is slightly too low).

Conditioning models to a limited (small) set of sensor data exhibits non-uniqueness in the parameterisation. Although conditioned models closely reflect the resaturation evolution at the twelve sensors, they are not sufficient to predict the state of the full bentonite stack. To further constrain the conditioning process, the extensive water content measurements could be used to recondition the models. However, it is likely that these data on their own would be insufficient to fully constrain the conditioning process; instead requiring experimental measurements from bentonite emplaced in several overcored boreholes. This final point suggests the non-uniqueness of the model system.

9.2 A summation of modelling BRIE

Task 8F follows on from Task 8C and Task 8D, which have previously been modelled by Amec Foster Wheeler, supported by RWM, and documented in Baxter et al. (2014a, b). Task 8C and Task 8D were concerned with the prediction of resaturation of the central probe boreholes of the BRIE, with limited data available for conditioning models. Task 8F revisits the BRIE, refining resaturation predictions using additional geometric and hydraulic data provided during dismantling of the experiment. Through these tasks, a number of high-level conclusions for modelling bentonite resaturation via a fractured host rock are determined:

Model features

- Experimental data from the BRIE illustrates the heterogeneity of bentonite resaturation from a fractured host rock. Therefore, models should provide an accurate representation of the fractured bedrock surrounding the emplaced bentonite and locations of groundwater ingress to the deposition holes to fully capture the hydration rates and profiles.
  - During Task 8C (Baxter et al. 2013a), the saturation rate of bentonite via a fractured host rock was found to be significantly affected by both the locations and total volume of groundwater ingress to the deposition holes. Task 8C identified the importance of a global scale analysis of fracture statistics for the background fracture network.
  - During the modelling of Task 8D (Baxter et al. 2014b) & Task 8F (current study), water producing intersections within the deposition holes have been specified deterministically. Through a local scale analysis, the fracture network has been conditioned at individual over-cored boreholes, and the resaturation rates and profiles of emplaced bentonite can be further constrained.
- For deposition holes sparsely intersected by fractures, the rock matrix provides a significant pathway for groundwater ingress to the deposition hole. This is particularly true for the driest region of the bentonite. Therefore the rock matrix, and its interaction with the fracture system, should be included within the conceptual model.
- The requirement to include fully coupled two-phase flow physics in the numerical representation of the conceptual model is dependent on the model parameterisation and construct. However, in the context of modelling the BRIE, the requirement to include fully coupled two-phase flow physics is not necessary.

Model uncertainties/parameterisation

- The process of conditioning models to a limited set of measurements likely provides a non-unique parameterisation of the system. To constrain model parameterisation further, a wide range of measurements should be considered for conditioning the system. This could include additional measurements of the same type already provided (e.g. additional relative humidity sensors distributed more widely across the bentonite), or, complimentary measurements such as the water content measurements taken upon completion of the experiment.
- The uncertainty in predicted resaturation profiles and times of bentonite emplaced in a fractured host rock can be reduced significantly by a detailed local fracture specification.
- Rock matrix permeability, measured at in situ stress conditions is critical to understanding resaturation rates in the driest regions of the deposition hole.
- Bentonite properties for relative permeability and pressure migration are significant for understanding the response of the bentonite buffer to groundwater ingress.

References

SKB's (Svensk Kärnbränslehantering AB) publications can be found at www.skb.com/publications.

AMEC, 2012a. NAMMU Technical Summary, Release 10.4. AMEC Report AMEC/ENV/CONNECTFLOW/8, AMEC, UK.

AMEC, 2012b. NAPSAC Technical Summary, Release 10.4 AMEC Report AMEC/ENV/CONNECTFLOW/12, AMEC, UK.

AMEC, 2012c. ConnectFlow Technical Summary, Release 10.4. AMEC Report AMEC/ENV/CPNNECTFLOW/15, AMEC, UK.

AMEC, 2012d. ConnectFlow Verification, Release 10.4 AMEC Report AMEC/ENV/CONNECTFLOW/16, AMEC, UK.

Baxter S, Holton D, Hoch A R, 2014a. Modelling Bentonite Resaturation in the Bentonite Rock Interaction Experiment (BRIE) – Task 8C. AMEC Report D.005529/13/01, AMEC, UK.

Baxter S, Holton D, Hoch A R, 2014b. Calibrated modelling of resaturation in the Bentonite Rock Interaction Experiment (BRIE) – Task 8D. AMEC Report 103453-AG-0001/T8012013/14, AMEC, UK.

Carta G, Baxter S, Holton D, Gordon A, 2016. Task Force on Engineered Barrier Systems, Code comparison and sensitivity analysis. Amec Foster Wheeler Report 204127-AA-UA00-00001-01-1.

Celia M, Bouloutas E T, Zarba R L, 1990. General mass-conservative numerical solution for the unsaturated flow equation. Water Resources Research, 26, 1483–1496.

Fatt I, Klikoff W A, 1959. Effect of fractional wettability on multiphase flow through porous media. Transactions AIME 216, 426–432.

Fransson Å, Åkesson M, Andersson L, 2017. Bentonite Rock Interaction Experiment. Characterization of rock and installation, hydration and dismantling of bentonite parcels. SKB R-14-11, Svensk Kärnbränslehantering AB.

Harrington J F, Horseman S T, 2003. Gas migration in KBS-3 buffer bentonite. Sensitivity of test parameters to experimental boundary conditions. SKB TR-03-02, Svensk Kärnbränslehantering AB.

Hartley L, Appleyard P, Baxter S, Hoek J, Roberts D, Swan D, 2012a. Development of a hydrogeological discrete fracture network model for the Olkiluoto Site Descriptive Model 2011, Volume I. Posiva Working Report 2012-32, Posiva Oy, Finland.

Hartley L, Appleyard P, Baxter S, Hoek J, Roberts D, Swan D, 2012b. Development of a hydrogeological discrete fracture network model for the Olkiluoto Site Descriptive Model 2011, Volume II. Posiva Working Report 2012-32, Posiva Oy, Finland.

Hjerne C, Nordqvist R, Harrström J, 2010. Compilation and analyses of results from cross-hole tracer tests with conservative tracers. SKB R-09-28, Svensk Kärnbränslehantering AB.

Holton D, Baxter S, Hoch A R, 2012. Modelling coupled processes in bentonite: recent results from the UK's contribution to the Äspö EBS Task Force. Mineralogical Magazine 76, 3033–3043.

Jackson C P, Hoch A R, Todman S, 2000. Self-consistency of a heterogeneous continuum porous medium representation of a fractured medium. Water Resources. Research 36, 189–202.

Joyce S, Simpson T, Hartley L, Applegate D, Hoek J, Jackson C P, Swan D, Marsic N, Follin S, 2010. Groundwater flow modelling of period with temperate climate conditions – Forsmark. SKB R-09-20, Svensk Kärnbränslehantering AB.

NDA RWMD, 2010a. Geological disposal. Generic environmental safety case main report. NDA/RWMD/021, Nuclear Decommissioning Authority (Radioactive Waste Management Directorate), UK.

NDA RWMD, 2010b. Geological disposal. Generic disposal facility designs. NDA/RWMD/048, Nuclear Decommissioning Authority (Radioactive Waste Management Directorate), UK.

Rhén I, Forsmark T, Hartley L, Joyce S, Roberts D, Gylling B, Marsic N, 2009. Bedrock Hydrogeolology: model testing and synthesis - Site descriptive modelling SDM-Site Laxemar. SKB R-08-91, Svensk Kärnbränslehantering AB.

Richards L A, 1931. Capillary conduction of liquids through porous mediums. Journal of Applied Physics 1, 318–333.

SKB, 2006. Long-term safety for KBS-3 repositories at Forsmark and Laxemar – a first evaluation. Main report of the SR-Can project. SKB TR-06-09, Svensk Kärnbränslehantering AB.

van Genuchten M T, 1980. A closed-form equation for predicting the hydraulic conductivity of unsaturated soils. Soil Science Society of America Journal 44, 892–898.

Vidstrand P, Stigsson M, Åkesson M, Fransson Å, 2017. SKB Task Forces EBS and GWFTS. Modelling the interaction between engineered and natural barriers. A compilation of Task 8 descriptions. SKB P-16-05, Svensk Kärnbränslehantering AB.

Wilson J, Savage D, Bond A, Watson S, Pusch R, Bennett D, 2011. Bentonite: a Review of key properties, processes and issues for consideration in the UK context. Quintessa Report QRS-1378ZG-1.1, Quintessa Ltd., UK.

Arkitektkopia AB, Bromma, 2019

SKB is responsible for managing spent nuclear fuel and radioactive waste produced by the Swedish nuclear power plants such that man and the environment are protected in the near and distant future.

skb.se